WL-TM-94-3077

LARGE AMPLITUDE NONLINEAR RESPONSE OF FLAT ALUMINUM, AND CARBON FIBER BEAMS AND

HOWARD F. WOLFE
CYNTHIA A. SHROYER

JUNE 1994

INTERIM REPORT FOR 10/01/92-09/01/93

APPROVED FOR PUBLIC RELEASE; DISTRIBUTION IS UNLIMITED.

FLIGHT DYNAMICS DIRECTORATE
WRIGHT LABORATORY
AIR FORCE MATERIEL COMMAND
WRIGHT PATTERSON AFB OH 45433-7562

NOTICE

When Government drawings, specifications, or other data are used for any purpose other than in connection with a definitely Government-related procurement, the United States Government incurs no responsibility or any obligation whatsoever. The fact that the government may have formulated or in any way supplied the said drawings, specifications, or other data, is not to be regarded by implication, or otherwise in any manner construed, as licensing the holder, or any other person or corporation; or as conveying any rights or permission to manufacture, use, or sell any patented invention that may in any way be related thereto.

This report is releasable to the National Technical Information Service (NTIS). At NTIS, it will be available to the general public, including foreign nations.

This technical report has been reviewed and is approved for publication.

Howard F. Wolfe, Aerospace Engineer
Acoustics & Sonic Fatigue Section

Cynthia R. Shroyer, Computer Scientist, Data Analysis Section

Coordination:

Ralph M. Shimovetz, Tech Manager
Acoustics & Sonic Fatigue Section

John T. Ach, Tech Manager
Data Analysis Section

Maj Joseph W. Moschler
Structural Dynamics Branch
Structures Division

If your address has changed, if you wish to be removed from our mailing list, or if the addressee is no longer employed by your organization, please notify WL/FIBGD, Wright-Patterson AFB, OH 45433-6553 to help maintain a current mailing list.

Copies of this report should not be returned unless return is required by security considerations, contractual obligations, or notice on a specific document.

DISCLAIMER NOTICE

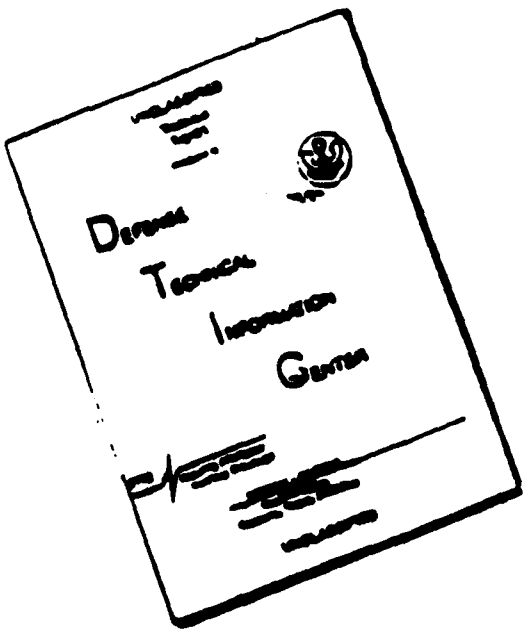

THIS DOCUMENT IS BEST QUALITY AVAILABLE. THE COPY FURNISHED TO DTIC CONTAINED A SIGNIFICANT NUMBER OF PAGES WHICH DO NOT REPRODUCE LEGIBLY.

REPORT DOCUMENTATION PAGE

Form Approved
OMB No. 0704-0188

1. AGENCY USE ONLY (Leave Blank)	2. REPORT DATE	3. REPORT TYPE AND DATES COVERED

4. TITLE AND SUBTITLE

MEASUREMENT OF NONLINEAR RESPONSE OF FLAT ALUMINUM, AND CARBON FIBER REINFORCED PLASTIC BEAMS AND PLATES

5. FUNDING NUMBERS

Program Element: 62201F
Project: 2401
Task: 04
Work Unit: 42

6. AUTHOR(S)

Howard F. Wolf, Cynthia A. Shroyer

7. PERFORMING ORGANIZATION NAME(S) AND ADDRESS(ES)

Flight Dynamics Directorate
Wright Laboratory
WPAFB OH 45433-6553

8. PERFORMING ORGANIZATION REPORT NUMBER

9. SPONSORING/MONITORING AGENCY NAME(S) AND ADDRESS(ES)

FLIGHT DYNAMICS DIRECTORATE
WRIGHT LABORATORY
AIR FORCE MATERIEL COMMAND
WRIGHT PATTERSON AFB OH 45433-7562

10. SPONSORING/MONITORING AGENCY REPORT NUMBER

WL-TM-94-3077

11. SUPPLEMENTARY NOTES

12a. DISTRIBUTION/AVAILABILITY STATEMENT

Approved for public release; distribution is unlimited.

12b. DISTRIBUTION CODE

13. ABSTRACT (Maximum 200 words)

This progress report presents the results of a continuing study to improve the understanding of nonlinear dynamic behavior of aerospace structures subjected to high levels of excitation. Tests were continued with a clamped-clamped (C-C) aluminum beam. A summary of the results is presented. Tests were conducted with a C-C carbon fiber reinforced plastic (CFRP) beam and a pinned-pinned (P-P) aluminum beam. A summary of these results is also presented. Flat plate tests began with an aluminum plate. The shapes of the total, axial and bending strain power spectral densities for the C-C aluminum and the CFRP beams were quite similar. Both showed a small frequency increase and slight peak broadening as the levels of excitation increased. The nonlinear displacement shapes for the two cases were also quite similar. Further analysis is needed for the P-P aluminum beam case. Finally, a method of estimating the RMS stress for the multimodal response of a panel is presented.

14. SUBJECT TERMS

Nonlinear bivration, sonic fatigue, clamped beams, clamped plates, dynamic testing, dynamic analysis.

15. NUMBER OF PAGES

90

16. PRICE CODE

17. SECURITY CLASSIFICATION OF REPORT	18. SECURITY CLASSIFICATION OF THIS PAGE	19. SECURITY CLASSIFICATION OF ABSTRACT	20. LIMITATION OF ABSTRACT
UNCLASSIFIED	UNCLASSIFIED	UNCLASSIFIED	UL

ABSTRACT

This progress report presents the results of a continuing study to improve the understanding of nonlinear dynamic behavior of aerospace structures subjected to high levels of excitation. Tests were continued with a continued clamped-clamped (C-C) aluminum beam. A summary of the results is presented. Tests were conducted with a C-C carbon fiber reinforced plastic (CFRP) beam and a pinned-pinned (P-P) aluminum beam. A summary of these results is also presented. Flat plate tests began with an aluminum plate. The shapes of the total, axial and bending strain power spectral densities for the C-C aluminum and the CFRP beams were quite similar. Both showed a small frequency increase and slight peak broadening as the levels of excitation increased. The nonlinear displacement shapes for the two cases were also quite similar. Further analysis is needed for the P-P aluminum beam case. Finally, a method of estimating the RMS stress for the multimodal response of a panel is presented.

CONTENTS

LIST OF FIGURES

FOREWORD

This memorandum summarizes the information contained in the M Phil./PhD Progress Report submitted in June 1993 to Professor R.G. White, Academic Supervisor, at the Institute of Sound and Vibration Research (ISVR), University of Southampton, England. The work was performed under the supervision of Professor R. G. White and R. M. Shimovetz, Technical Manager, Acoustics and Sonic Fatigue Section, Structural Dynamics Branch, Wright Laboratory, Wright-Patterson Air Force Base (WPAFB). The initial work at ISVR, published in WL-TM-91-311-FIBG, has been continued at WPAFB. A second memorandum was published, WL-TM-93-352-FIBG.

1. INTRODUCTION

This is the third memorandum summarizing the progress made on an in-house research project entitled "Nonlinear Aspects of Aerospace Structures at High Excitation Levels." The first and second memoranda [1 and 2] were published in May 1991 and December 1992. The goal of the project is to improve the understanding of the nonlinear dynamic behavior of aerospace structures subjected to high excitation levels. Aluminum and carbon fiber reinforced plastic (CFRP) beams and plates were studied analytically and experimentally.

2. BEAM TEST RIG

The test rig for testing the beams was modified to reduce alignment problems when lightly tensioning the beams and clamping the beams to the bed plate as shown in Fig 1. Steel blocks were machined with protrusions to fit the grooves in the vibration isolation bed plate. This change permitted static test measurements to be taken by applying a load axially to the beam with the threaded rod assembly. One of the beam clamps was kept loose to allow movement and static tension loads to be placed on the beam. This method revealed errors in the strain gauge measurements close to the clamping block, as well as the other gauges and is discussed in the beam test sections of this report.

The annular permanent magnet mounting was changed when the force produced by the coil in the magnetic field was found to be nonlinear with coil travel. Originally, two magnets were mounted together which modified the magnetic field of the magnet being used. The one magnet arrangement was found to be satisfactory. New coil-magnet calibration curves were obtained relating the coil current to force for sinusoidal and random excitation.

The strain bridge amplifiers that were used can be either AC coupled or DC coupled. DC coupling was selected since the in-plane stretching results in a DC offset or a mean value other than zero in the strain time histories. The in-plane stretching or axial strain was one of the primary effects of interest in this study. Many sources of electronic errors can contaminate the strain data when the bridges are DC coupled. Any DC offset in the force excitation circuit can result in a DC shift in strain. Some possible sources are the band pass filter, current modifier, amplifier, strain bridge amplifier and recording system. Each source was carefully checked before the start of a test to eliminate electronic DC offsets.

A new constant current modifier was designed and built to replace the one developed at the Institute of Sound and Vibration Research (ISVR). The new modifier in combination with the new constant current amplifier provided a flatter narrow band random

input spectrum to excite the beams.

3. CLAMPED-CLAMPED (C-C) ALUMINUM BEAM EXPERIMENTS

Static deflection shapes were obtained by applying DC current to the coil and measuring the displacements with a dial gauge. The results, shown in Figs 2 and 3, will be useful in checking large displacement static bending theories.

Static strain gauge measurements were made and compared with dial gauge measurements of the elongation of the beam. These values can be compared since the strain is equal to the amount of elongation divided by the length of the beam ($\Delta\ell/\ell$). The strain gauge locations are shown in Fig 4. Gauges 3 and 6, installed back-to-back, were very close to the clamping block. This yielded erroneous data due to the clamping pressure applied to the end of the beam and distortion of the bonding surface. The active element of gauges 3 and 6 was 0.8128 mm in length and mounted 1 mm from the clamp location to obtain data close to the stress concentration. The torque values to tighten the clamping plate were selected to prevent beam slippage. The clamping block was moved 19 mm from gauges 3 & 6 to determine accuracy and the effect of clamping close to the gauges. Fig 5 shows the results of the tests. Although the gauge measurements were reasonably linear, 4 out of 6 gauges were 30 microstrain below the 800 microstrain level, about 4 % accuracy. When the clamping block was moved to 2 mm from gauges 3 & 6 (Fig 6) the results were similar except for gauges 3 & 6. Gauges 3 & 6 were reasonably linear but 34% low in level. Different adhesives, coatings, strain gauges and beams were evaluated with similar results. The major source of error was found to be the method of bonding the strain gauges to the beams. The static bending results, shown in Fig 7, show the nonlinear increase in strain as the static load increases.

Total, axial and bending strain measurements were measured again with random excitation at different load levels with a variety of bandwidths to determine the effects of exciting the following modes of vibration: first mode only, third mode only, fifth mode only, first and third modes and first, third and fifth modes. These tests were conducted to study modal coupling effects, if any. Preliminary results showed the modes well separated in frequency and no modal coupling. One example of the total, axial and bending strain results is shown in Fig 8. Sine dwell tests were also conducted and are shown in Fig 9.

Displacements at the center of the beam were also measured using a laser vibrometer and sine dwell excitation as shown in Fig 10. The beam was then excited with slow sine sweeps at low levels to determine damping for the first mode using the half power point bandwidth method. The following relationship was

used: * With the exciter coil attached to the beam, the loss factors measured were 1.89%, 1.85% and 1.92%. No measurable difference in damping for the beam was found with or without retro-reflective laser tape used to lower noise in vibrometer measurements. An example of a sine sweep is shown in Fig 11.

* $\zeta = \frac{c}{c_c} = \frac{\Delta f}{2 f_o}$

Displacement measurements of the clamping block were taken with the vibrometer in the direction of beam motion. Only 0.00305 mm peak-to-peak was measured with sinusoidal excitation of the first mode at a maximum level of 85 ma, 64.6 Hz, 230 microstrain at the center of the beam, and 2.3 mm peak-to-peak displacement. The percent displacement of the block relative to the beam peak displacement was only 0.133%, but the test was not performed with a perfectly clamped boundary condition.

4. CLAMPED-CLAMPED (C-C) CARBON FIBER REINFORCED PLASTIC (CFRP) BEAM DYNAMIC TESTS

The two CFRP beams fabricated, APC-2 Graphite/PEEK, were scrapped because distortion built up in the beams. Two more attempts to fabricate thermoplastic beams were also unsuccessful. Fabrication of graphite epoxy beams $(0°/\pm45°/90°)_{2s}$ with Hercules AS4/3501-6 prepreg tape yielded flat beams suitable for testing. The dimensions were the same as the aluminum beams (2x20x631 mm) except the thickness was increased from 2 mm to 2.21 mm to obtain a symmetric ply lay-up.

Tests conducted on the graphite epoxy beam were similar to past tests for the aluminum beam using the same test rig. The results from the static tension tests were similar for the two types of beams, however, the gauge measurements on the graphite epoxy beam were about 100 microstrain lower at the 800 microstrain level but still linear. Static tension test results are shown in Fig 12 and 13. Static bending test results, shown in Fig 14, were also similar to the aluminium beam results. The displacement versus strain data are shown in Fig 15 for strain gauges 1 & 3.

The sine dwell total, axial and bending strain and displacement data at high excitation levels are shown in Fig 16. The peak frequency increased from 56.5 Hz to 75.3 Hz. The total and axial strains for all 6 gauges are shown in Figs 17 and 18. The axial strain for the gauges at the clamped edge for the maximum load case was about 65 microstrain, whereas, the other gauge locations were about 75 microstrain. This amounts to 14% lower measurement than the other locations, otherwise, the axial strains were about equal for all excitation loads. The strain

versus displacement data are shown in Fig 19.

For the frequency sweep tests, the frequency was slowly swept from low to high and high to low for the first mode of vibration to determine the jump characteristics. An example is shown in Fig 20. Likewise, amplitude effects at three different frequencies were determined by slow amplitude sweeps from low to high. Sine sweeps were also recorded to determine the first mode damping.

Locating the third and fifth modal frequencies was more difficult than the first. Two distorted third modes appeared at 388.6 Hz and 406.7 Hz as shown in Figs 21 and 22. At the lower frequency the left peak was much higher than the right and at the higher frequency, the opposite was true. The coil and beam torsional resonances were at 2200 Hz and above, so they were dismissed as sources of contamination and coupling. The plastic screw attaching the coil to the beam was machined to align the coil more nearly perpendicular to the beam. This resulted in the higher frequency, 406.7 Hz, being more predominant although the lower frequency third mode still appeared. The instance of two third modes did not occur with the same test rig for the aluminum beam case. One explanation is the possibility that the composite material properties, which were not present in the C-C aluminum case, may result in distortion in the higher mode of vibration. Likewise, the fifth mode was also distorted as seen in Fig 23. More examples of this phenomena can be seen from the random excitation plots in Figs 24 through 28.

Two bandwidths were selected for the random tests, 10 - 600 Hz and 10 - 1300 Hz. The power spectral densities for the 10 - 1300 Hz cases for three strain gauge locations are shown in Figs 24, 25, and 26. The displacement and current power spectral densities are shown in Figs 27 and 28. The first mode had one peak at all levels of excitation as did the first mode for the aluminum beam. The third and fifth modes each occurred at two different frequencies at strain locations 2 and 3 as shown in Figs 25 and 26. The fifth mode peaks were not symmetric. The lower of the two frequencies shifted to lower frequencies at high excitation levels which is characteristic of a soft spring nonlinearity. The power spectral densities for the displacements are shown in Figure 27. The double peak phenomenon for the third and fifth modes was not apparent since the displacements at the center of the beam were much smaller than those for the first mode. The power spectral densities for the current are shown in Fig 28. The total, axial and bending strains for the displacement in the 10 - 600 Hz random case are shown in Fig 29.

5. PINNED-PINNED (P-P) ALUMINUM BEAM DYNAMIC TESTS

A pinned-pinned beam and fixture were fabricated and

installed in the test rig as shown in Figs 30 and 31. A longer exciter coil was also fabricated in order to maintain a linear current-force relationship since the displacements were much higher for the P-P case than the C-C case. The mass of the new coil assembly was 66 g, 39.6 g heavier than the coil assembly for the C-C case. The current modifier was changed to handle the higher currents required.

The static bending test results are shown in Fig 32. The displacement data are shown with the strain data in Fig 33.

The frequency was repeatedly swept from low to high and high to low for the first mode using increasly higher force levels in order to observe the jump phenomenon (Figs 34 and 35). Five frequencies were selected around the first mode and the amplitudes were slowly increased and decreased (amplitude sweeps) as shown in Figs 36 and 37. These sweeps describe the two bistable states in which the beam vibrates.

Combined plots of the strain spectral densities for the total strain at gauge locations 1 and 2 are shown in Figs 38 and 39 for the random excitation tests. The axial and bending strain spectral densities are shown in Figs 40 and 41. A comparison of the total, axial and bending strain spectral densities for gauge location 1 is shown in Fig 42.

6. LARGE AMPLITUDE DISPLACEMENT SHAPES AND ANALYSIS

Nonlinear displacement shapes were obtained experimentally for two clamped-clamped beams, an aluminium one and a CFRP one, and one pinned-pinned aluminium beam by sinusoidally exciting them at large amplitudes of vibration. These experiments were conducted as part of a study to more fully understand nonlinear effects in sonic fatigue analysis of structures. Many recent advances have been made in the technology of scanning laser doppler sensors. The rapid scanning capability as well as automatic data collection and display methods are particularly advantageous in measuring mode shapes and large amplitude surface velocities. The upper velocity limit of 1 m/s has recently been increased to 10 m/s, which facilitates the measurement of displacement shapes to very high amplitudes with a high degree of accuracy. The inherent accuracy of these sensors is due to the small wavelength of the light beam. These capabilities plus many other features have made the scanning laser doppler sensor very favorable for obtaining experimental displacement data for high amplitude vibration of beams, as well as many other structures of interest.

Nonlinear displacement shapes are dependent upon the excitation force and the tuning frequency. This differs from mode shapes which are mathematically linear, amplitude

independent and occur at a single frequency. The nonlinear behavior exhibited characteristics similar to a cubic stiffness term in the equations of motion.

The surface velocity measurements from the scanning laser vibrometers were electronically integrated to yield displacement shapes. The beams were sinusoidally excited from low to high to obtain one resonant frequency in the nonlinear region of response. A second frequency was also obtained when the frequency was swept from high to low, but this frequency was not as interesting since its amplitude was much lower. All displacement shapes were obtained by dwelling at a frequency found by sweeping the frequency of oscillation from below a particular resonance to a point just prior to jump through.

Curvature in the beam is related to the bending and axial strains as shown in the following expressions: [3]

$$\varepsilon_b = \frac{t}{2}\frac{d^2w}{dx^2} \quad \text{and} \quad \varepsilon_a = \frac{1}{2\ell}\int_o^\ell \left(\frac{dw}{dx}\right)^2 dx = \Delta\ell/\ell$$

where: ε_b = bending strain
ε_a = axial strain
t = thickness of the beam
ℓ = length of the beam

Second derivative estimates of the displacement shapes can be obtained by differentiating the curve fit of the raw measured data twice. Derivatives of the displacement shapes can be quite sensitive to instrument noise and ripple effects in the raw data since the amplitudes are very small compared to the length of the beam. Various smoothing methods were explored in an attempt to approximate the raw data. Smoothing was accomplished with a seventh order polynomial calculated by a commercial curve fitting routine. Examples of first and third mode nonlinear displacement shapes for a clamped-clamped aluminium beam are shown in Figs 43 and 44. The frequencies increased from 54.8 Hz to 67 Hz from the smallest to the largest displacement shapes. The maximum slopes and curvatures increased with increasing levels of excitation. The slopes and curvatures were calculated from the first and second derivatives with respect to distance along the length of the beam. Examples of these are shown in Figs 45 and 46. Errors in the second derivatives were noticed near the clamps. A fourth order polynomial fit is shown in Fig 47 and the first and second derivatives are shown in Figs 48 and 49. The fourth order fit seems to be more reasonable than the seventh order fit. The maximum curvature was about 3.4×10^{-4} per millimeter or 340 microstrain, which is comparable to the strain measured. The normalized displacement shapes are shown in Fig 50.

Other schemes are quite plausible to obtain better accuracy in estimating the bending strain. The axial strain can be

was found by determining the change in length divided by the original length of the beam. Displacement shapes of the third mode (see Fig 44) were not equal in amplitude. Mode shapes were measured at low acoustic excitation levels without the coil mass attached. Both even and odd modes were obtained. The third mode shape is shown in Fig 51.

Comparing the third and the fifth displacement shapes with and without the exciter coil attached indicated a reduction in the amplitude at the center of the beam.

Other examples are shown in Fig 52 for a CFRP beam. In this case the raw data are shown with similar results to the aluminum beam. Likewise, similar results were obtained for the fourth order polynomial fit, shown in Fig 53, the first derivative, shown in Fig 54, the second derivative, shown in Fig 55 and the normalized displacement shapes, shown in Fig 56.

The displacement shapes (raw data) for the P-P aluminium beam case are shown in Fig 57, the fourth order polynomial fit in Fig 58, the derivatives in Figs 59 and 60 and the normalized displacement shapes in Fig 61. Since the polynomial fit altered the shape of the data to resemble the clamped case, the derivatives were useless. The slope should be zero at the center of the beam and maximum at the ends for the pinned boundary condition.

Experimental nonlinear displacement shapes of beams with various boundary conditions can be obtained with relative ease using scanning laser vibrometers. The axial and bending components of strain can be obtained from the nonlinear displacement shapes and then be used to determine the stress in the material for the sinusoidal forced vibration case.

7. MAGNETIC FIELD EFFECTS ON STRAIN GAUGE MEASUREMENTS

The magnetic field produced by the permanent magnet coil exciter can affect the strain gauge measurements. The strain gauges on an aluminum beam were moved close to a strong magnetic field produced by a 12,000 pound shaker. The shaker was moving at full power with 310 amperes in the field coil at 90 Hz while the strain gauges were moved through the magnetic field. The maximum change in strain measurements due to moving the gauges in and out of the field was only 6 microstrain. Since the shaker magnetic field is much larger than the coil magnet arrangement used in the beam tests, the change in strain measurement from a smaller magnetic field would be even less. Thus, errors due to magnetic field effects were considered insignificant.

8. CLAMPED-CLAMPED (C-C) ALUMINUM SHAKER TEST PANEL

Shaker tests of panels provide a convenient method for studying modal coupling effects since they provide well defined forcing functions. An aluminum panel was torqued down in an aluminum clamping frame arrangement before installing the strain gauges. The unclamped size was 260 x 210 x 1.27 mm. Mode shapes with acoustic excitation were measured with the vibrometer as shown in Figs 62, 63, 64 and 65. An unfortunate choice in aspect ratio, 1.24 (length divided by width), resulted in a 2:2 modal frequency at 656 Hz, which was within 1 Hz of a 3:1 mode. Another skewed 3:1 mode also appeared at 662 Hz. Hopefully, the nonlinear effects from higher amplitude excitation on a large shaker and installation of the strain gauges will help to separate these modes.

9. CARBON FIBER REINFORCED PLASTIC (CFRP) SHAKER TEST PANELS

Three clamped-clamped (C-C) CFRP shaker panels are being fabricated for the same fixture used for the aluminum panel shaker tests. The material will be the same as the CFRP beams, AS4/3501-6 unidirectional prepreg with AS4 fibers in a 3501-6 matrix. The size will be the same as the aluminum panel except the thickness of the 8 plies (0/±45°/90)$_s$ will be 1 mm.

Two C-C CFRP acoustic panels are being fabricated in the plane progressive wave tube (PWT). The unclamped size will be 587 x 387 x 1 mm.

A P-P CFRP beam is being fabricated for testing in the beam test rig. The same length, width and thickness of the C-C beam will be used.

10. FINITE ELEMENT METHODS (FEM)

A finite element beam program is being developed by Professor Chuh Mei at Old Dominion University. Table I shows the linear theoretical resonant frequencies and the FEM results for pretensioning the C-C aluminum beam and adding the coil mass at the center of the beam [4]. Adding a coil mass tends to lower the resonant frequencies and pretensioning tends to increase the resonant frequencies. The resonant frequencies from the FEM program with 100 microstrain pretension and a 26.4 g coil mass compared favorably with the experimental results. The maximum deflections measured for the C-C aluminum beam compared with FEM results for various excitation levels are shown in Fig 66. Comparisons of the strain measurements at the center of the beam and at the clamped edges are shown in Figs 67 and 68.

11. RECTANGULAR PLATES UNDER LARGE DEFLECTIONS

Chien and Yuan [5] solved the static problem of a uniformly loaded, clamped, rectangular plate under large deflection. They compared their experimental results, their theoretical results, and results from investigators Levy and Wey. At high deflection and high load, their theory did not agree very well with their experiments. An example of their experimental results is shown in Fig 69.

Although comparing plate data with beam data can be misleading, similar trends could be expected. The static test results for the C-C aluminum beam are shown in Fig 70. Chien and Yuan's axial strains for a plate seem to increase at a faster rate than for the beam, and bending strains seem to decrease at a slower rate. Their theory follows that of many other investigators.

12. ESTIMATING MULTIMODAL RANDOM RESPONSE OF PLATES

Integrations of the strain spectral densities of the plate response at both low levels and high levels of random excitation suggest that at higher levels of excitation, the third and fifth modes contribute significantly to the overall response levels. The response energy, primarily due to the first modal response at lower levels of excitation, appears to shift from the first modal response to a smeared or less distinct first, third and fifth modal response at higher levels of excitation. The less distinct results of the integrations suggest modal coupling and nonlinear frequency response.

The mean square stress may be expressed as:

$$\sigma^2(t) \approx \frac{\pi}{4\zeta} f_n G_x(f_n) \sigma_0^2$$

where: σ_0 = static stress
$G_x(f_n)$ = sound power spectral density
f_n = resonant frequency
ζ = damping ratio

This equation uses only the first mode response and assumes that the static and dynamic deflected shapes are identical and that the acoustic pressure is in phase over the whole panel. Assuming the first, third and fifth modes are the major contributing sources of response, an estimate of the total mean square stress may be expressed as:

$$\sigma^2 \approx A_1 \frac{\pi}{4\zeta_1} f_1 G_x(f_1) \sigma_1^2 + A_3 \frac{\pi}{4\zeta_3} f_3 G_x(f_3) \sigma_3^2 + A_5 \frac{\pi}{4\zeta_5} G_x(f_5) \sigma_5^2$$

Where: $A_1+A_3+A_5 = 1000$

A modified version of the Miles equation [6] is expressed as:

$$\sigma = \frac{1.63 \times 10^{-9} \quad (E/\rho)^{1/2} a^{1.25} S_p(f_{11}) (b/a)^{1.75}}{h^{1.75} \zeta^{0.25} [3(b/a)^2+3(a/b)^2+2]^{0.84}} \text{ ksi}$$

$$S_p(f_{11}) = \sqrt{G_p(f_{11})}$$

Where: E = Youngs modulus
ρ = density
a = width of the plate
b = length of the plate
h = thickness

For a specific plate size and material most of the terms may be expressed as a constant C or:

$$\sigma = A_1 C_1 \frac{S_p(f_{11})}{\zeta_{11}^{0.56}} + A_3 \frac{C_3 S_p(f_{31})}{\zeta_{31}^{0.56}} + \frac{A_5 C_3 S_p(f_{51})}{\zeta_{51}^{0.56}}$$

The static pressure assumption for the first mode assumes a length "b" and a width "a" of a plate. Further approximating the third and fifth mode as a length of b/3 and b/5 would facilitate an estimate of their modal contribution.

13. CONCLUSIONS

a. The shapes of the total, axial and bending strain spectral densities for the clamped-clamped CFRP beam and the clamped-clamped aluminum beam were very similar. The amplitudes of the peaks were somewhat similar, more so, however, than either case compared to the peaks in the strain spectral densities for the P-P aluminum beam.

b. The nonlinear displacement shapes for the clamped-clamped CFRP beam and the clamped-clamped aluminum beam were also quite similar. The nonlinear displacement shapes for the pinned-pinned aluminum beam were noticeably different from either of the other two cases. The clamps at the ends of the beam prevent it from rotating and result in large curvatures.

c. The coil mass attached to the center of a beam, mass loads the beam and decreases the resonant frequencies. The mass also significantly lowers the amplitude at the center of the displacement shapes of the third and fifth modes.

10. REFERENCES

1. Wolfe, H.F., "Nolinear Aspects of Aerospace Structures at High Excitation Levels, Flat Aluminium Beams and Plates Studied-Progress Report Oct 89-Sep 90," WL-TM-91-311-FIBG, Wright-Patterson AFB, OH, May 1991.

2. Wolfe, H.F. and Shroyer, C.A., "Large Amplitude Nonlinear Response of Flat Aluminum Beams and Plates - Progress Report Oct 90-Sep 92," WL-TM-92-352-FIBG, Dec 1992.

3. Bennouna, M.M. and White, R.G., "The Effect of Large Vibration Amplitude on the Fundamental Mode Shape of a Clamped-Clamped Uniform Beam," Journal of Sound and Vibration (1984) 96(3), P. 281-308.

4. Blevins, R.D., Formulas for Natural Frequency and Mode Shapes, Robert E. Kreiger Publishing Co., Malabar, Florida, 1984.

5. Chien, W.Z., and Yuan, K.Y., "On the Large Deflection of Rectangular Plates," Proceedings 9th International Congress Applied Mechanics, Brussels, Vol 6, P. 403, 1957.

6. Rudder, F.F. and Plumblee, H.E., "Sonic Fatigue Design Guide For Military Aircraft," AFFDL-TR-74-112, AD-B004-600L, AFFDL, Wright-Patterson AFB, OH, May 1975, P. 315.

TABLE 1
ALUMINUM BEAM MODAL FREQUENCIES
405 X 20 X 2 mm

$$\omega_n = \frac{\lambda n^2}{L^2}\sqrt{\frac{EI}{\rho}} \quad (Ref\ 4)$$

	Theoretical* C-C Hz	Theoretical* S-S Hz	FEM** C-C Hz	FEM** S-S Hz	Test** Sine Hz	FEM*** C-C Hz	Test*** C-C Random Hz	
$\lambda_1 = 4.73$	$f_1 = 70.8$	31.2	99.4	70.3	85	64.7	67	65
$\lambda_2 = 7.853$	$f_2 = 195.2$				205			
$\lambda_3 = 10.10$	$f_3 = 382.6$	281	431	339	380	352	350	348
$\lambda_4 = 14.14$	$f_4 = 632.8$				612			
$\lambda_5 = 17.28$	$f_5 = 944.9$	781	1000	842	898	865		

* no preload, no coil mass
** 100 microstrain preload, no coil mass
***100 microstrain preload in tension, 26.4g coil attached @ center

More than 3 beam thickness - consider Poisonn's effect which increases frequencies 4.8%

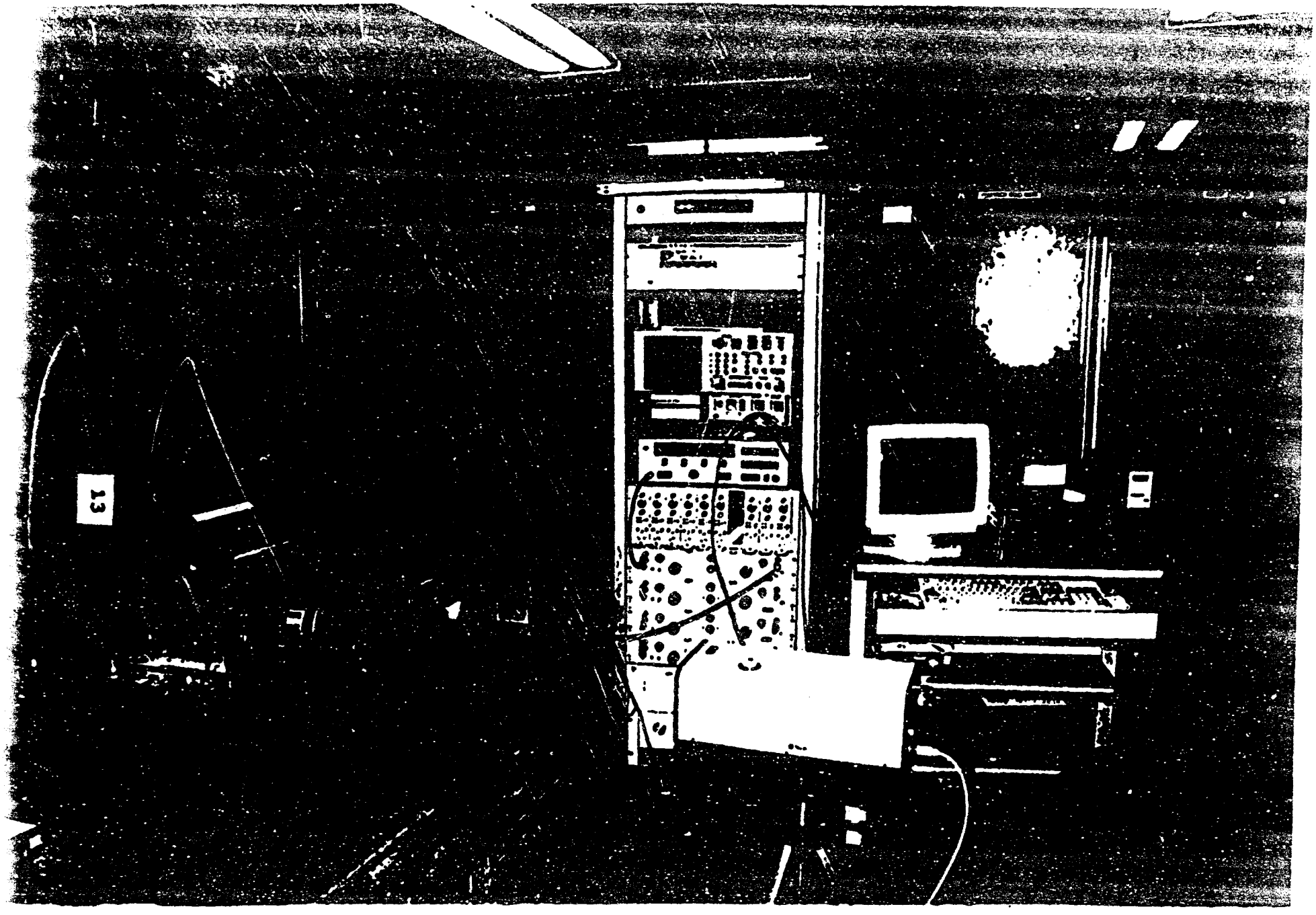

FIGURE 1 BEAM TEST RIG, CLAMPED-CLAMPED (C-C) FIBER REINFORCED PLASTIC (CFRP) BEAM

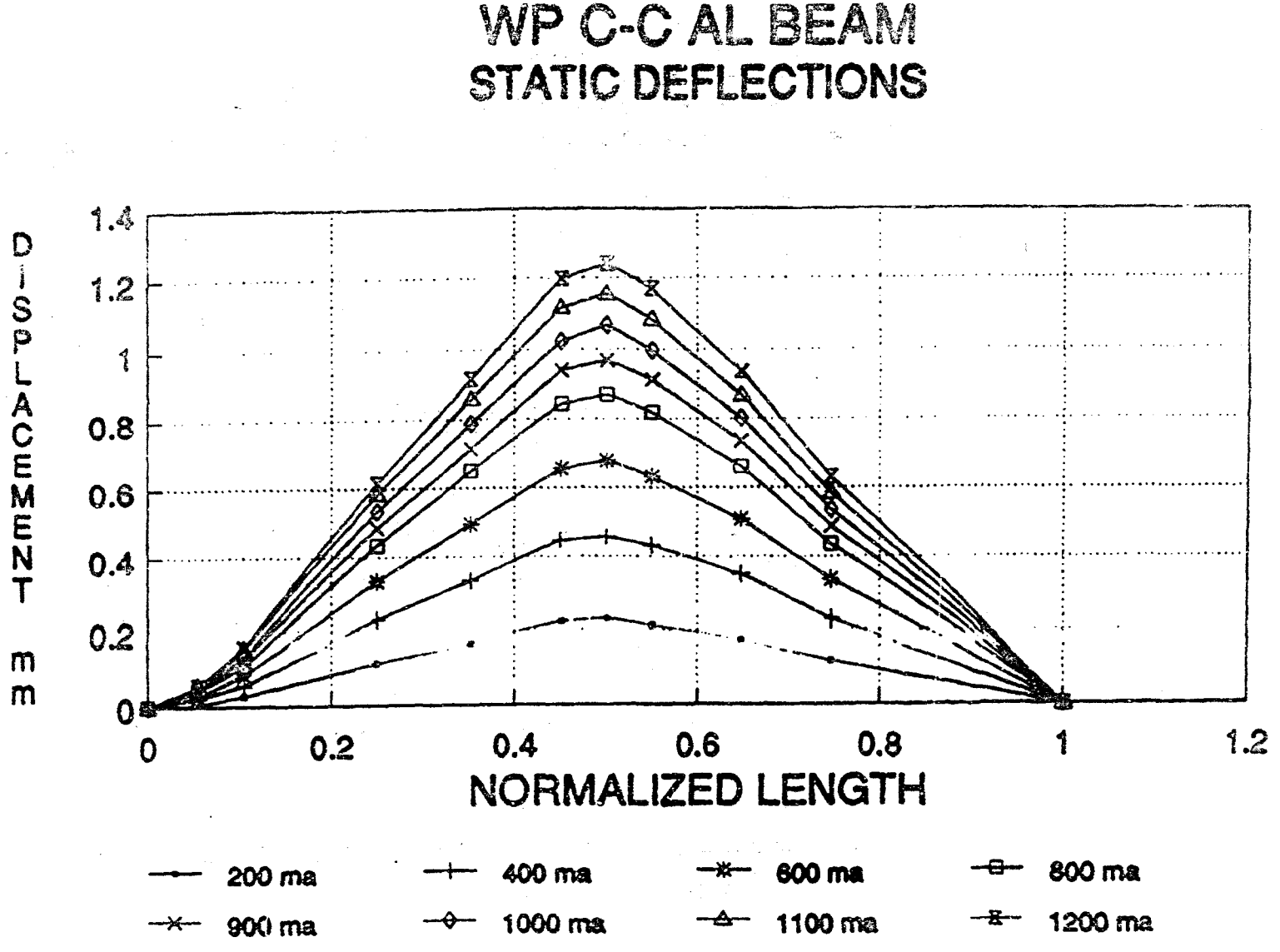

HW64 23JUL92

FIGURE

WP C-C AL BEAM
STATIC DEFLECTIONS

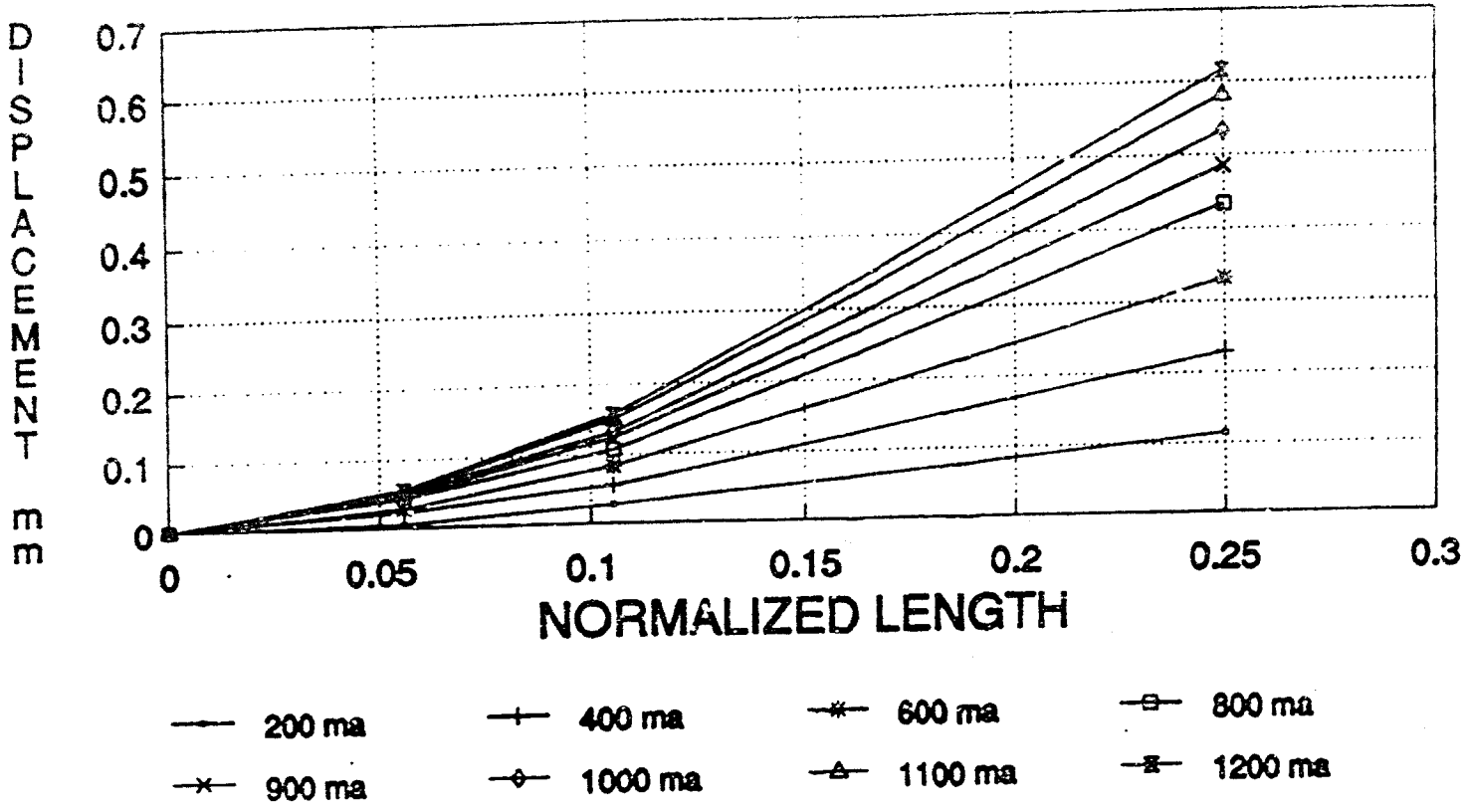

HW65 23JUL92

FIGURE 3 STATIC DEFLECTION SHAPES, EDGE EFFECTS, C-C ALUMINUM BEAM

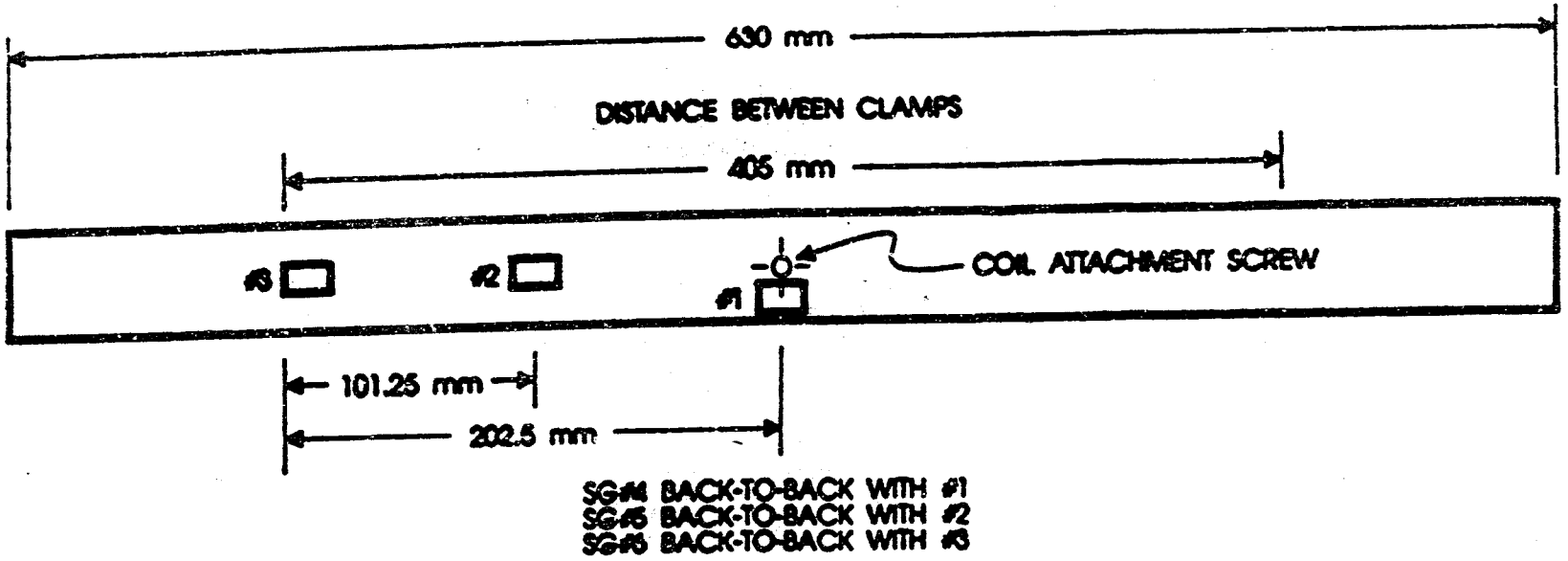

FIGURE 4 STRAIN GAUGE LOCATIONS, ALUMINUM BEAM

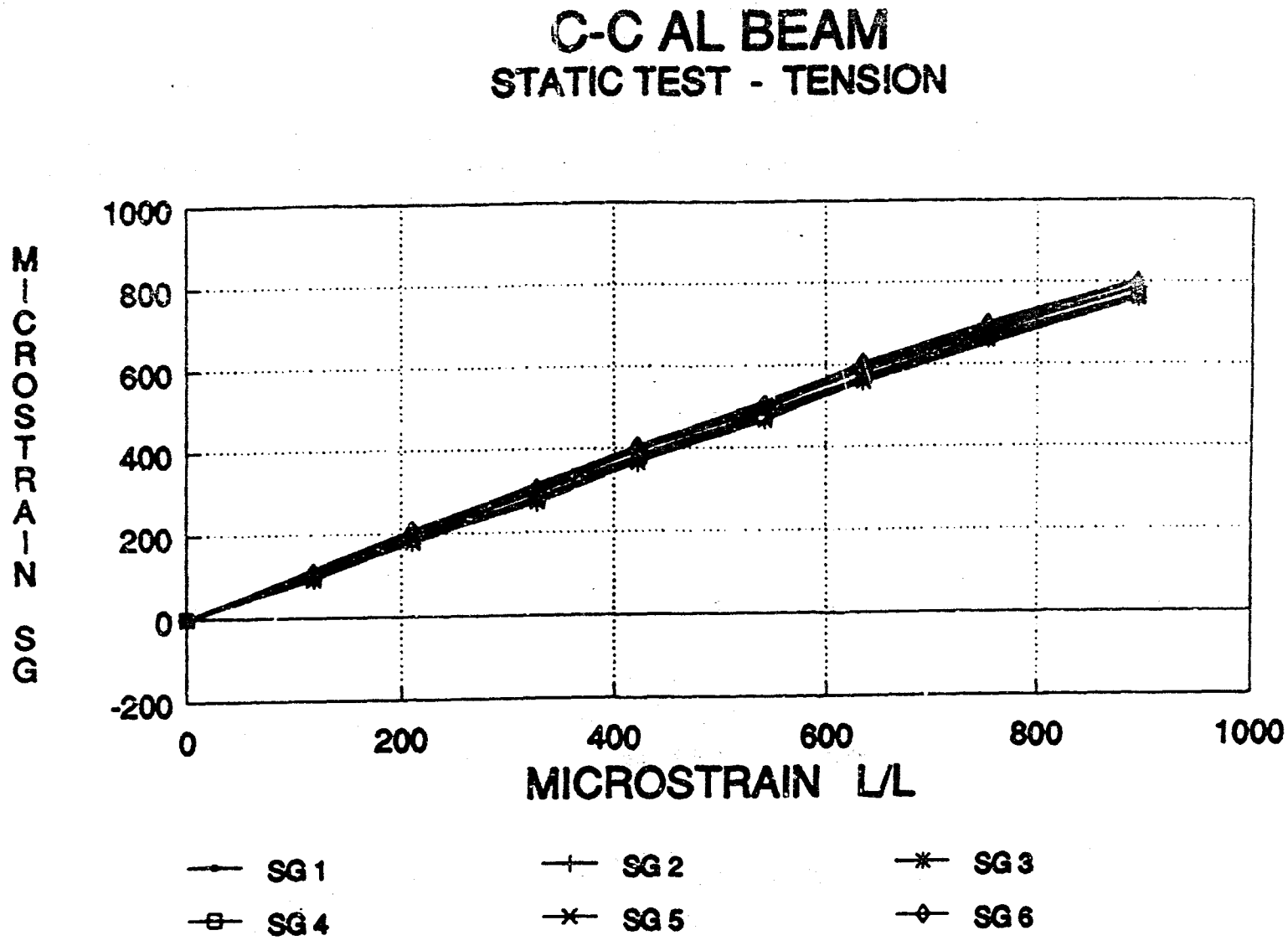

HW103A 425mm 3DEC92

FIGURE 5 STATIC TENSION TEST, CLAMPING BLOCK 20mm FROM SG 3&6, C-C ALUMINUM BEAM

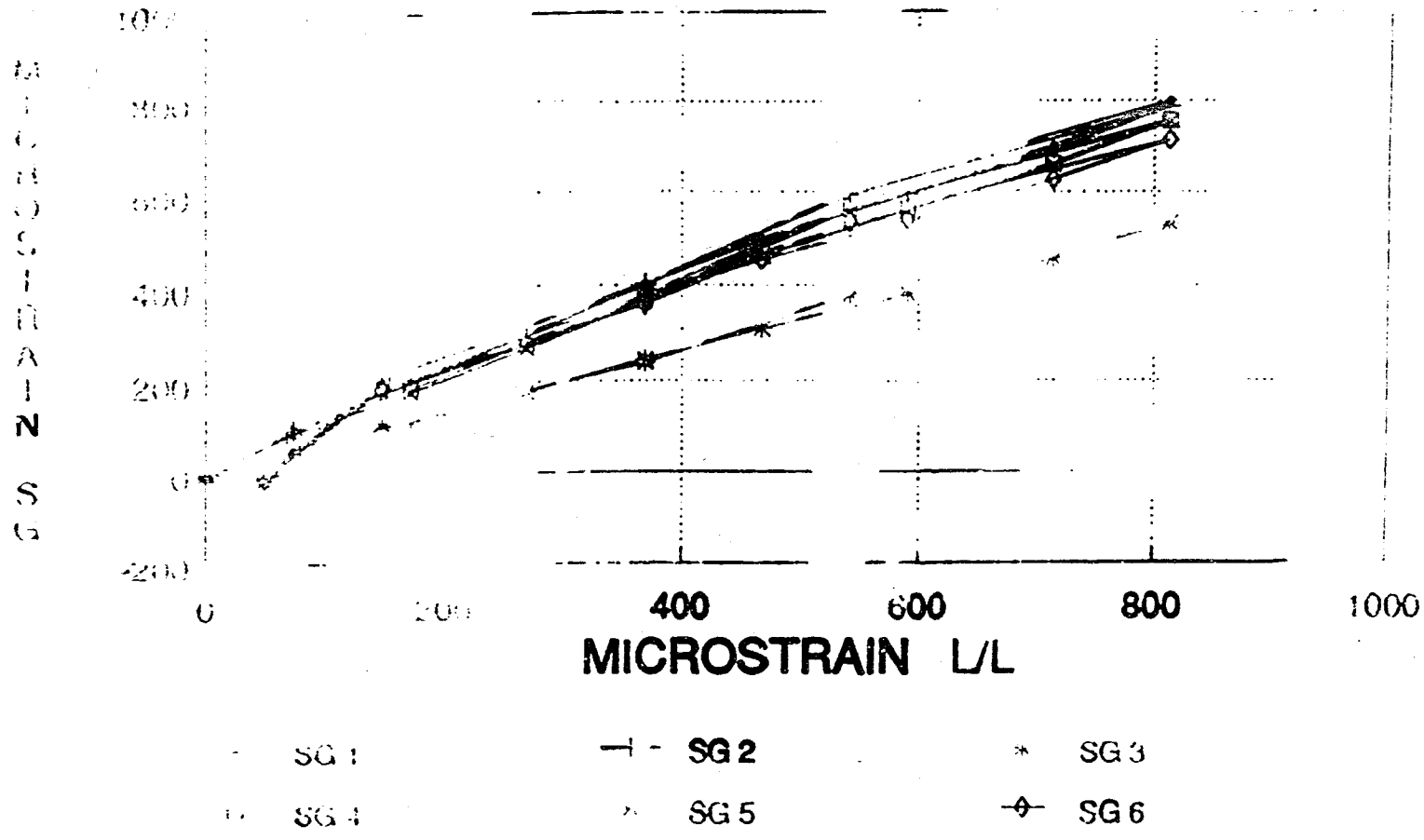

HW:03 406mm 3DEC92

FIGURE 6 STATIC TENSION TEST, CLAMPING BLOCK 1mm FROM SG 3&6, C-C ALUMINUM BEAM

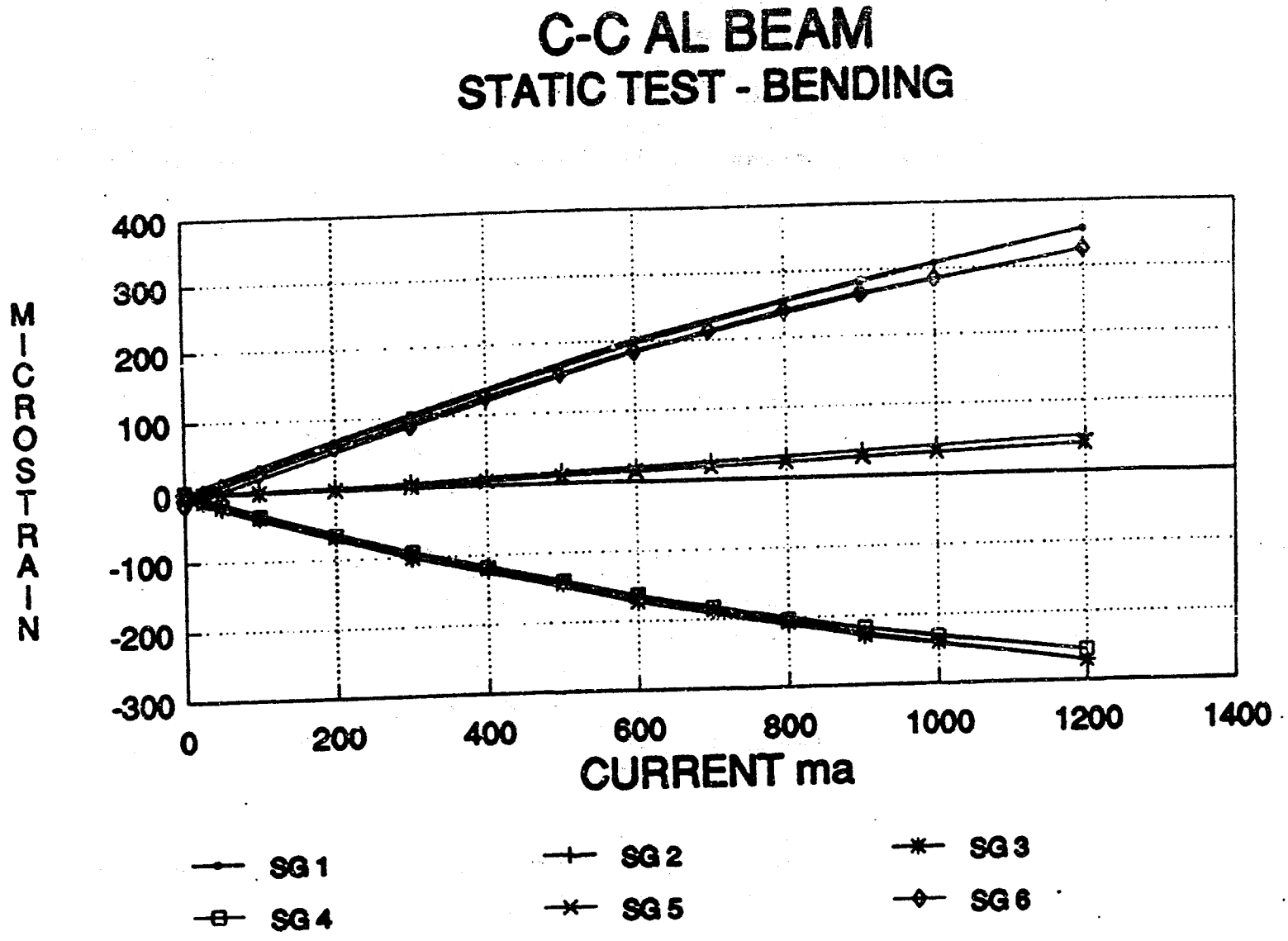

FIGURE 7 STATIC BENDING TEST, C-C ALUMINUM BEAM

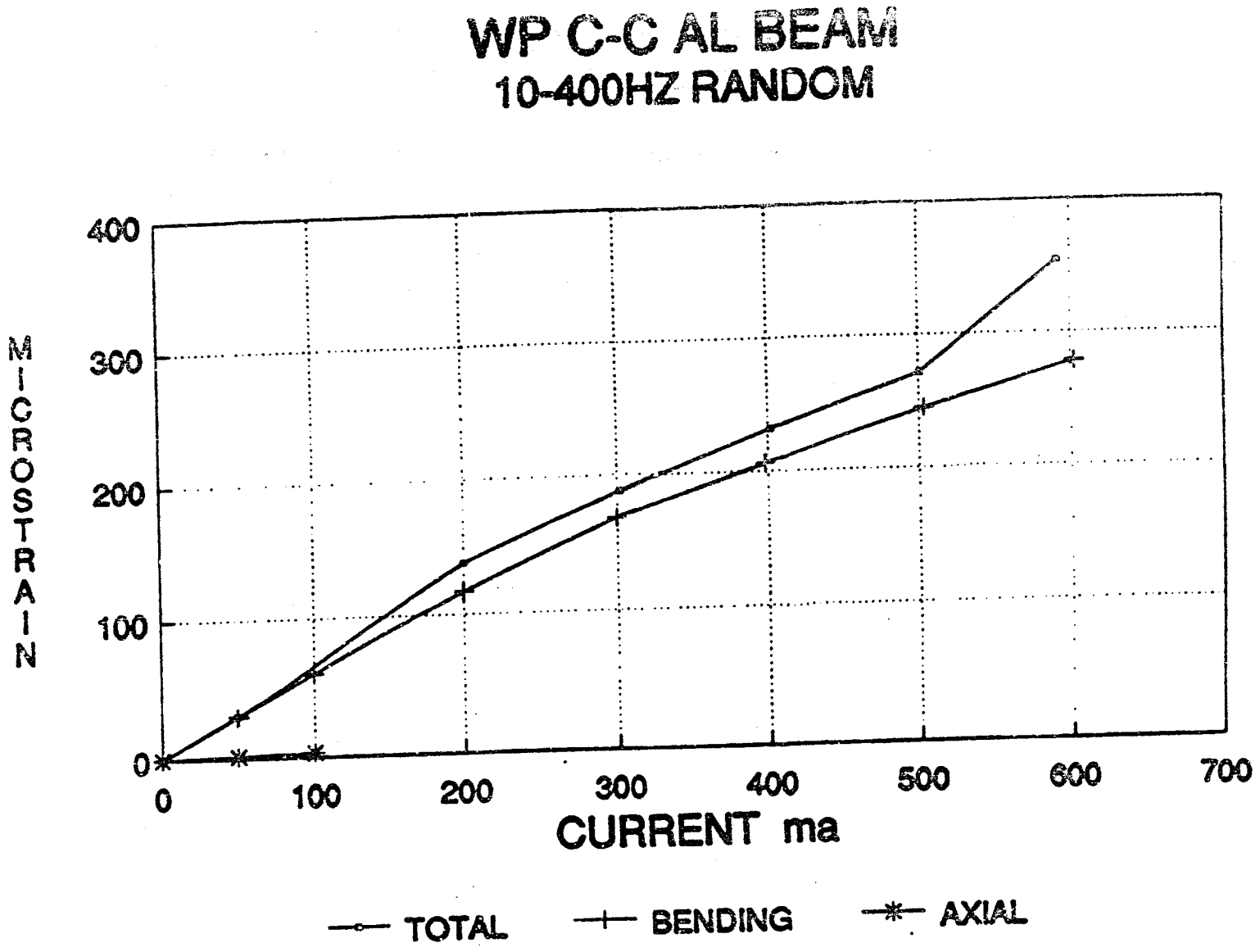

FIGURE 8 TOTAL, BENDING AND AXIAL STRAINS, 10-400 HZ RANDOM, C-C ALUMINUM BEAM

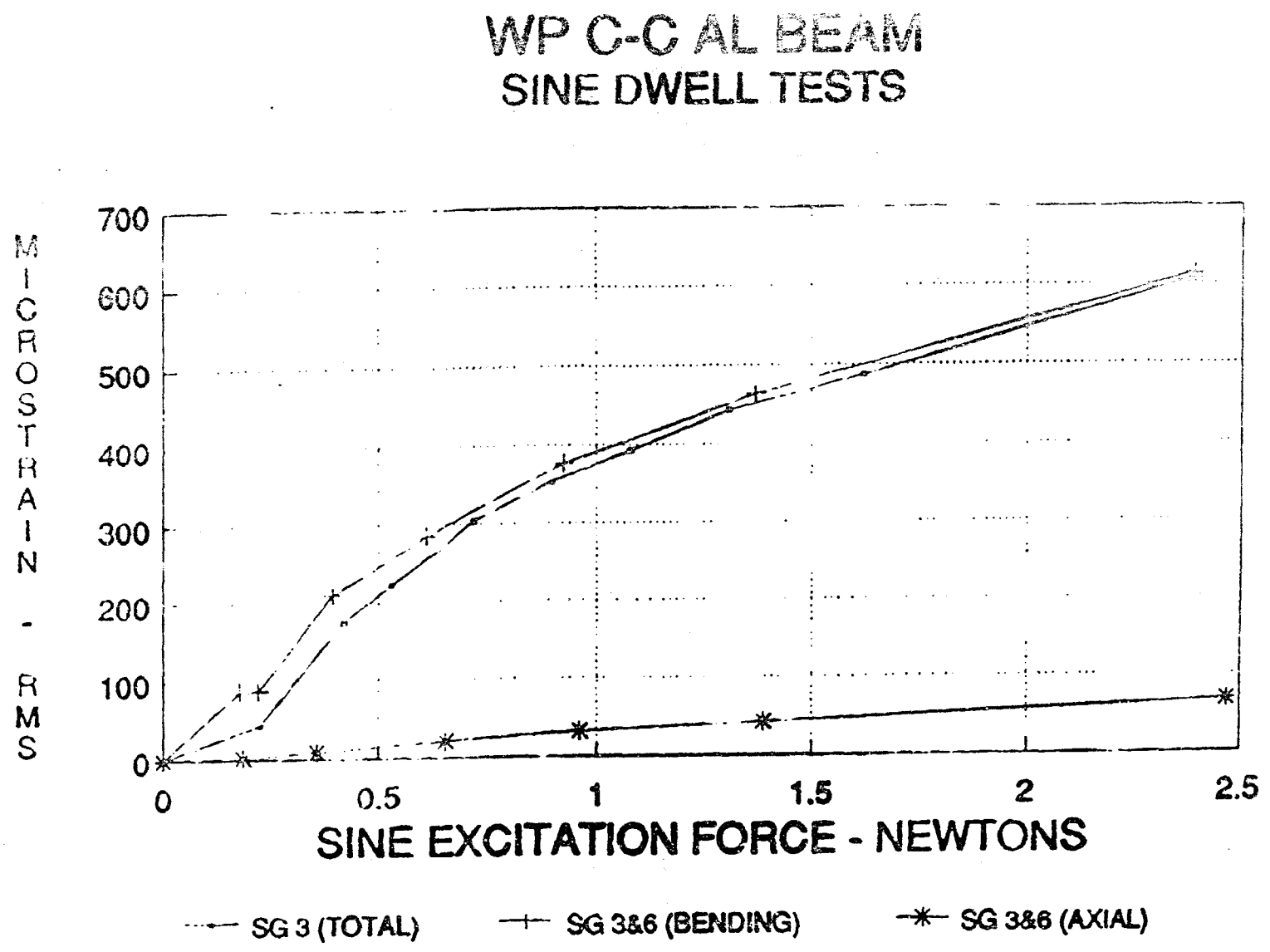

HW 2 29SEP92

FIGURE 9 TOTAL, BENDING AND AXIAL STRAINS, SINE DWELL, C-C ALUMINUM BEAM

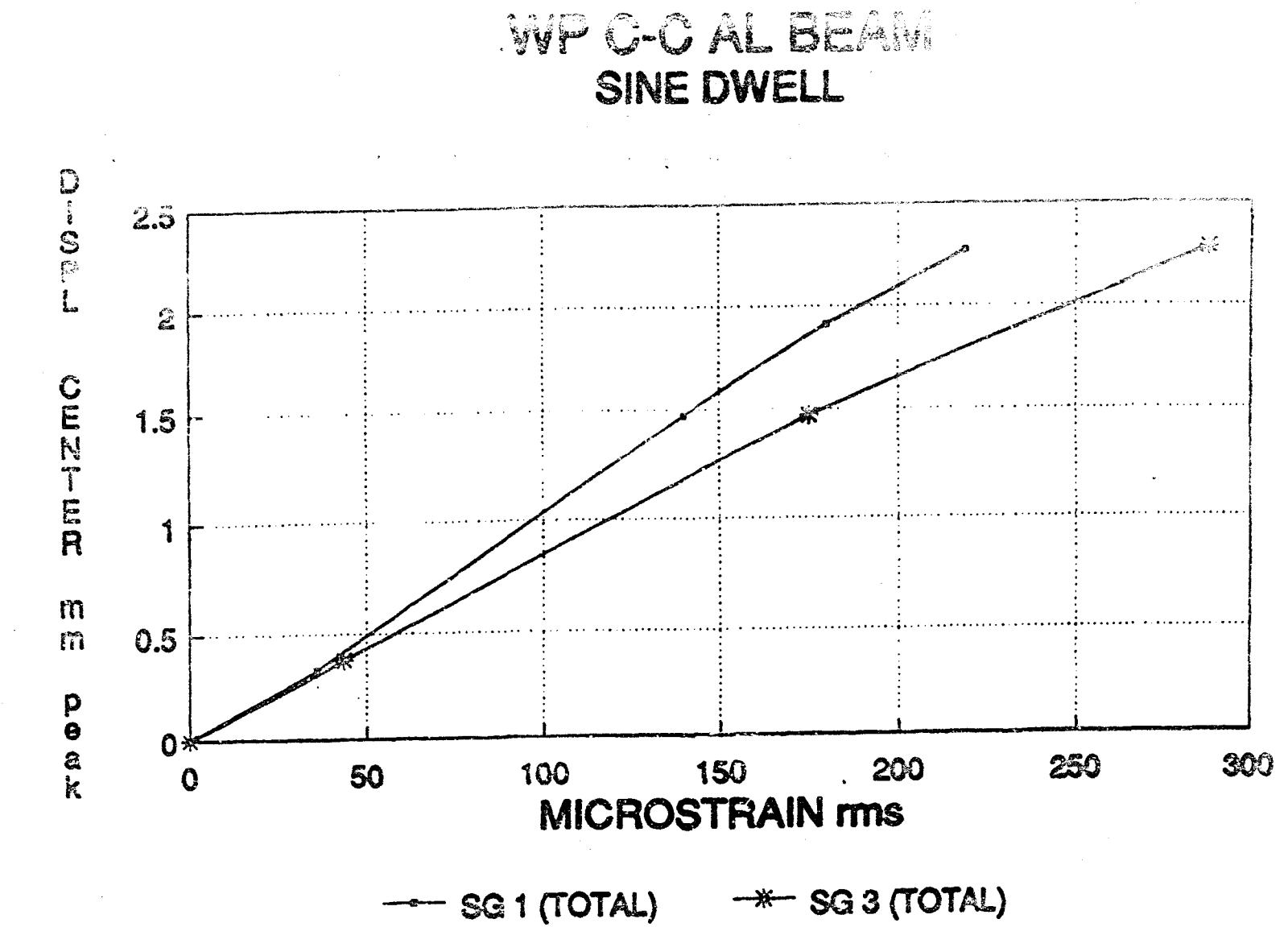

FIGURE 10 STRAIN VS DISPLACEMENT, SINE DWELL, C-C ALUMINUM BEAM

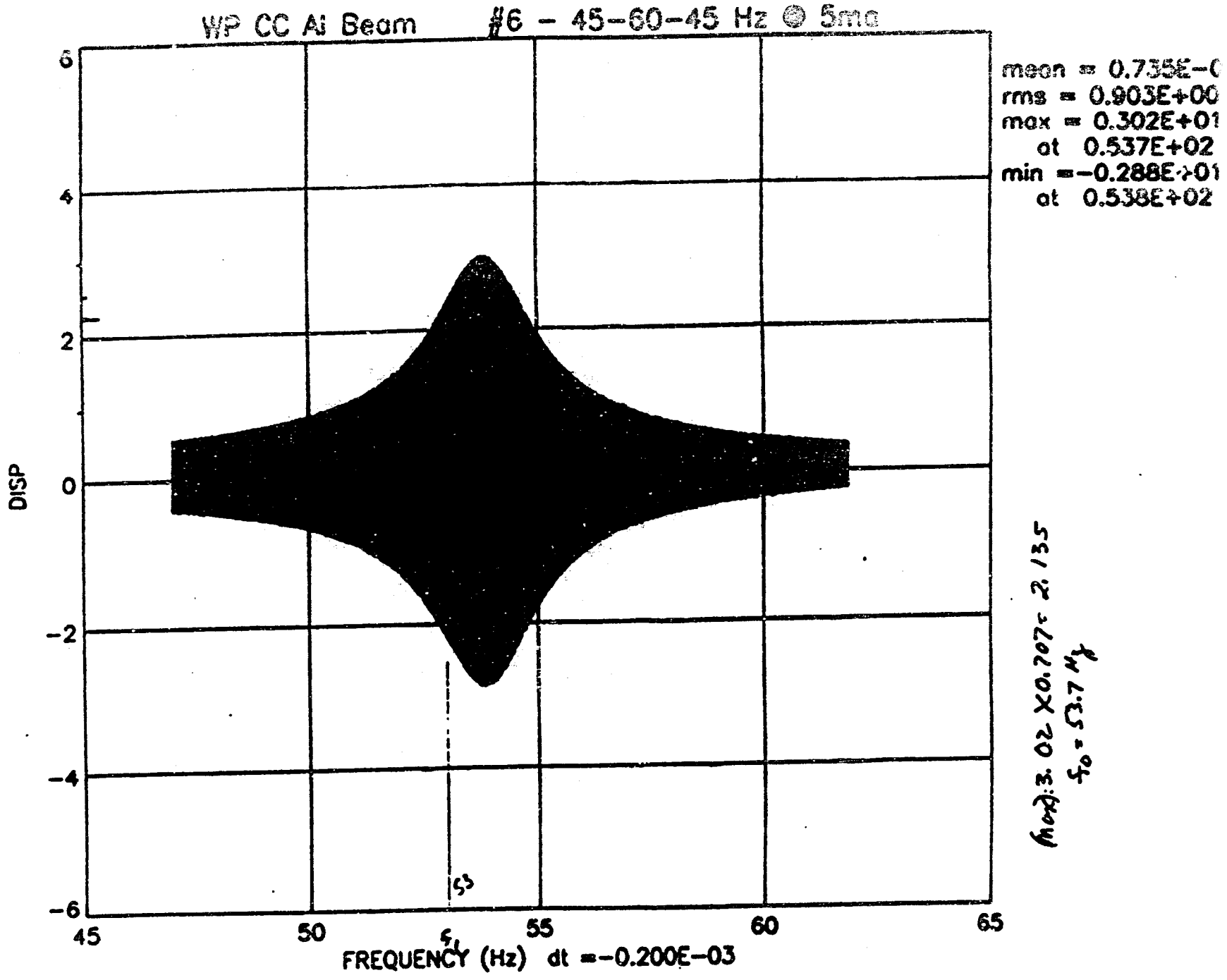

FIGURE 11 SLOW FREQUENCY SWEEP, C-C ALUMINUM BEAM

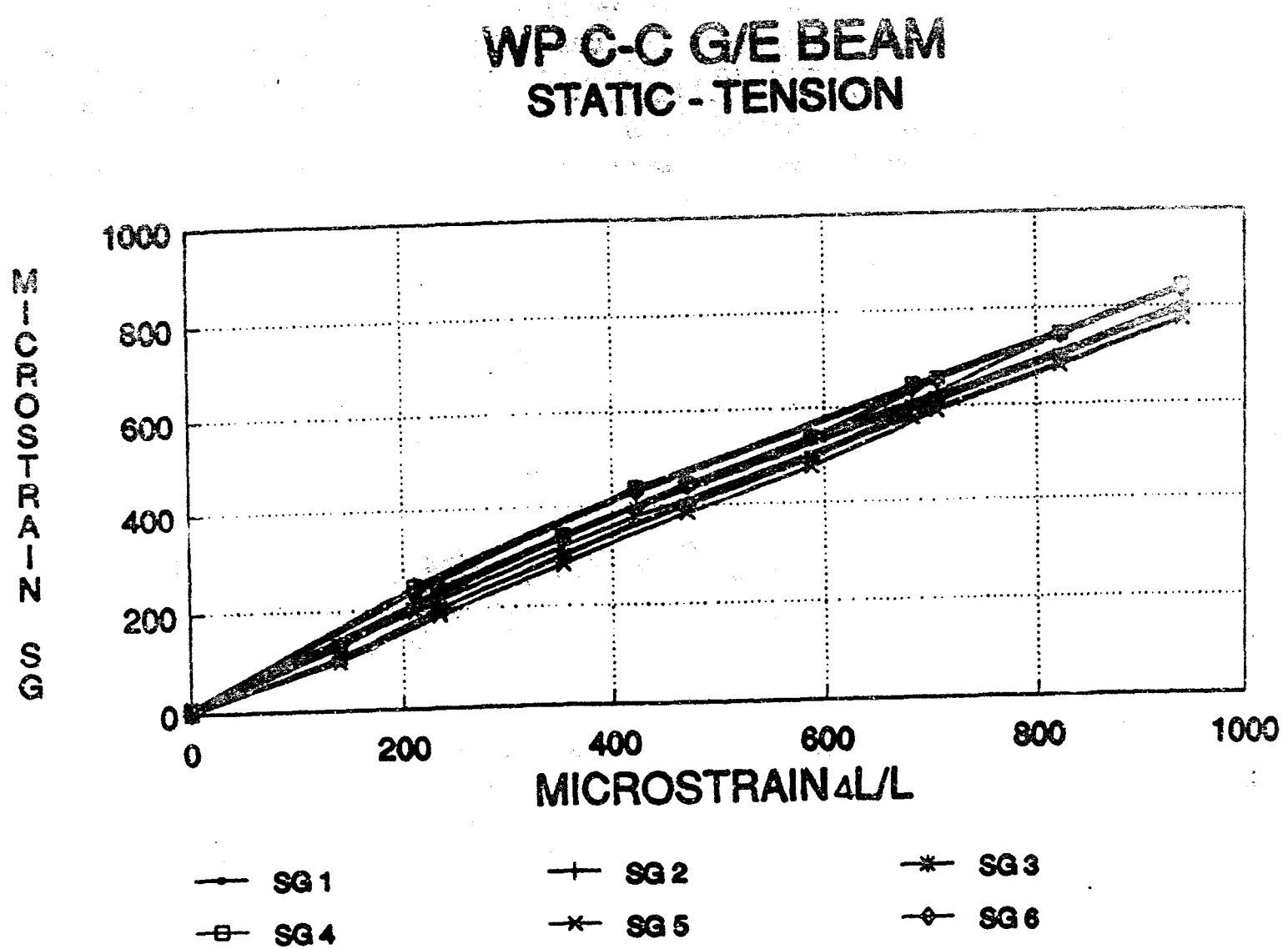

FIGURE 12 STATIC TENSION TEST, CLAMPING BLOCK 20mm FROM SG 3&6, C-C CFRP BEAM

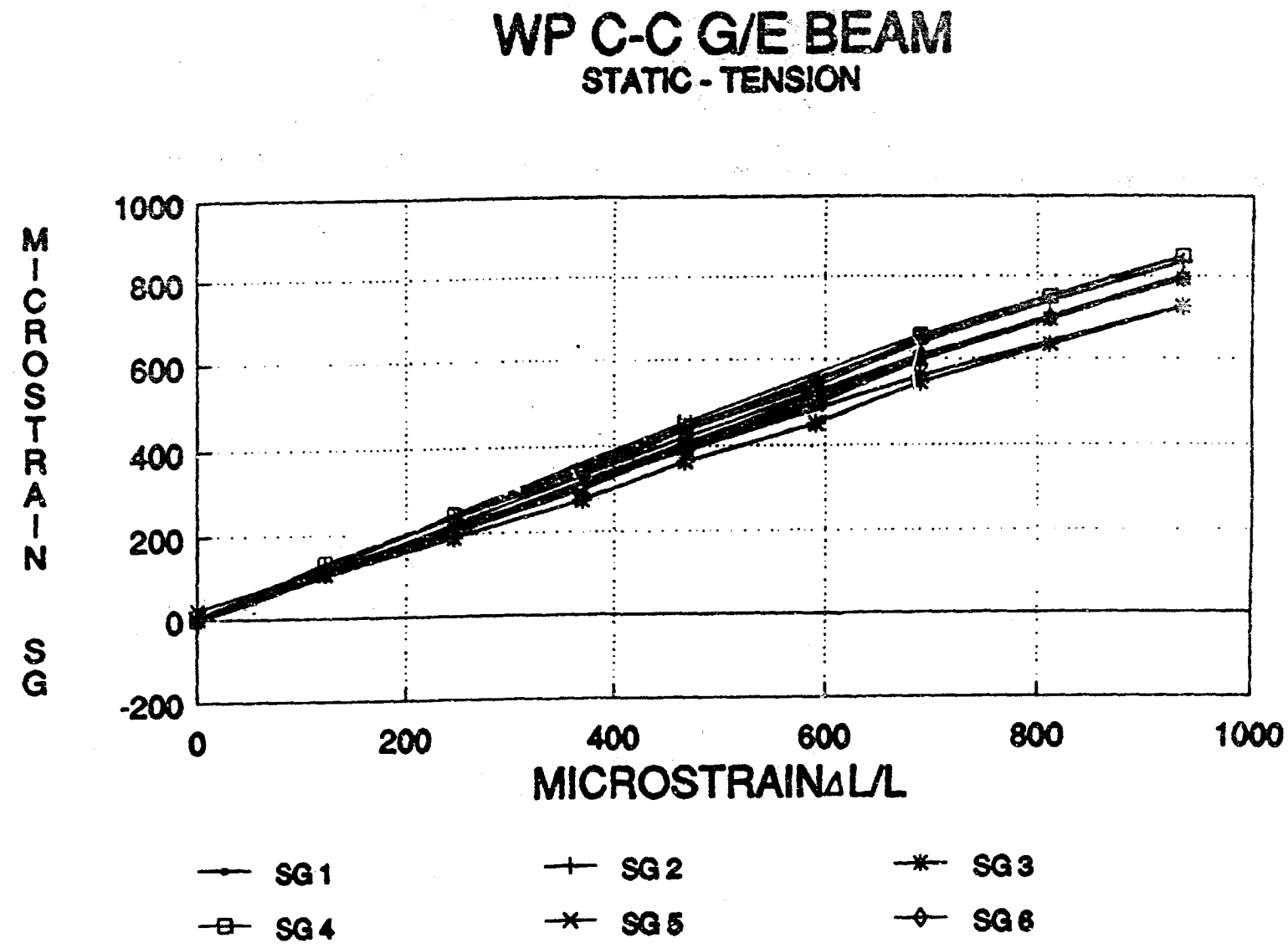

HW107 406mm 15DEC92

FIGURE 13 STATIC TENSION TEST, CLAMPING BLOCK 1mm FROM SG 3&6, CFRP BEAM

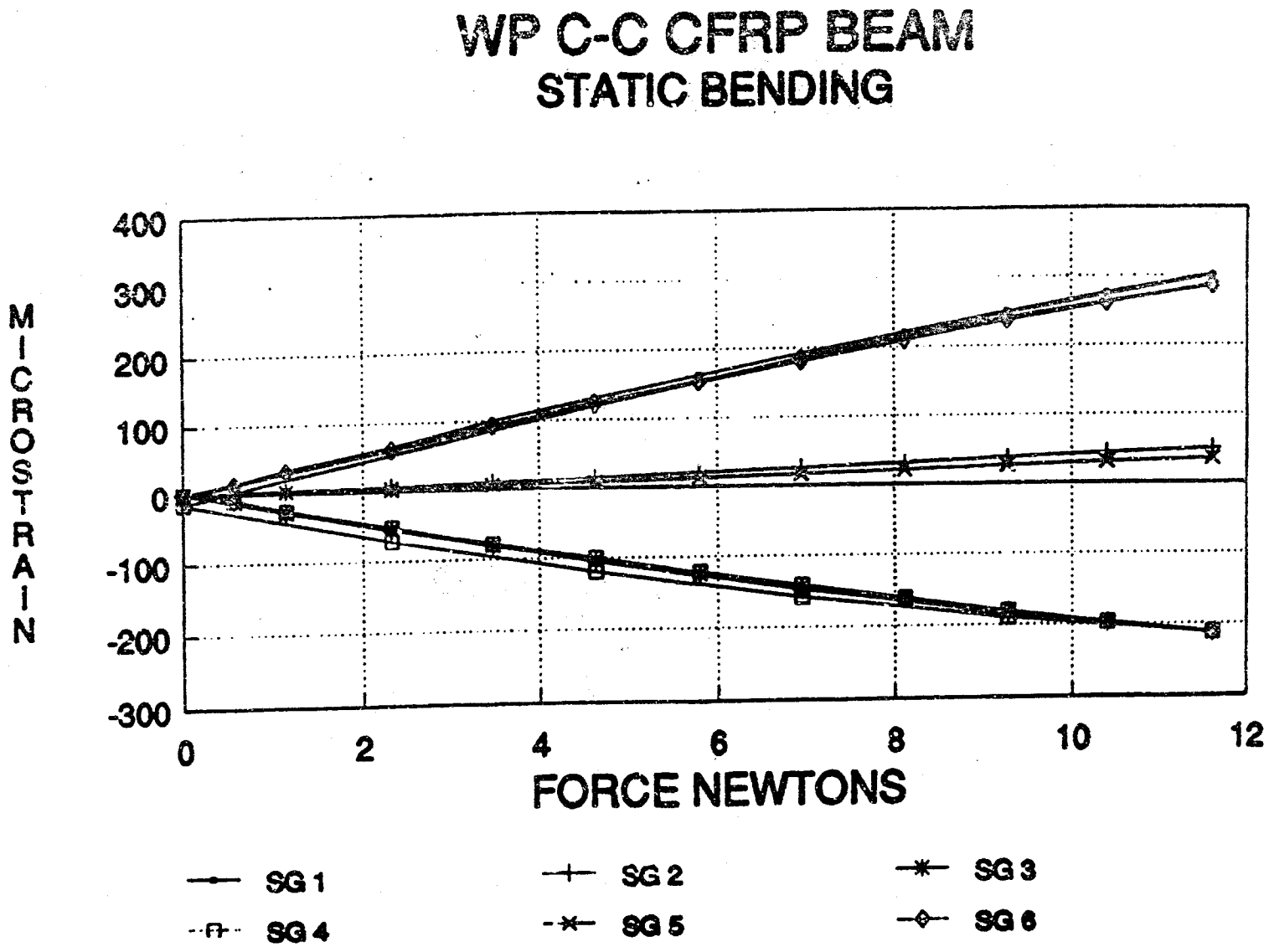

FIGURE 14 STATIC BENDING TEST, C-C CFRP BEAM

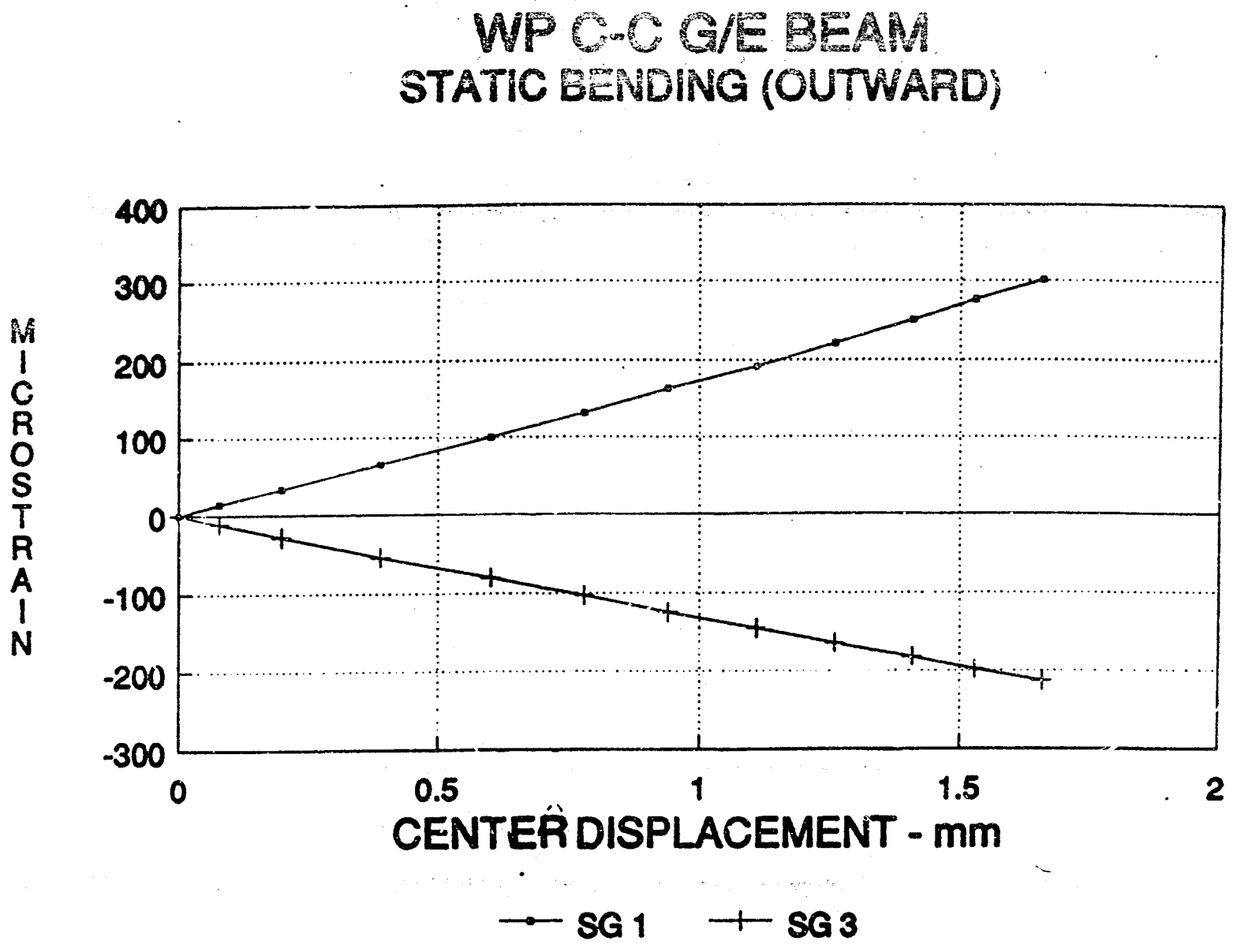

FIGURE 15 STATIC DISPLACEMENT VS STRAIN, C-C CFRP BEAM

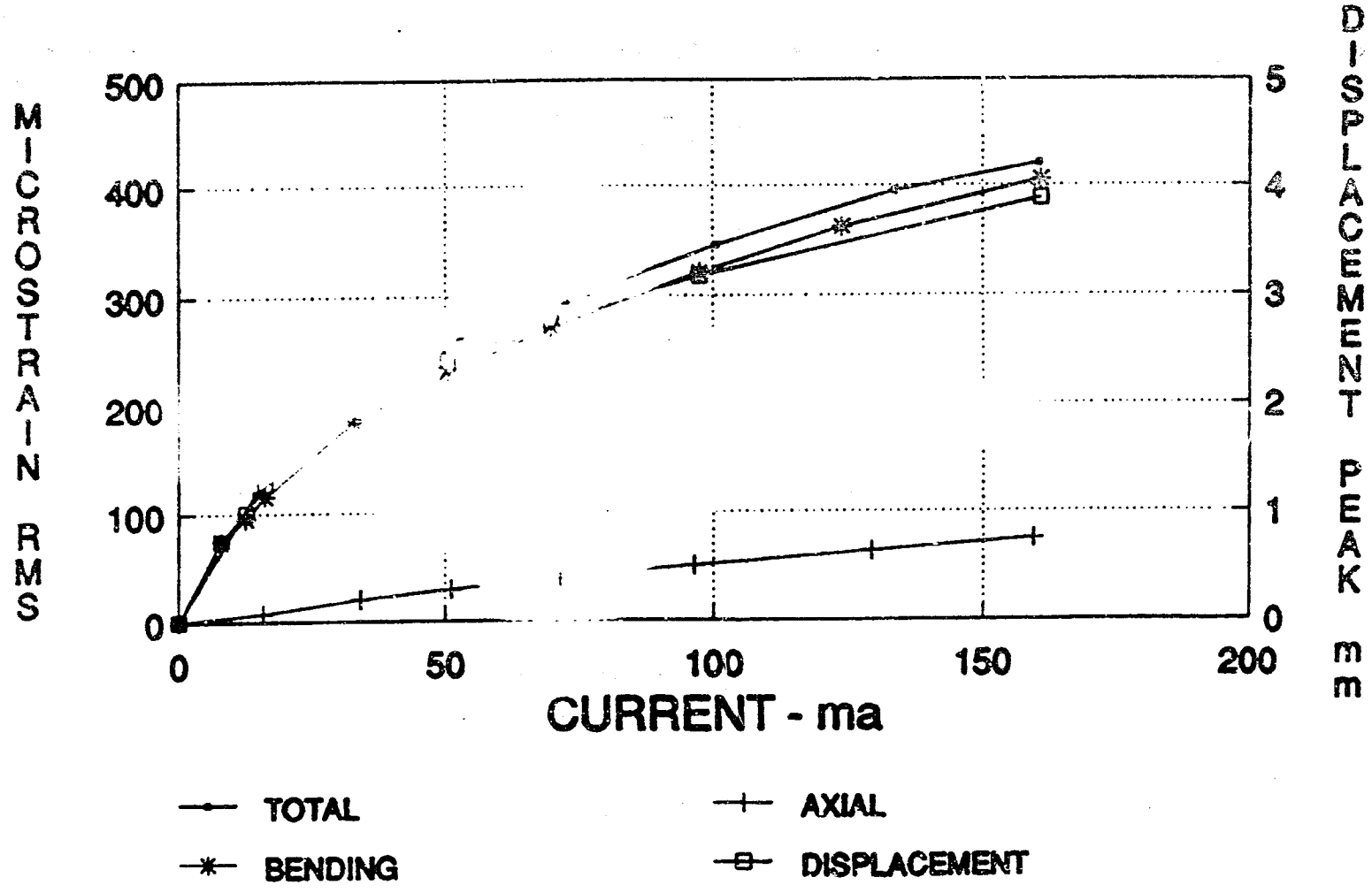

HW111AA 406mm 24DEC92

FIGURE

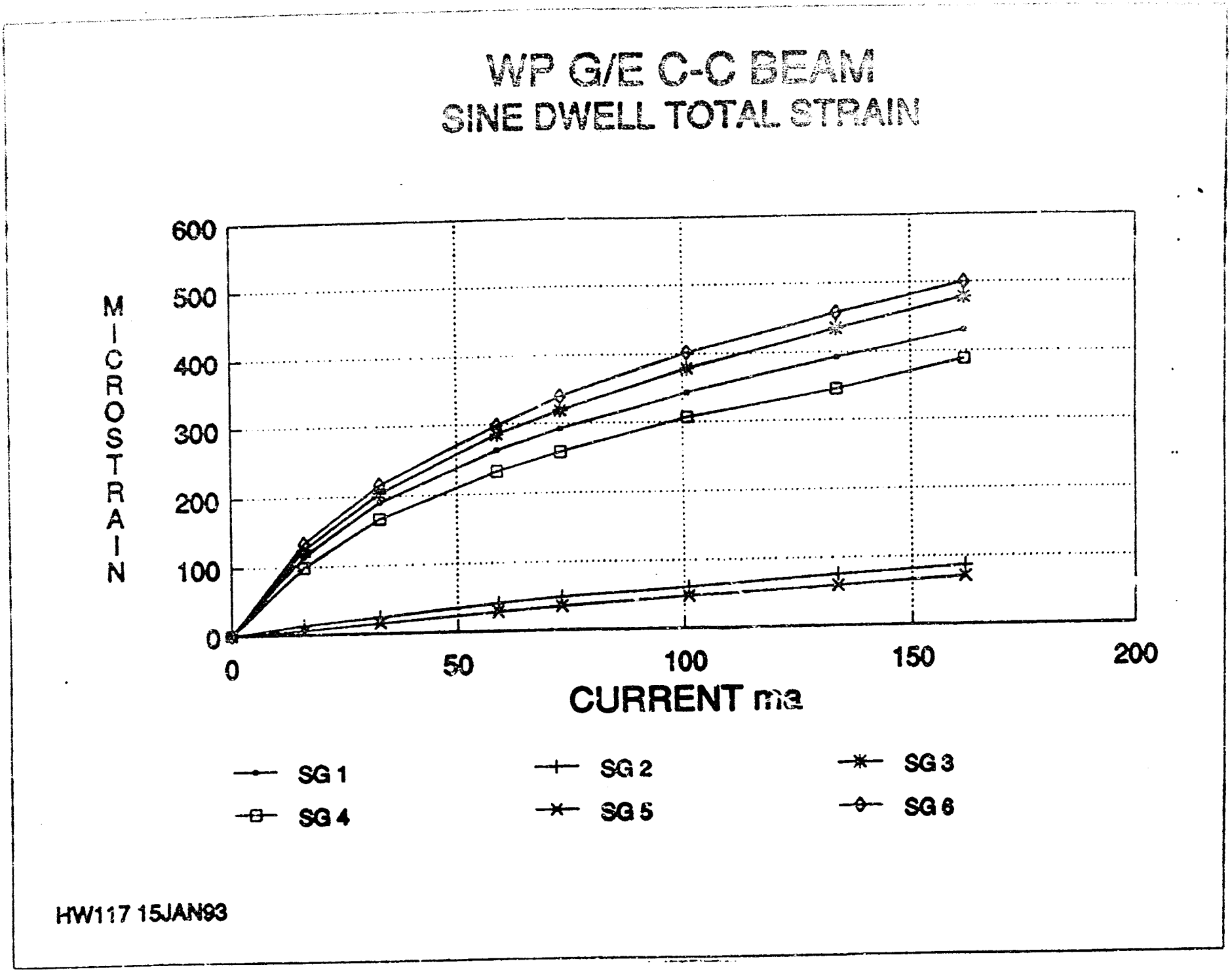

FIGURE 17 CURRENT VS TOTAL STRAIN, SINE DWELL, CFRP BEAM

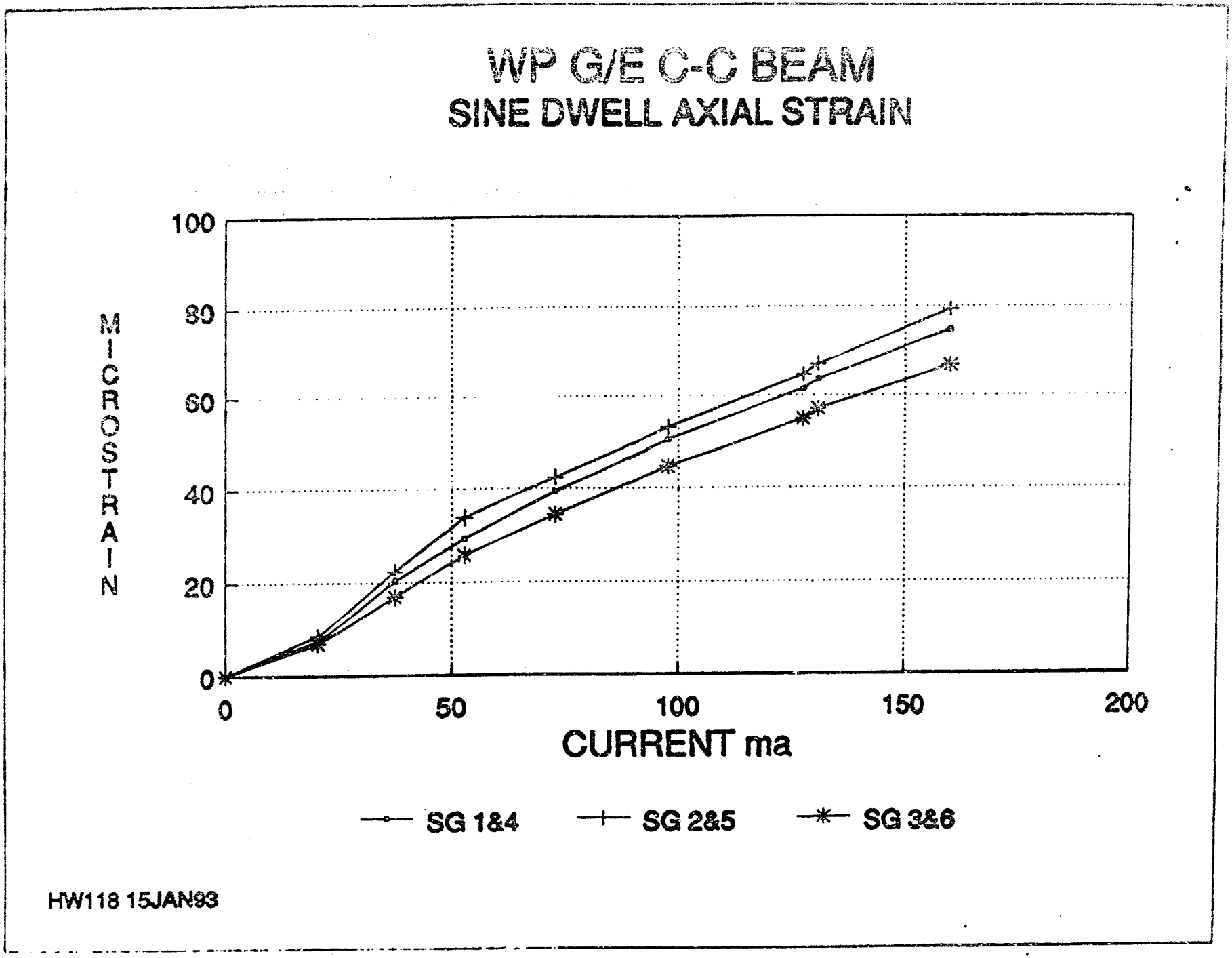

FIGURE 18 CURRENT VS AXIAL STRAIN, SINE DWELL, CFRP BEAM

WP C-C G/E BEAM

DISPL VS STRAIN SINE DWELL

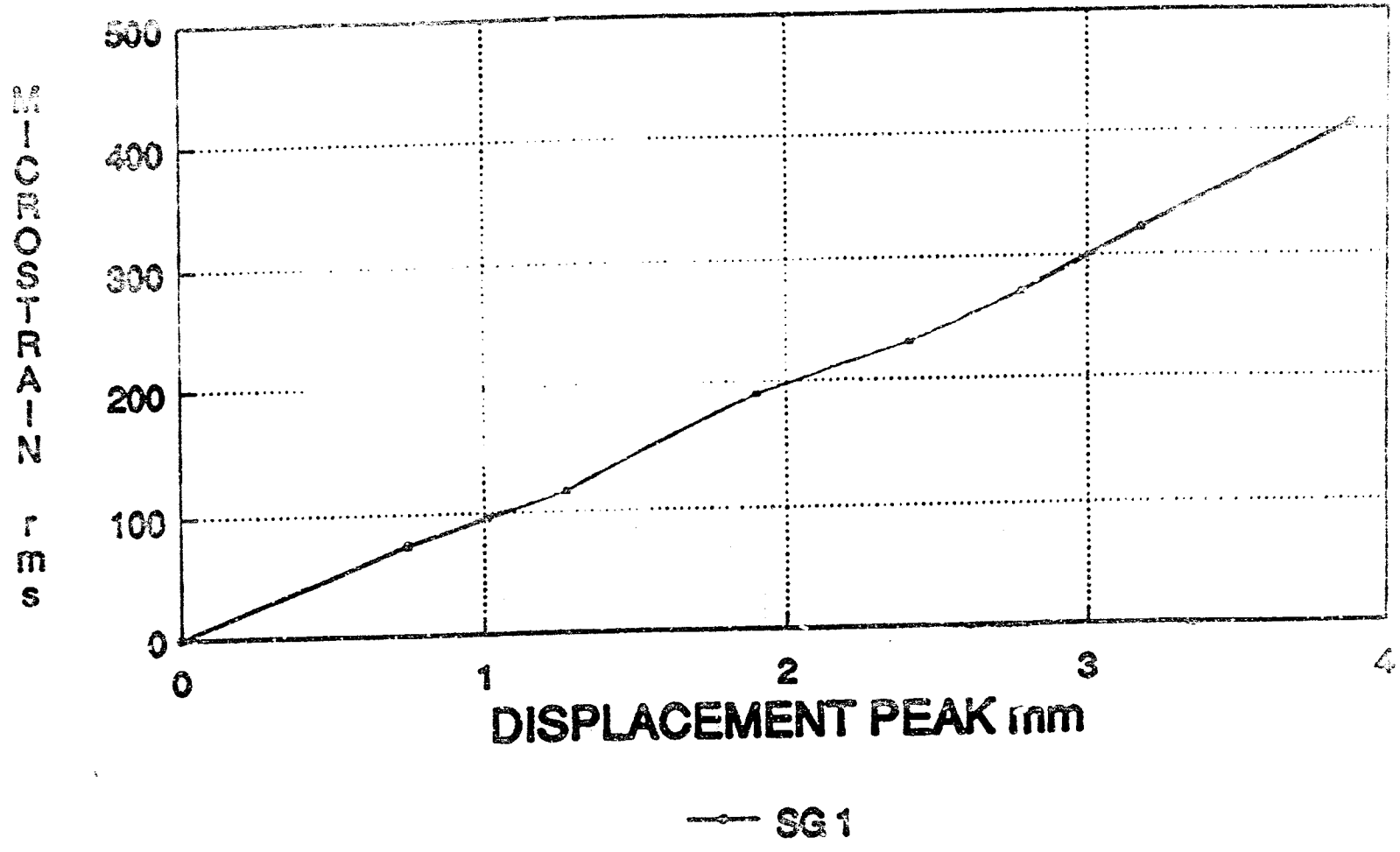

HW115 406mm 24DEC82

FIGURE

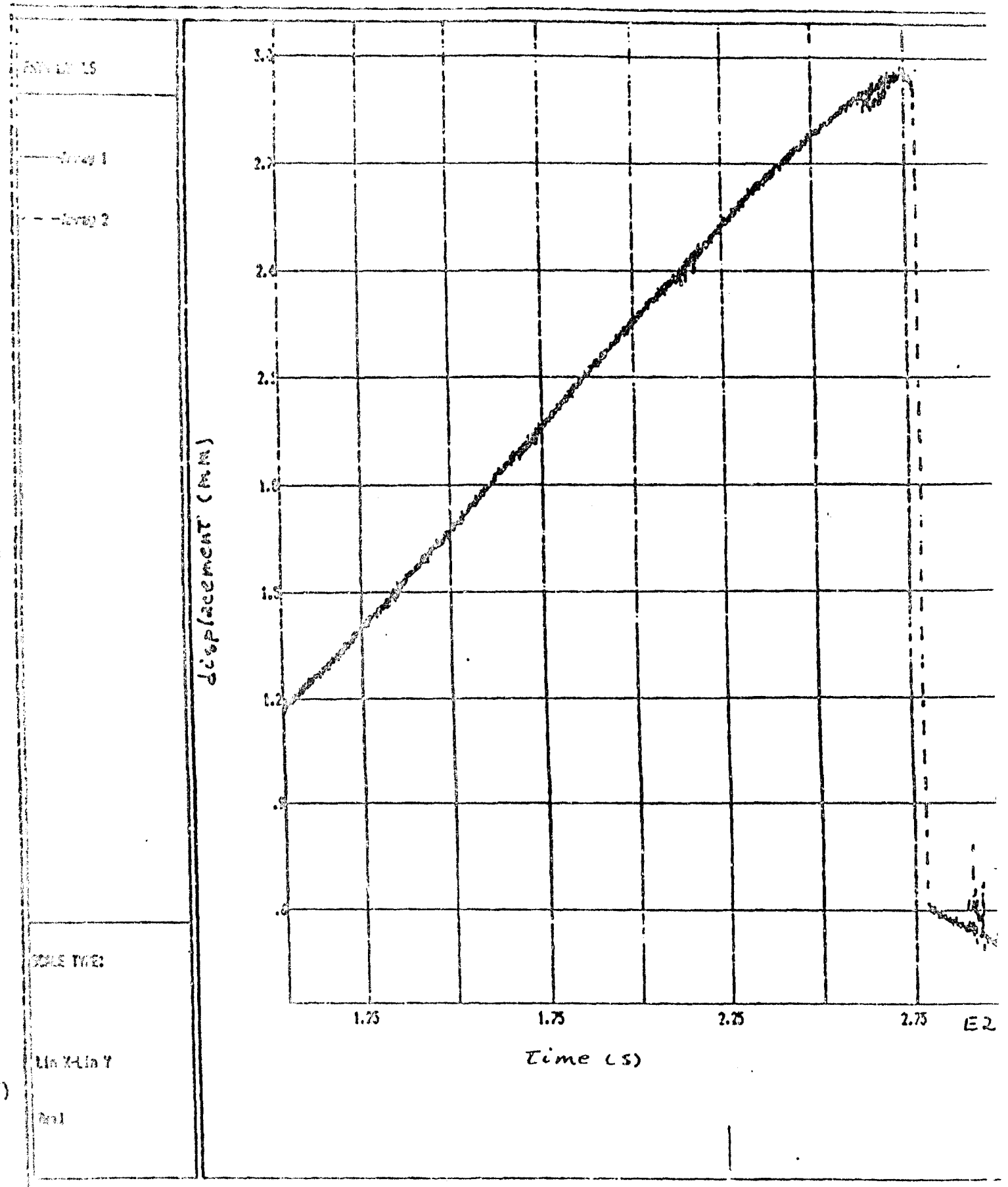

FIGURE 20 FREQUENCY SWEEP, JUMP EFFECT OF FIRST MODE, C-C CFRP BEAM

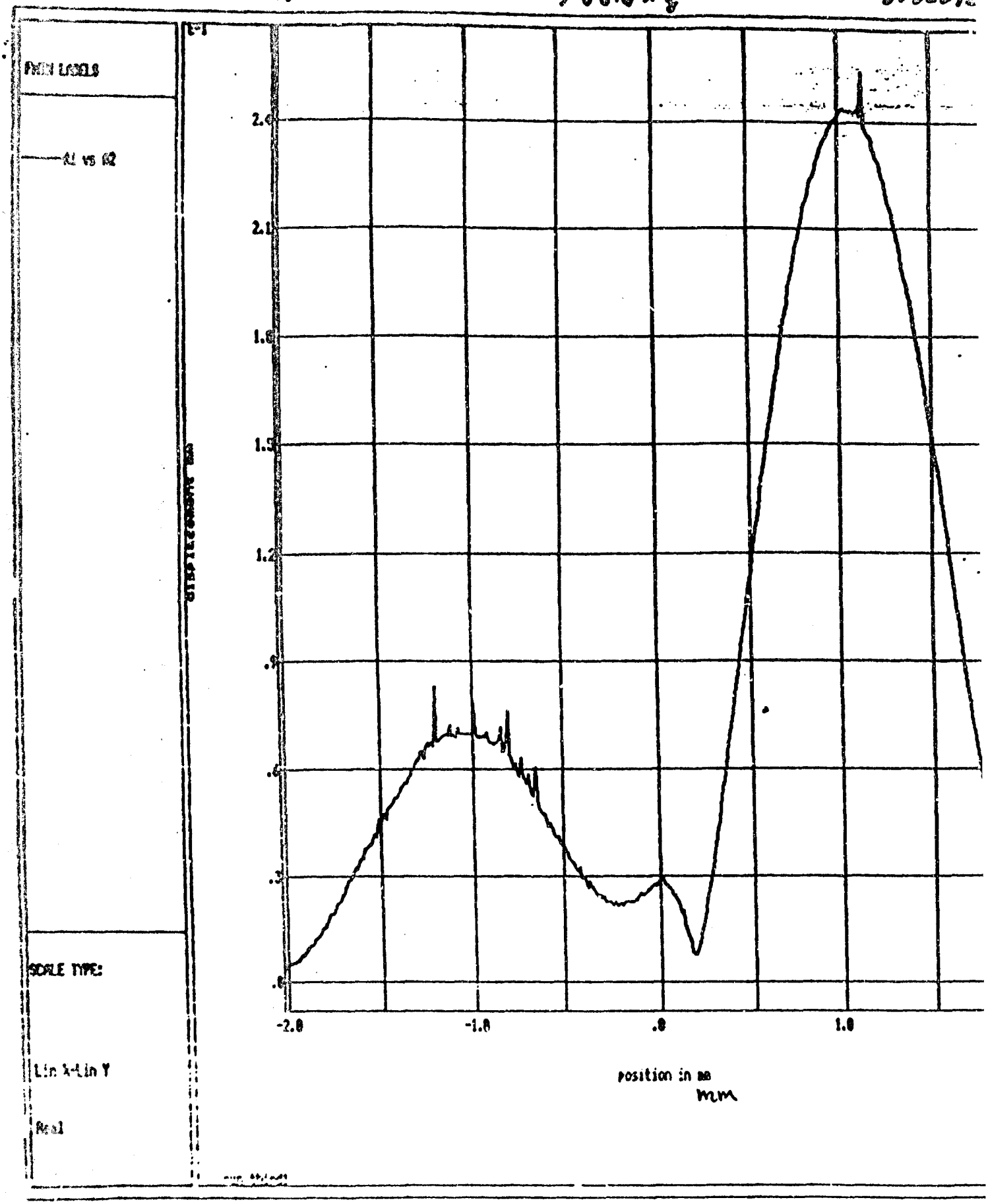

FIGURE 21 DISTORTED DISPLACEMENT SHAPE, THIRD MODE, 388.6 HZ CFRP BEAM

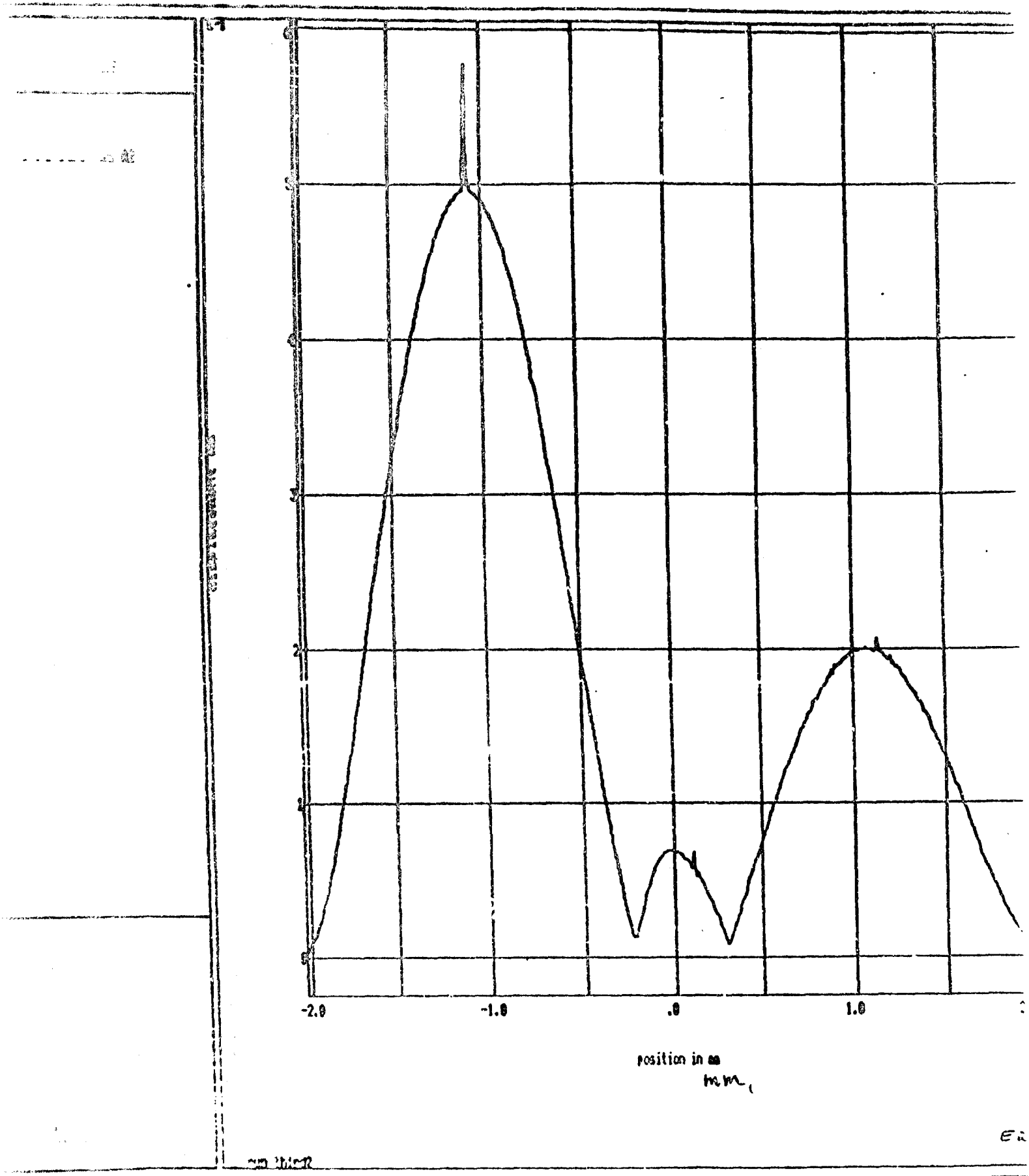

FIGURE 22 DISTORTED DISPLACEMENT SHAPE, THIRD MODE, 406.7 HZ, CFRP BEAM

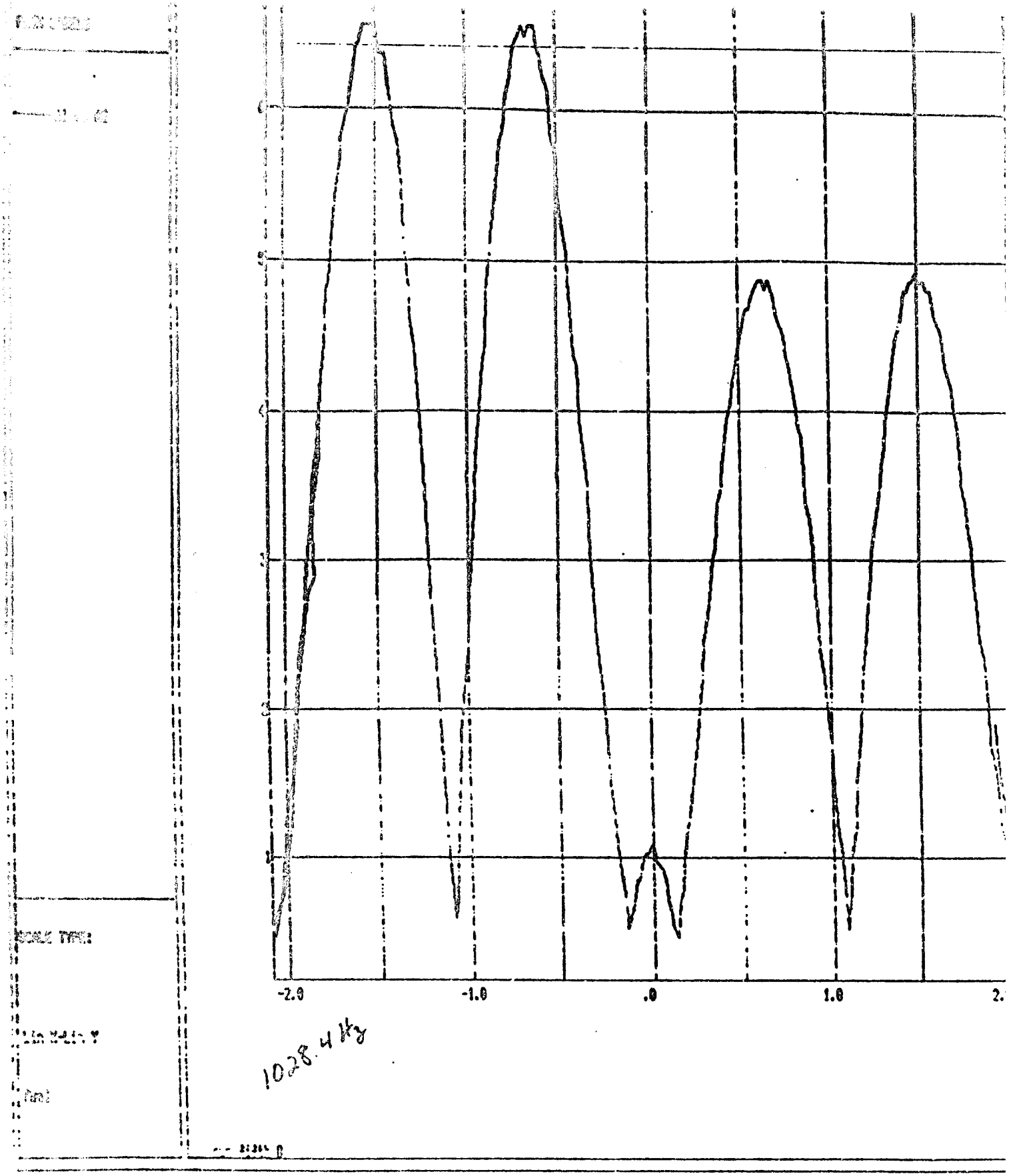

FIGURE 23 DISTORTED DISPLACEMENT SHAPE, FIFTH MODE, 1028.4 HZ, CFRP BEAM

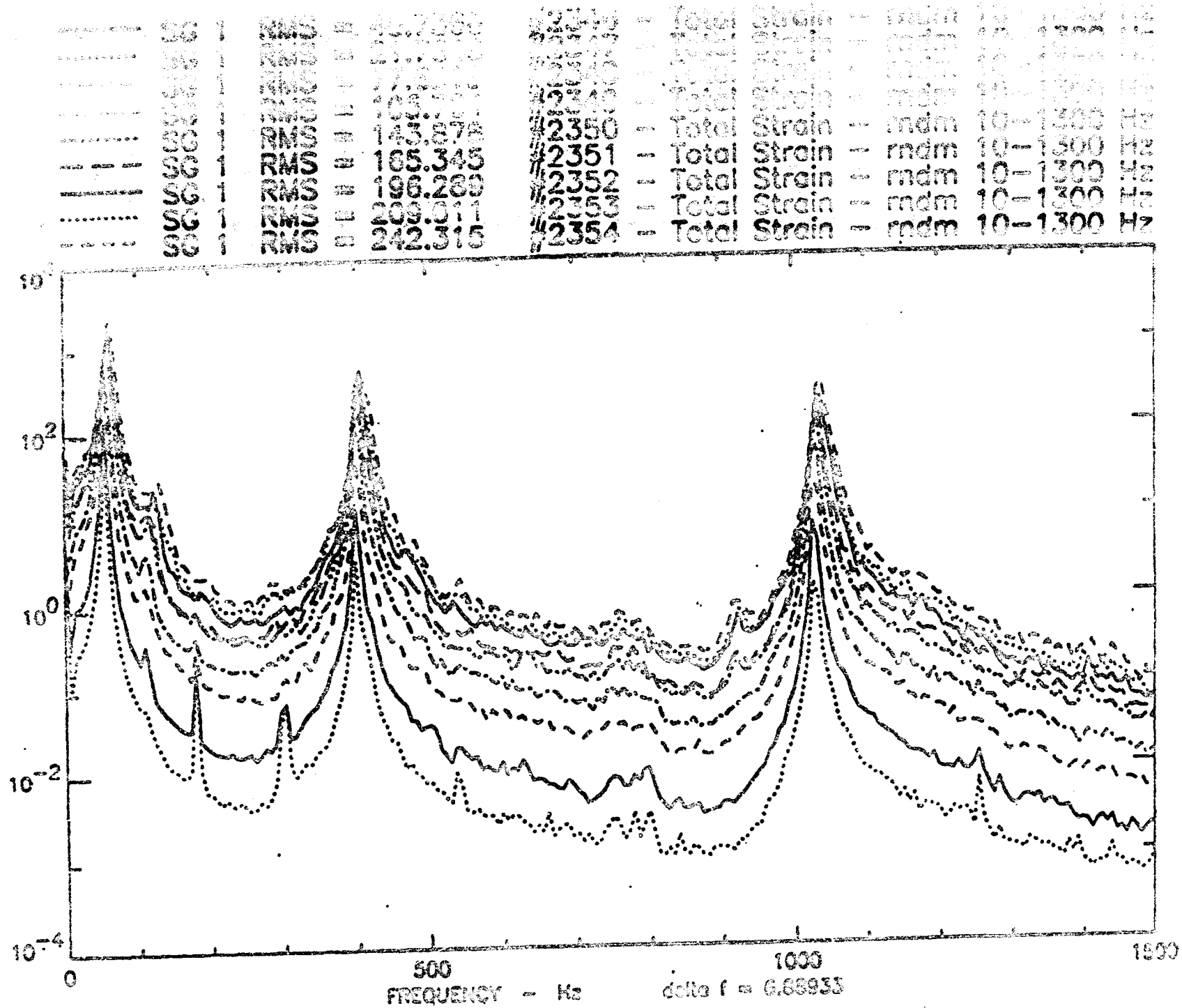

FIGURE 24 STRAIN SPECTRAL DENSITIES, SG 1, 10-1300 Hz RANDOM, C-C CFTO LEMM

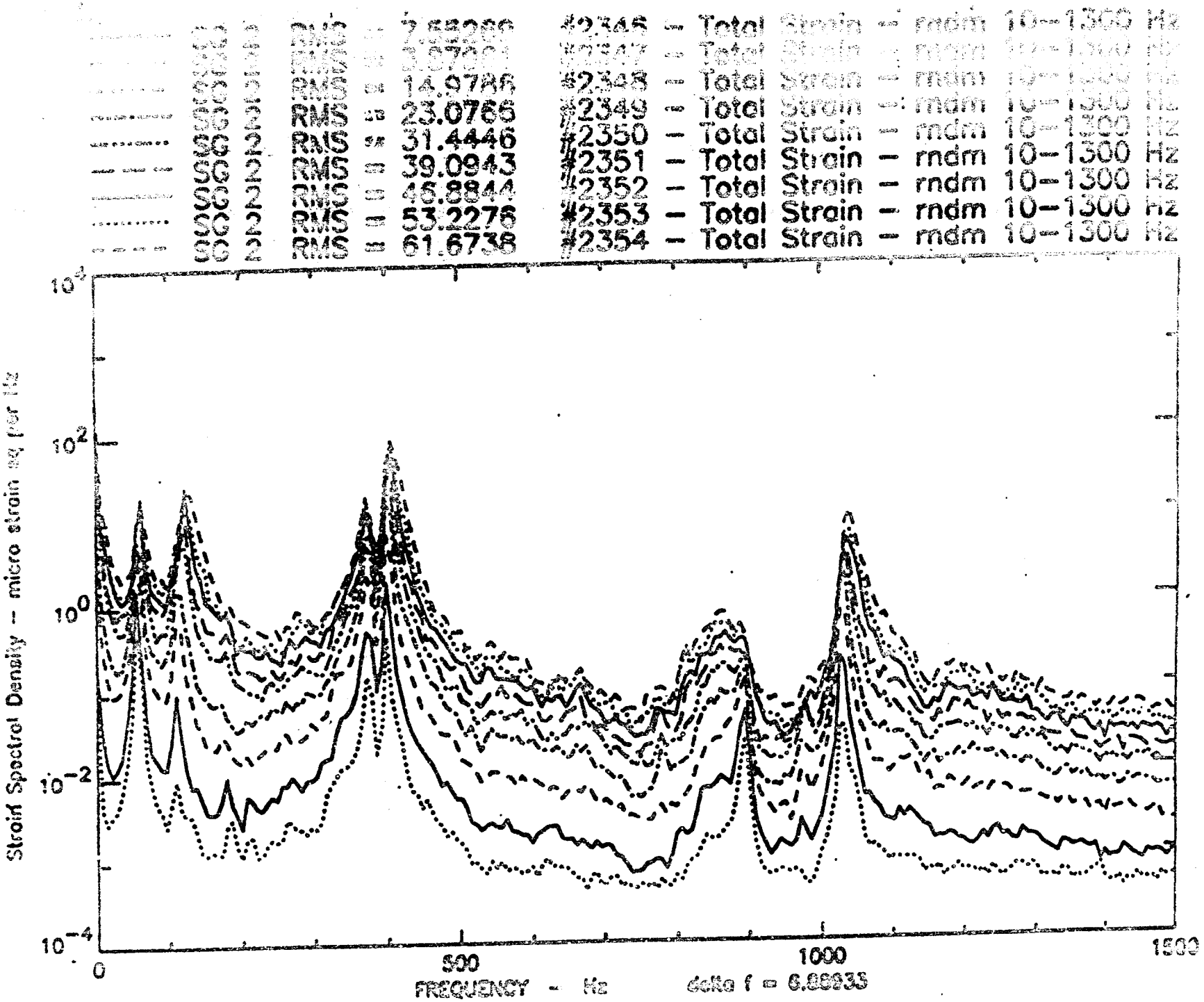

FIGURE 25 STRAIN SPECTRAL DENSITIES, SG 2, 10-1300 HZ RANDOM, C-C CFRP BEAM

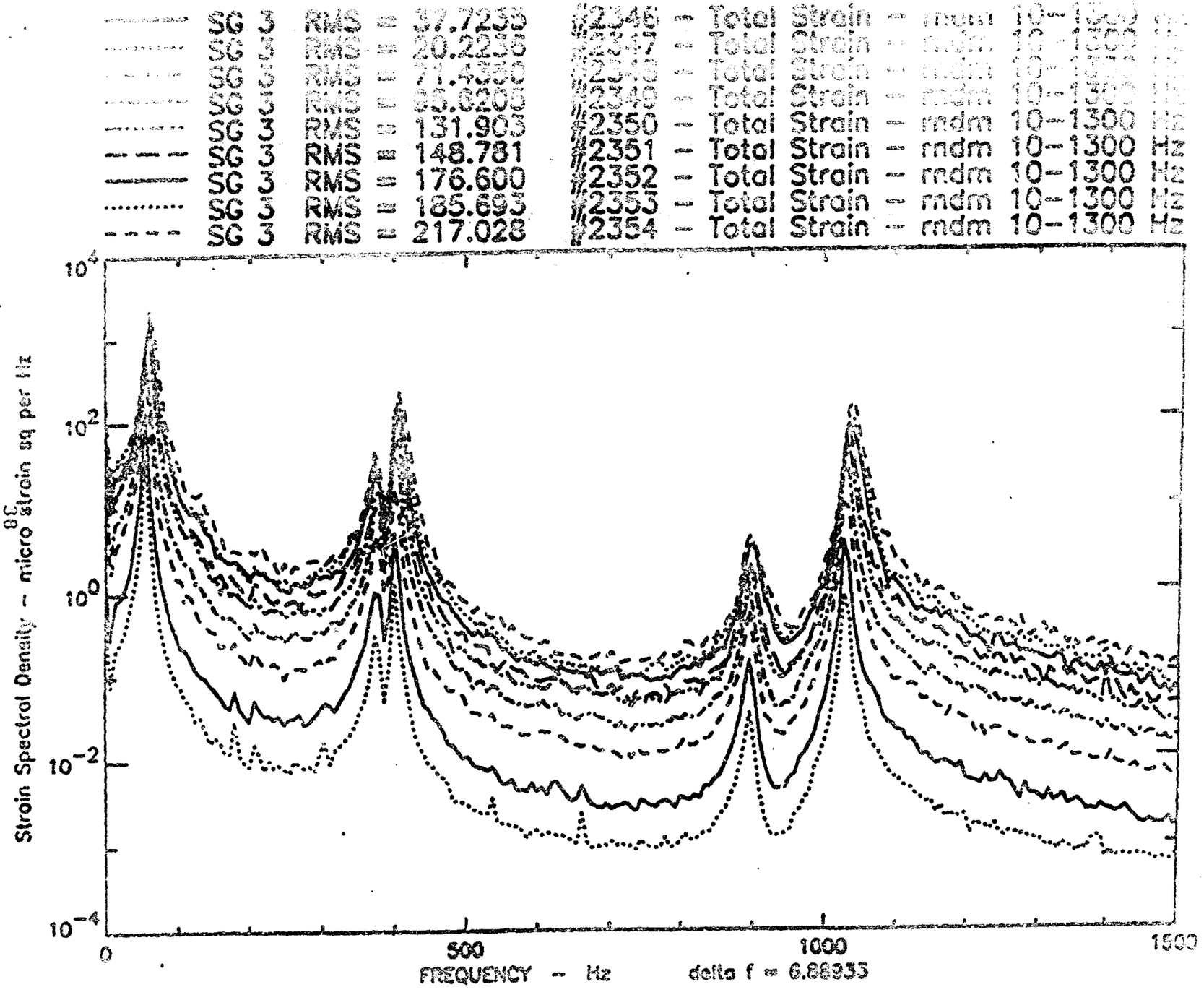

FIGURE 26 STRAIN SPECTRAL DENSITIES, SG 3, 10-1300 HZ RANDOM, C-C CFRP BEAM

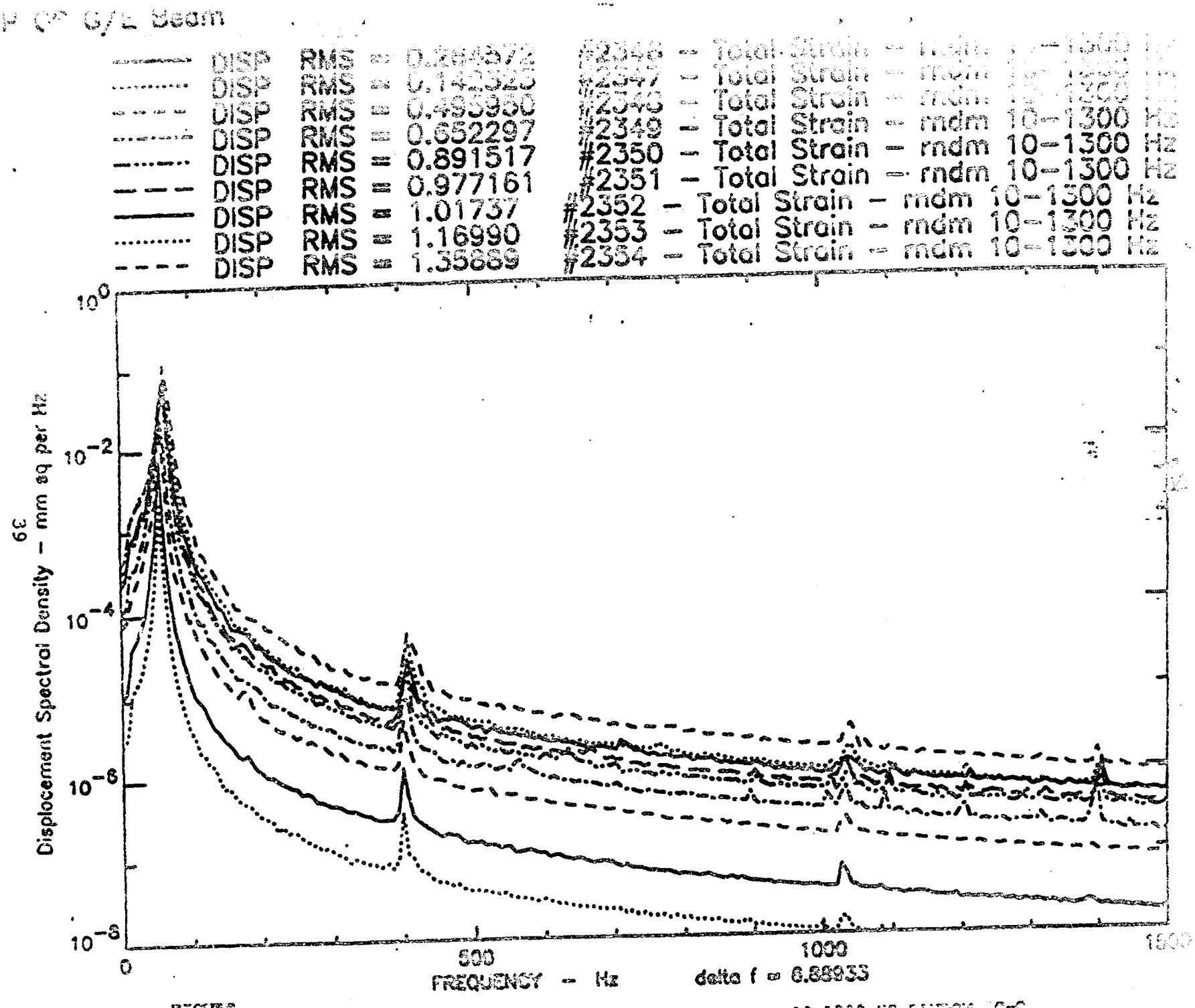

FIGURE 57 DISPLACEMENT SPECTRAL DENSITIES, BEAM CENTER, 10-1300 HZ RANDOM, C-C

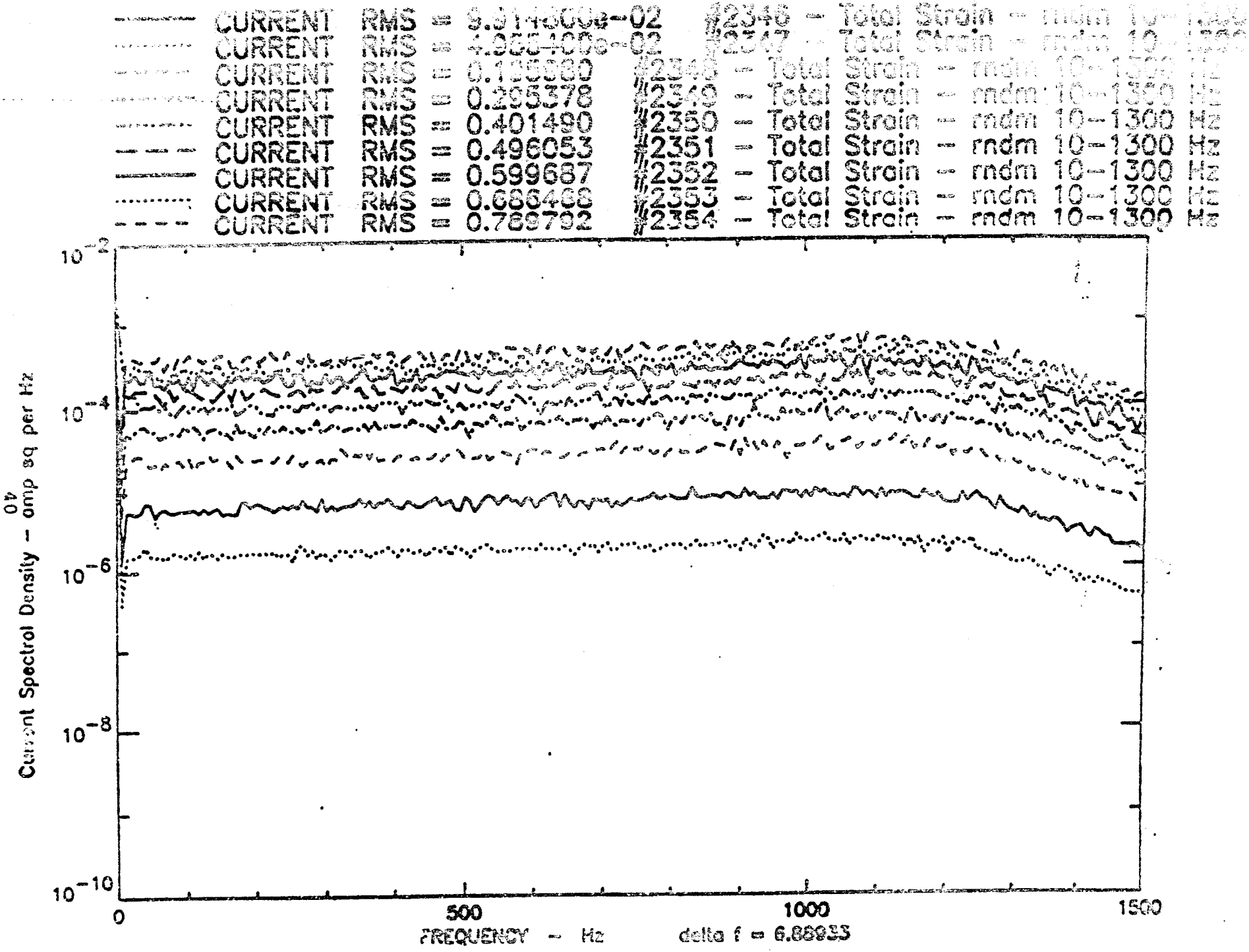

FIGURE 20 CURRENT SPECTRAL DENSITIES, 10-1300 HZ RANDOM, C-C CERP BEAM

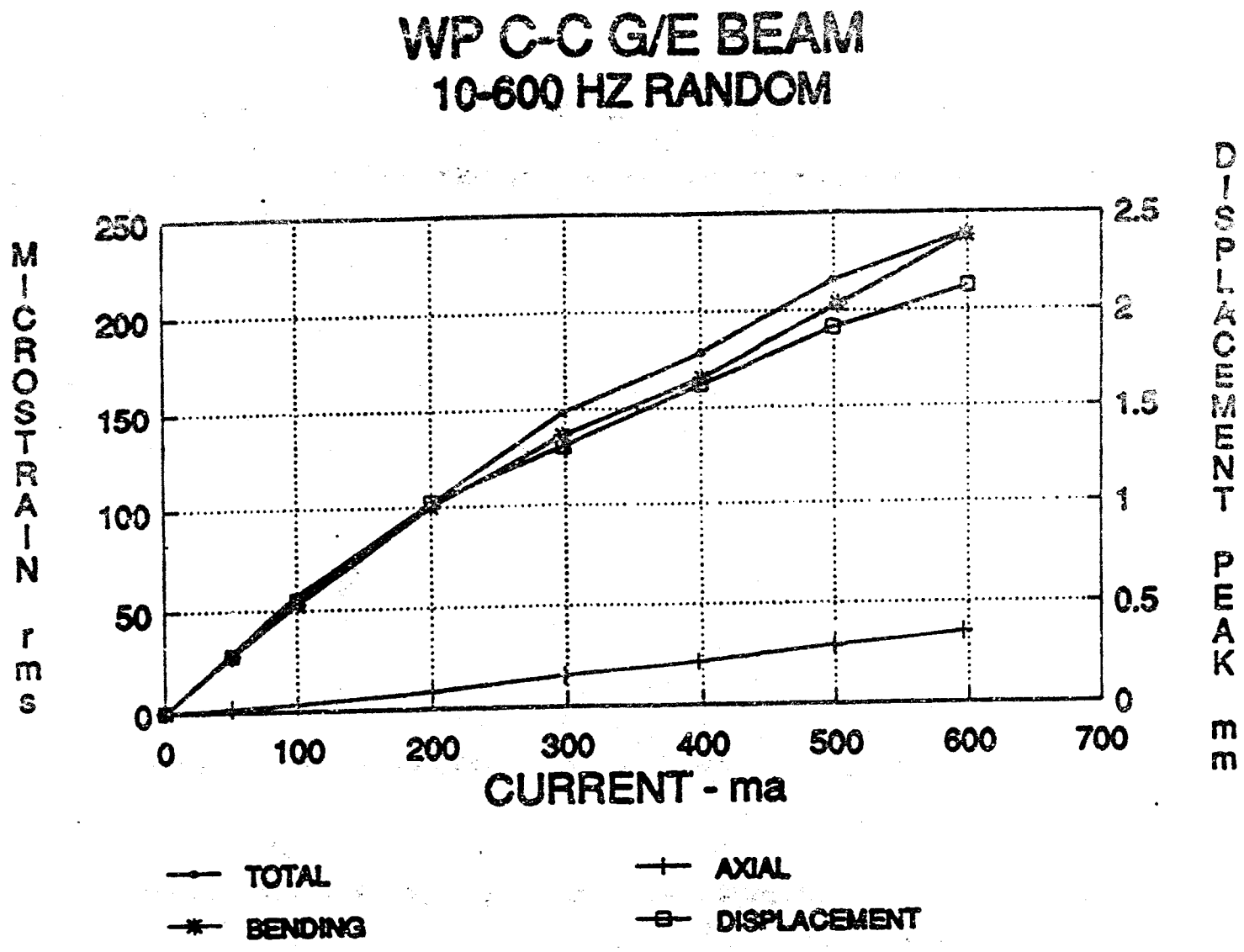

FIGURE 29 CURRENT VS DISPLACEMENT AND STRAIN, 10-600 HZ RANDOM, C-C CFRP BEAM

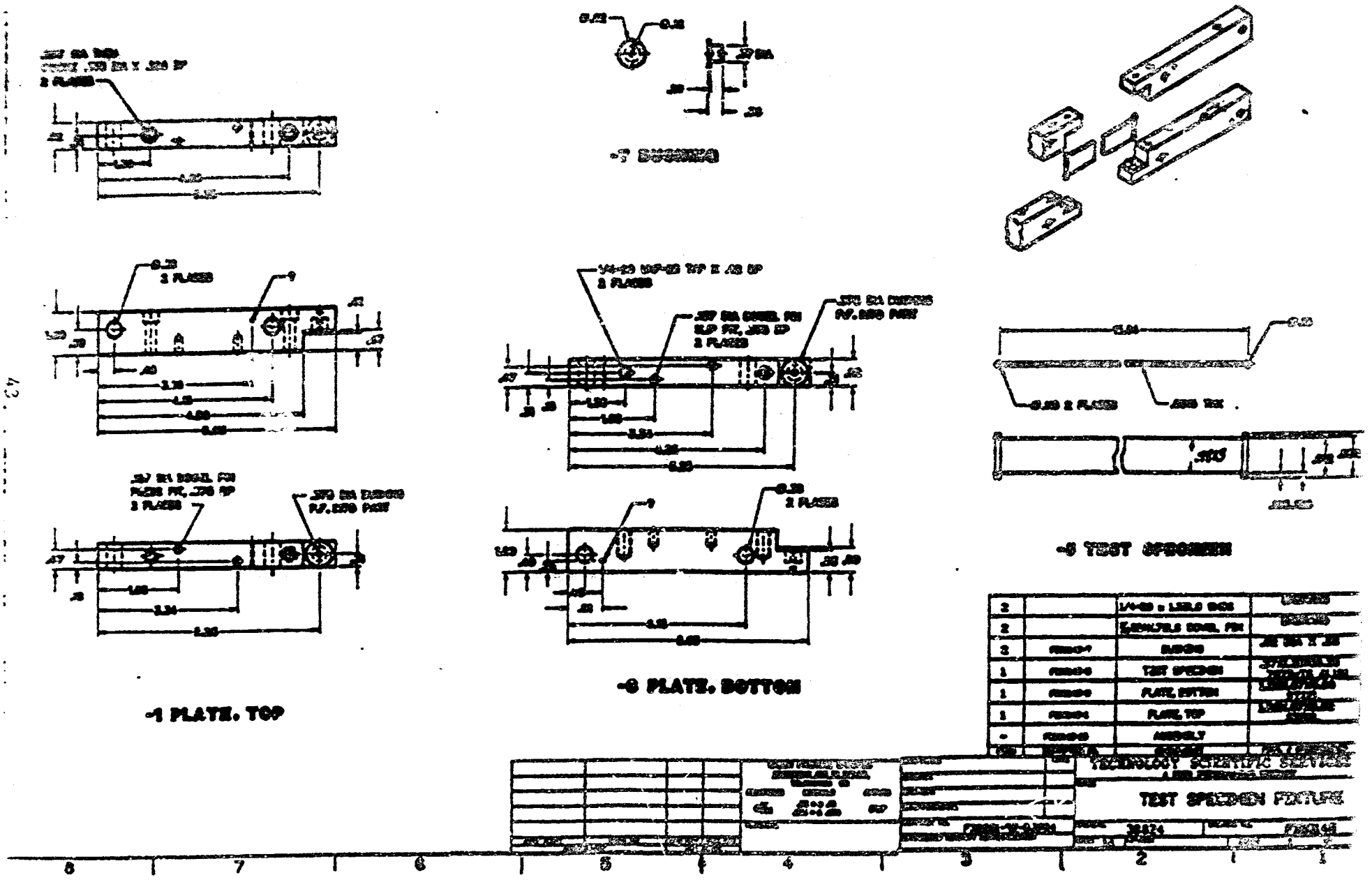

FIGURE 31 F-P ALUMINUM BEAM AND FIXTURE DESIGN

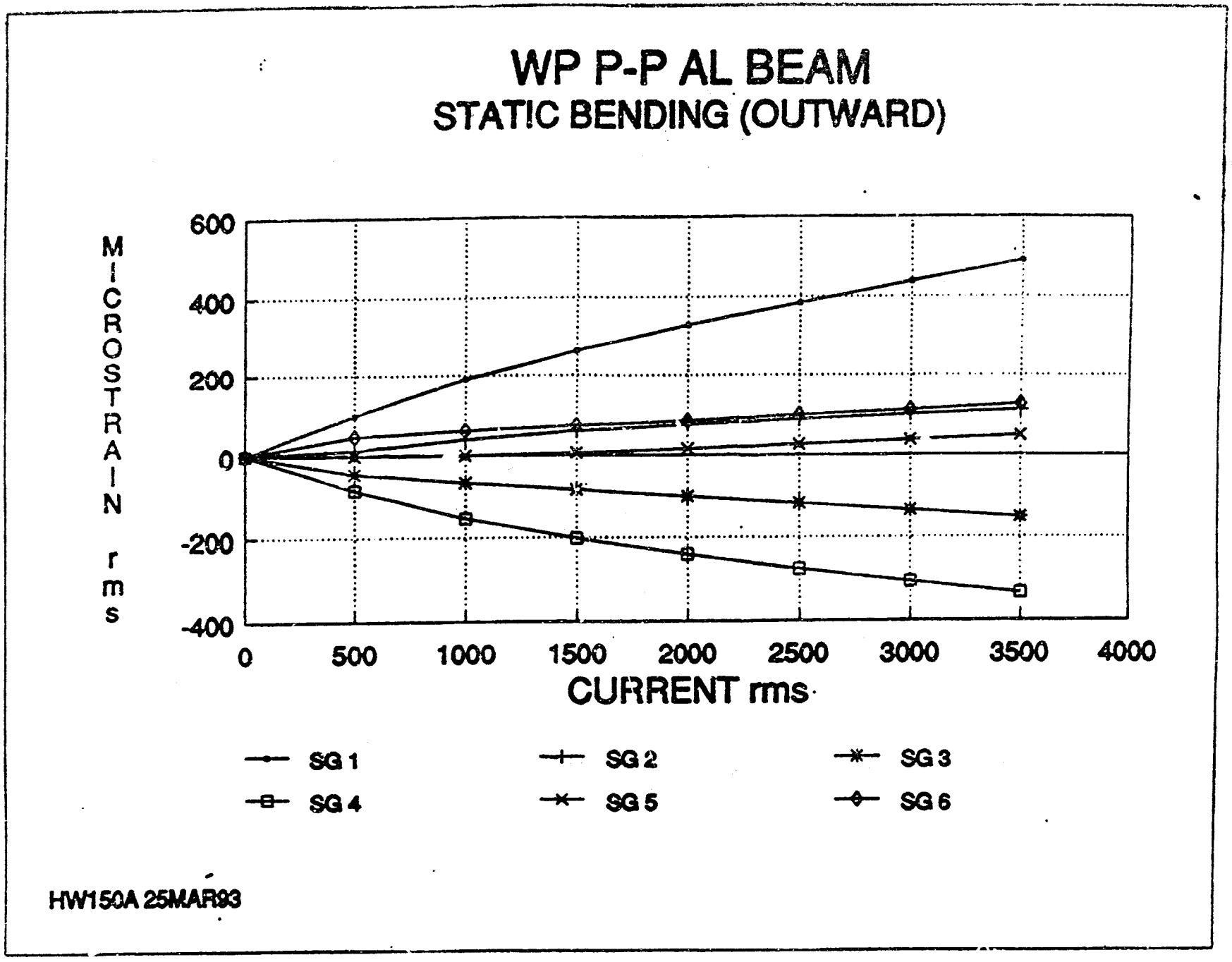

FIGURE 32 P-P ALUMINUM BEAM STATIC BENDING TEST

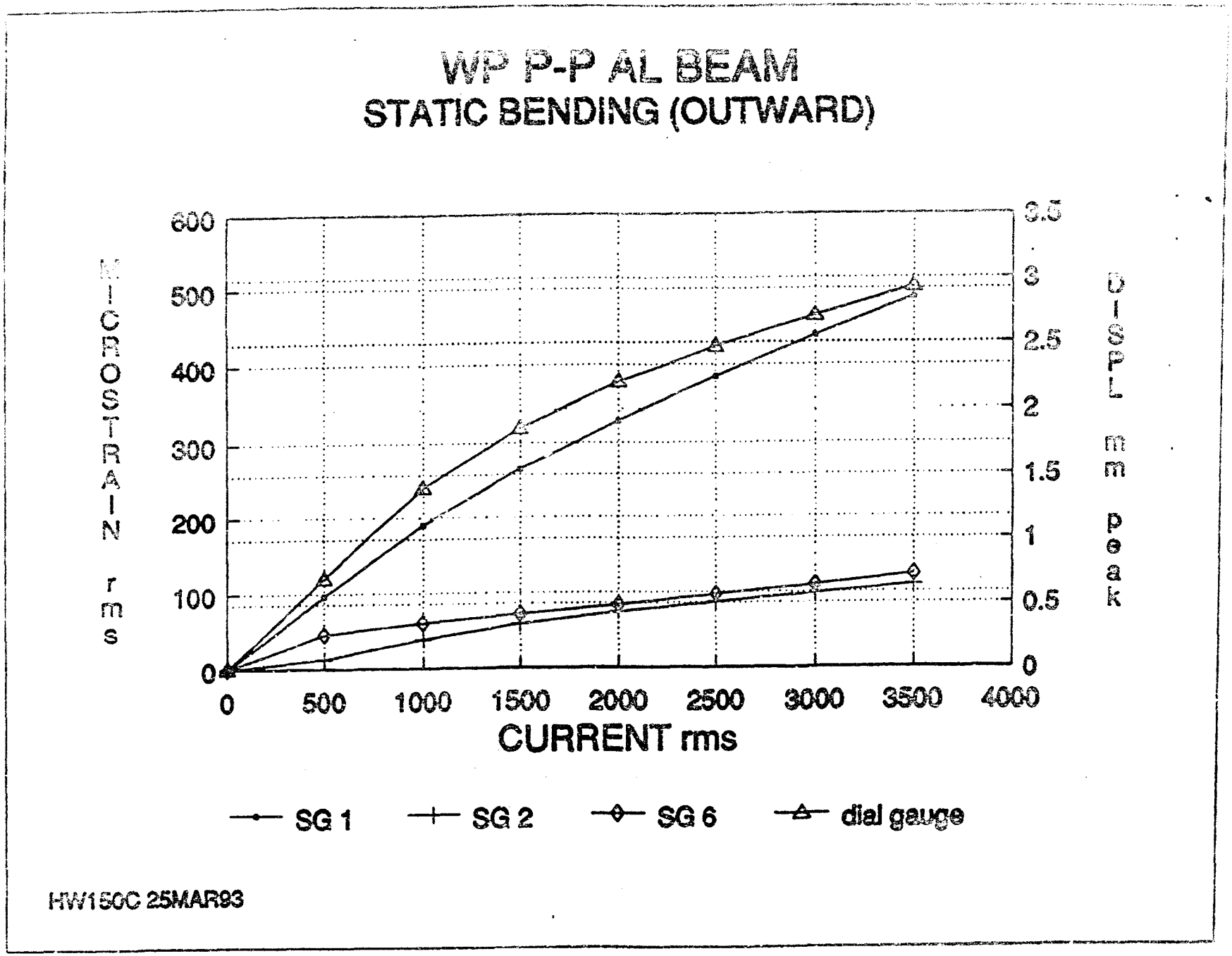

FIGURE 33 CURRENT VS DISPLACEMENT AND STRAIN, P-P ALUMINUM BEAM

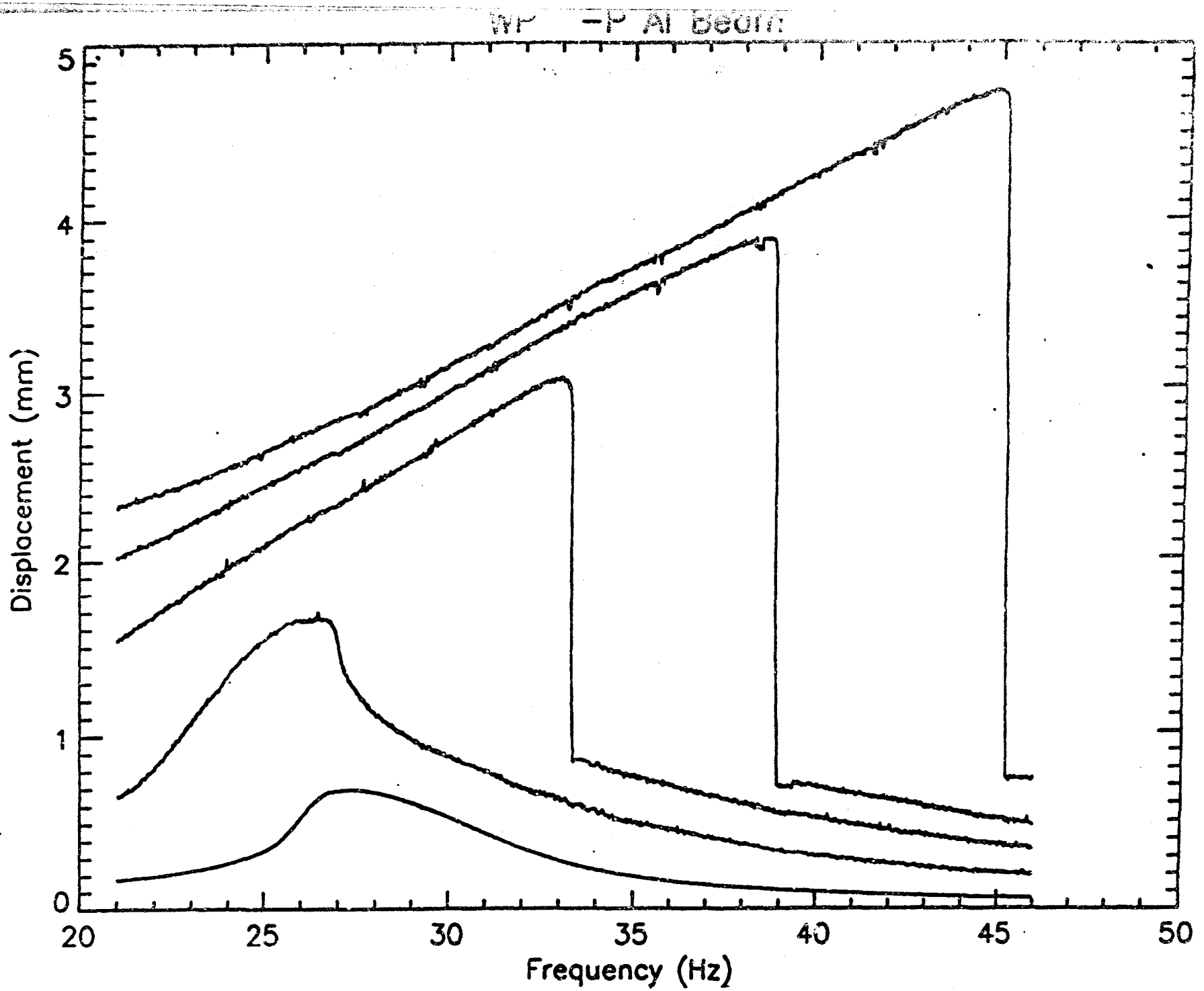

FIGURE 34 INCREASING FREQUENCY SWEEP, JUMP EFFECT OF FIRST MODE, P-P ALUMINUM BEAM

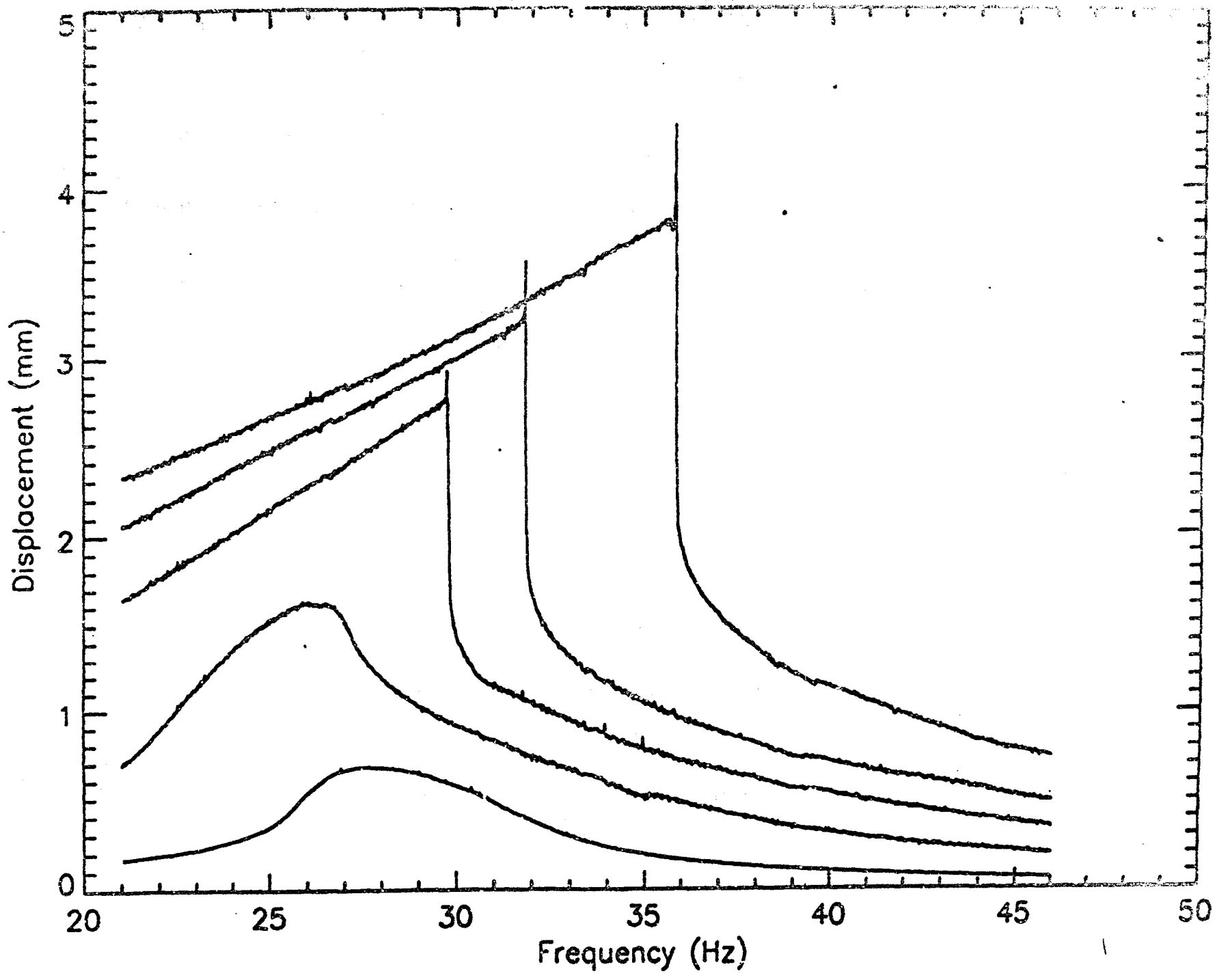

FIGURE 35 DECREASING FREQUENCY SWEEP, JUMP-UP EFFECT OF FIRST MODE, P-P ALUMINUM BEAM

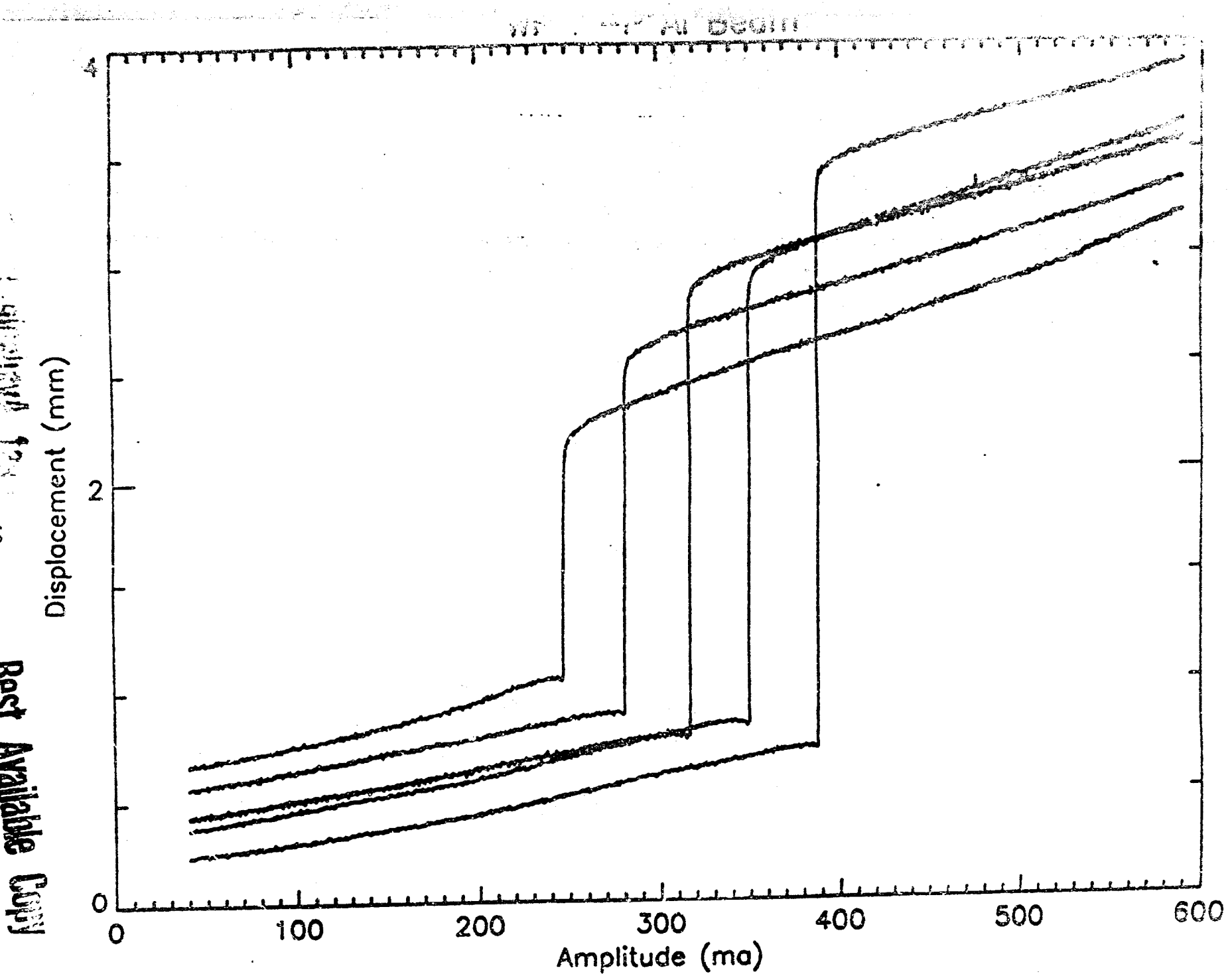

FIGURE 36 DECREASING AMPLITUDE SWEEP, JUMP-DOWN EFFECT, FIRST MODE, P-P ALUMINUM BEAM

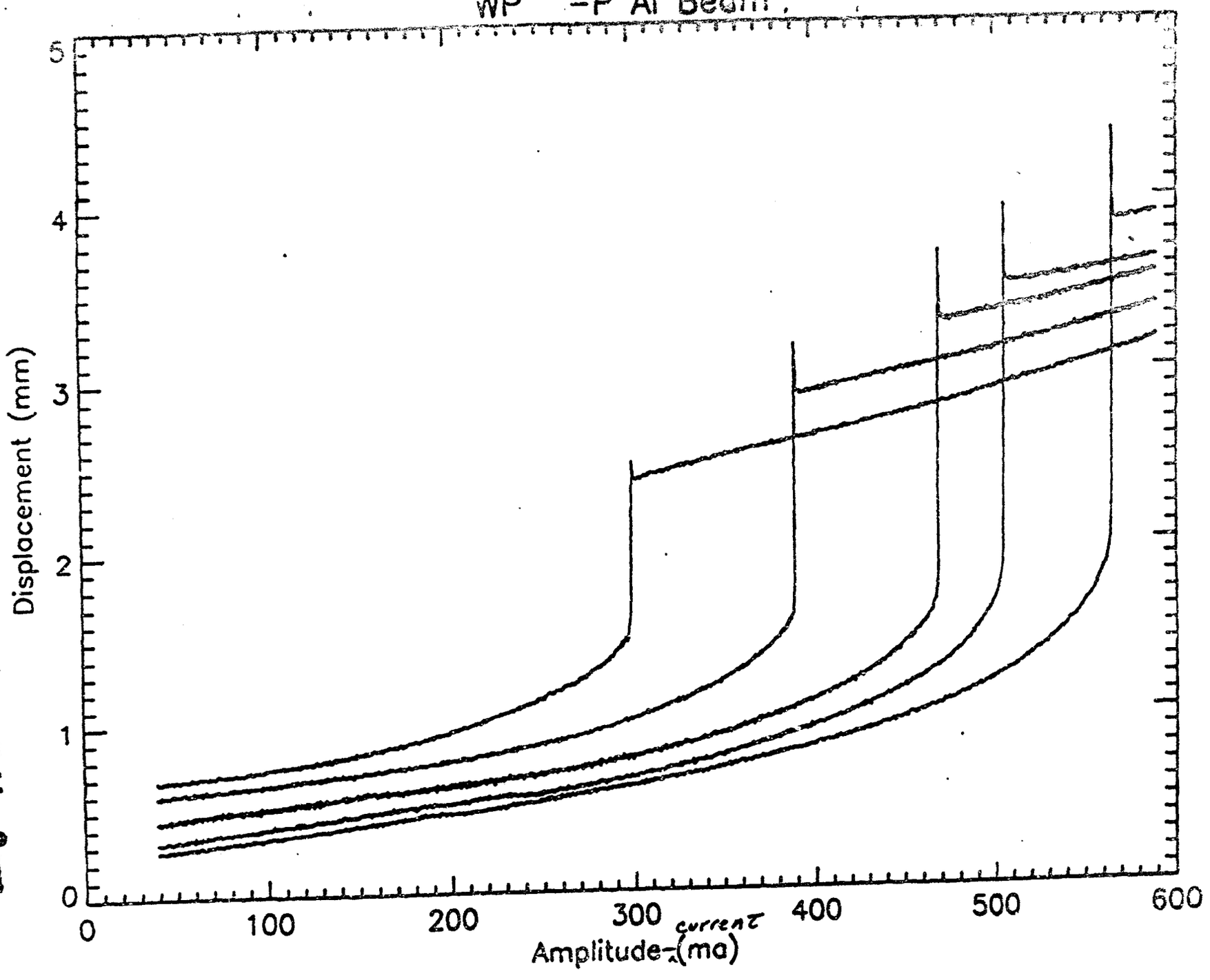

FIGURE 37 DECREASING AMPLITUDE SWEEP, JUMP-UP PHENOMENA, FIRST MODE, P-P

WP PF Al Beam

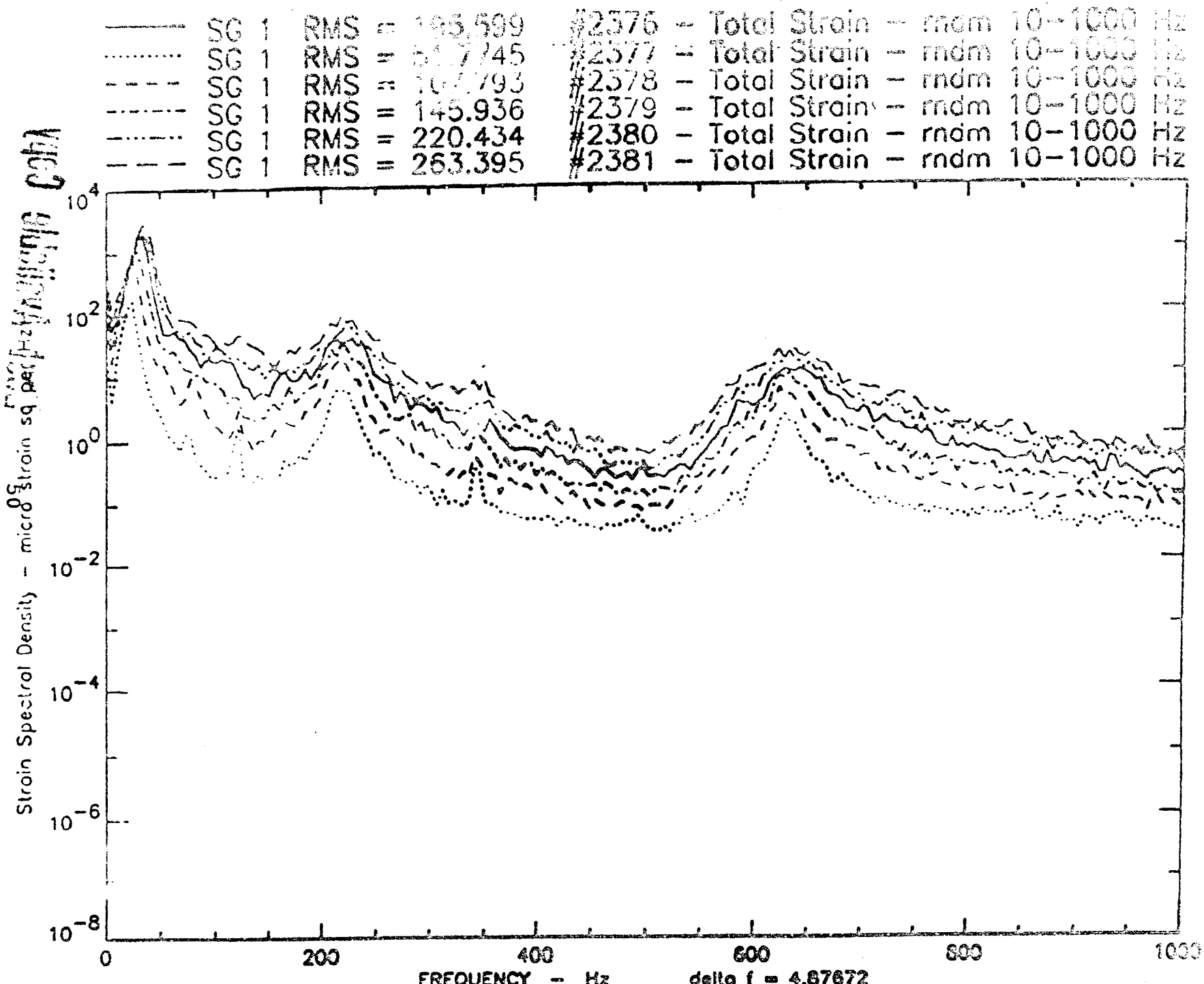

FIGURE

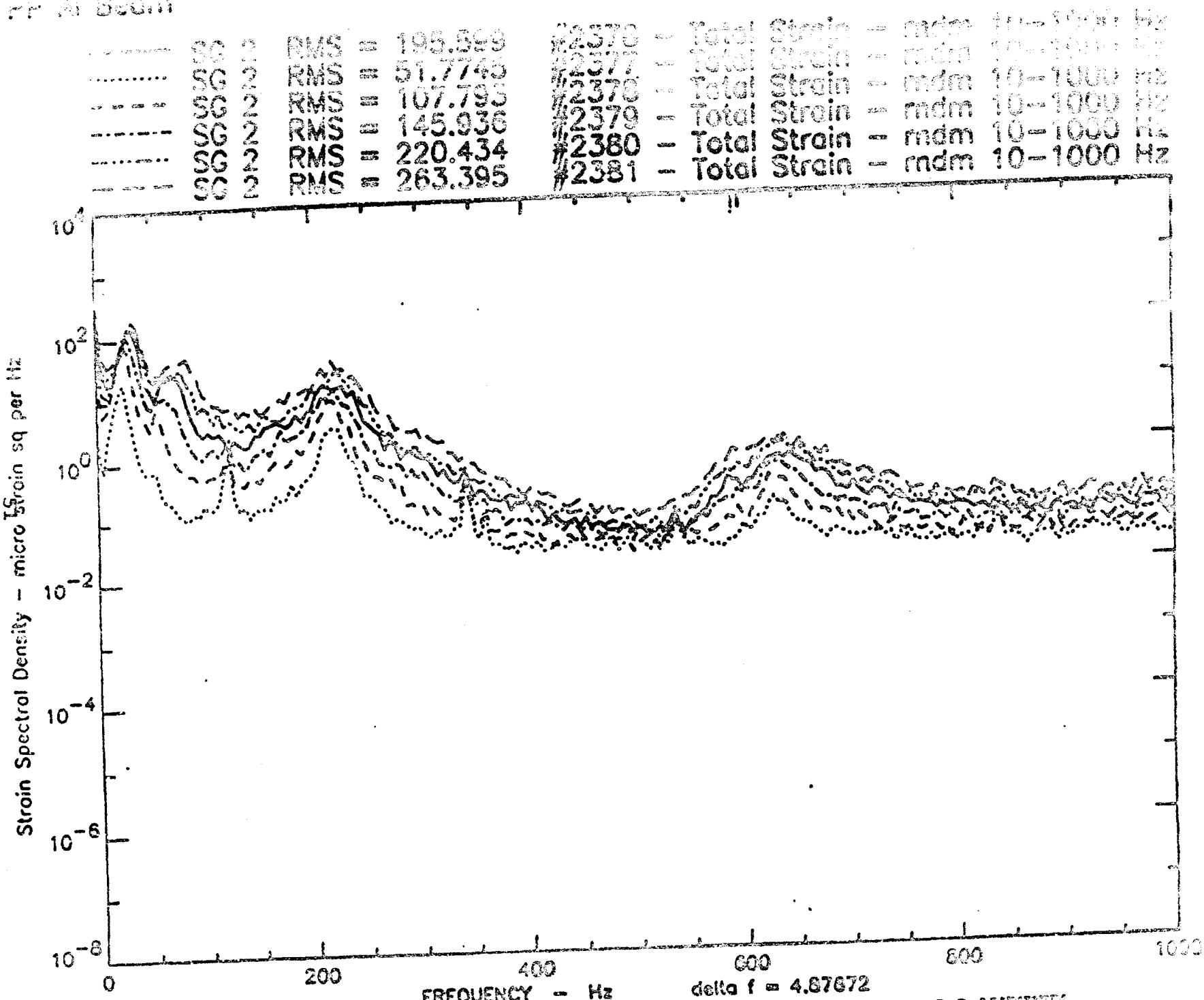

FIGURE 30 SOIL STRAIN SPECTRAL DENSITIES, SG 2, 10-1000 Hz RANDOM, F-F ALUMINUM

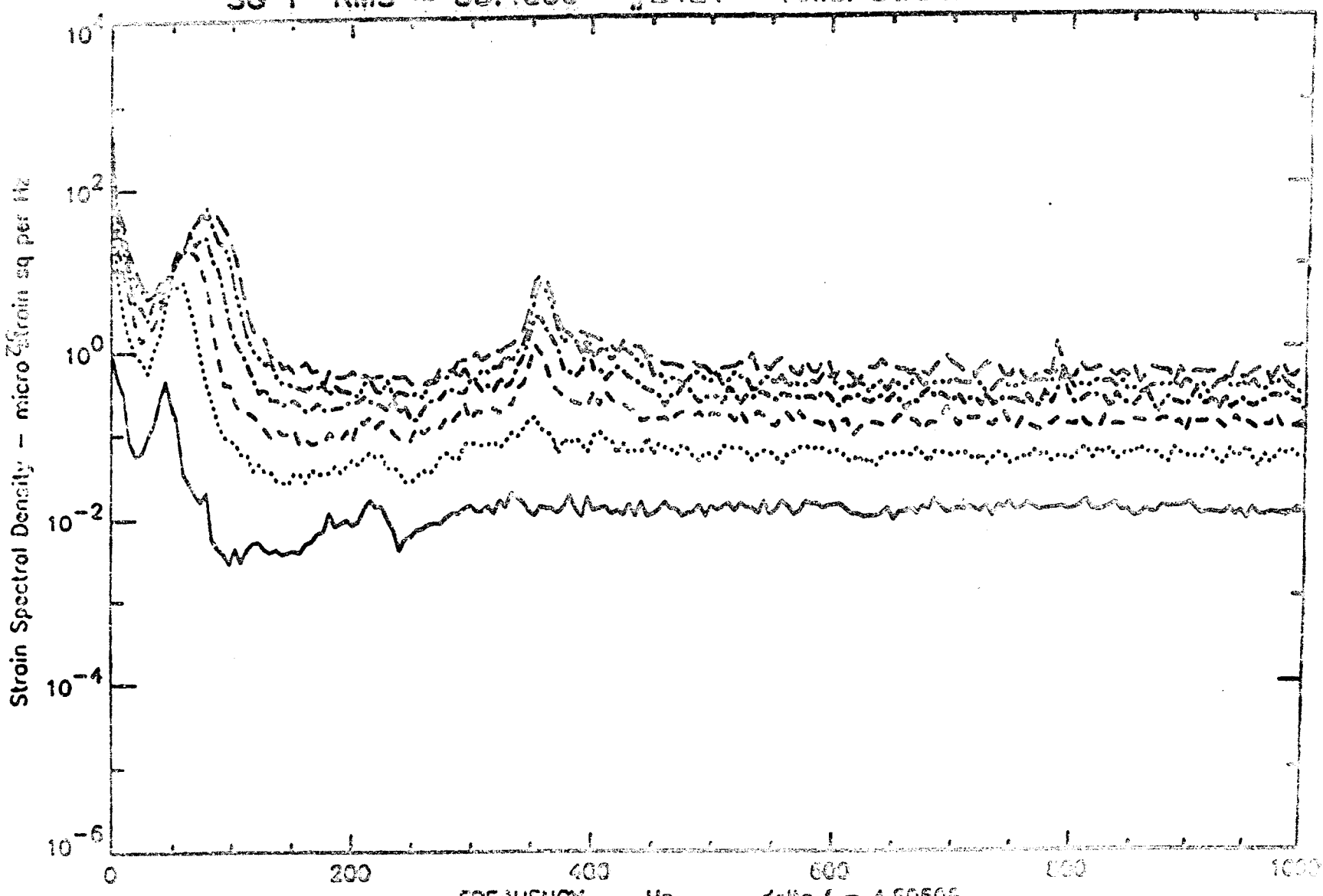

FIGURE 40 AXIAL STRAIN SPECTRAL DENSITIES, SG 1 10-1000 HZ FATIGUE, 0°F ENVIRONMENT

WP P-.' Al Beam

SG 1 4	RMS = 46.3378	#2437	– Bending Strain 10–1000 Hz
SG 1 4	RMS = 96.3615	#2438	– Bending Strain – 10–1000 Hz
SG 1 4	RMS = 145.156	#2439	– Bending Strain – 10–1000 Hz
SG 1 4	RMS = 185.406	#2440	– Bending Strain – 10–1000 Hz
SG 1 4	RMS = 213.312	#2441	– Bending Strain – 10–1000 Hz
SG 1 4	RMS = 244.731	#2442	– Bending Strain – 10–1000 Hz

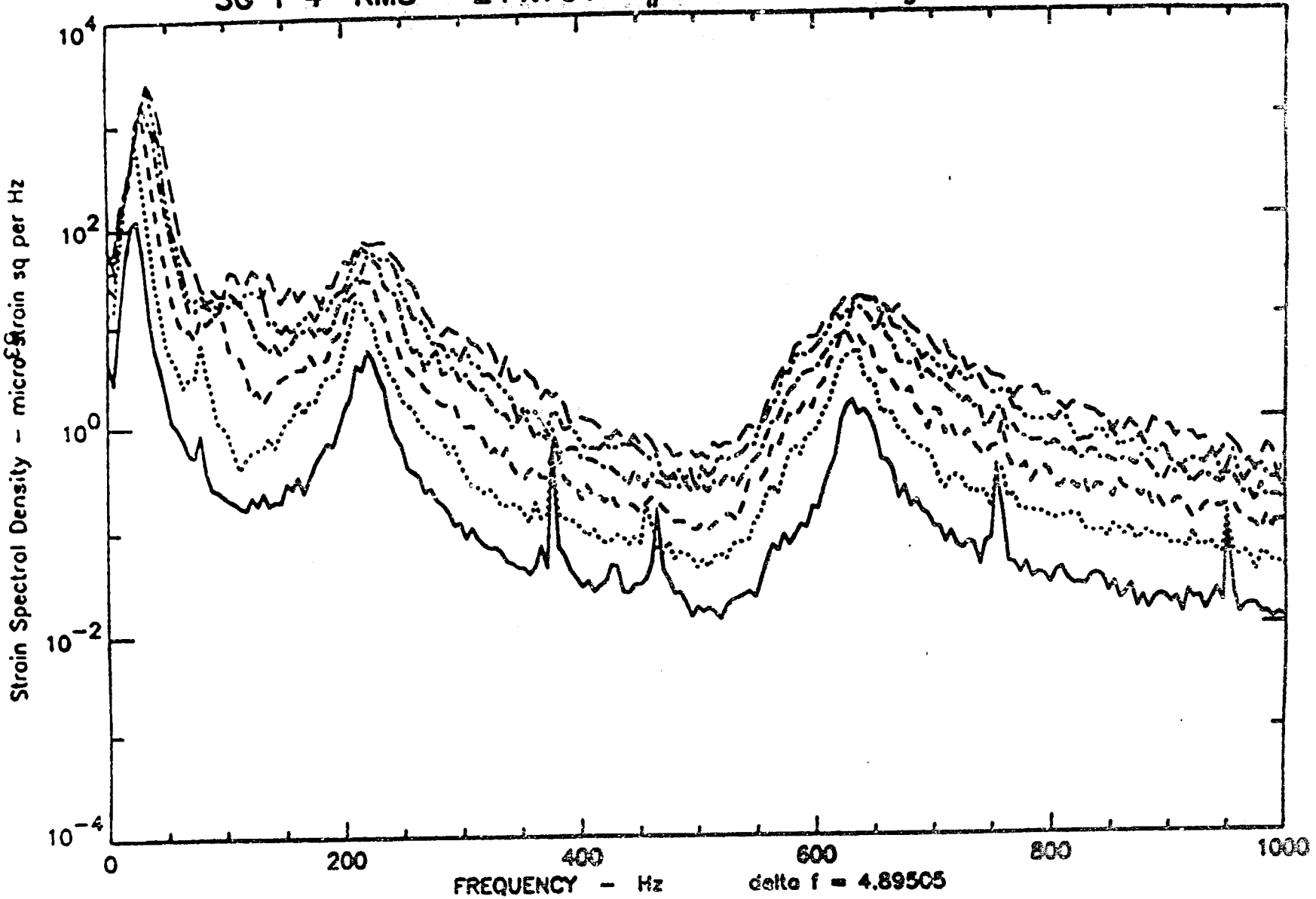

FIGURE

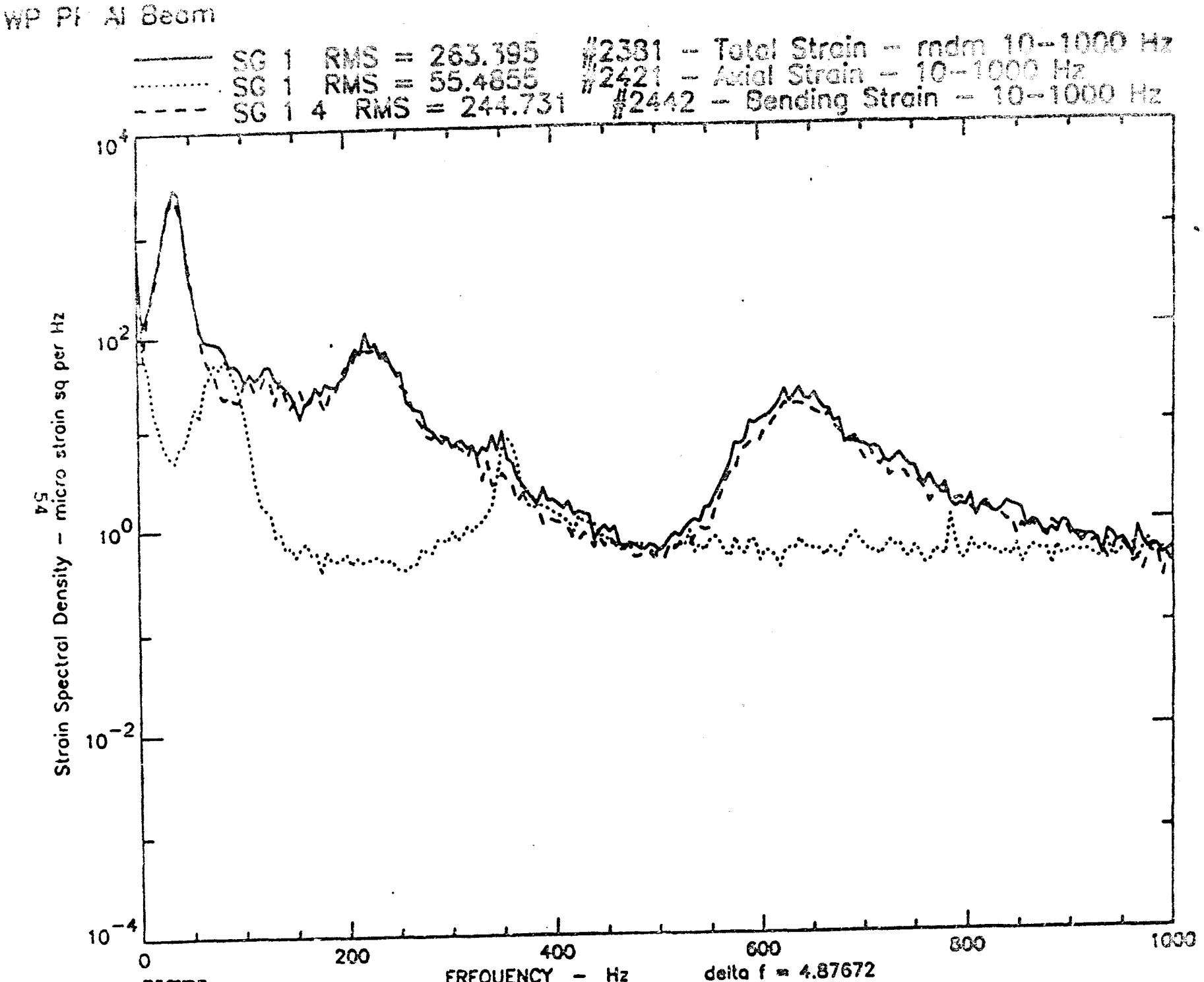

FIGURE 42

TOTAL, AXIAL AND BENDING STRAIN SPECTRAL DENSITIES, SG 1, 10-1000 HZ,

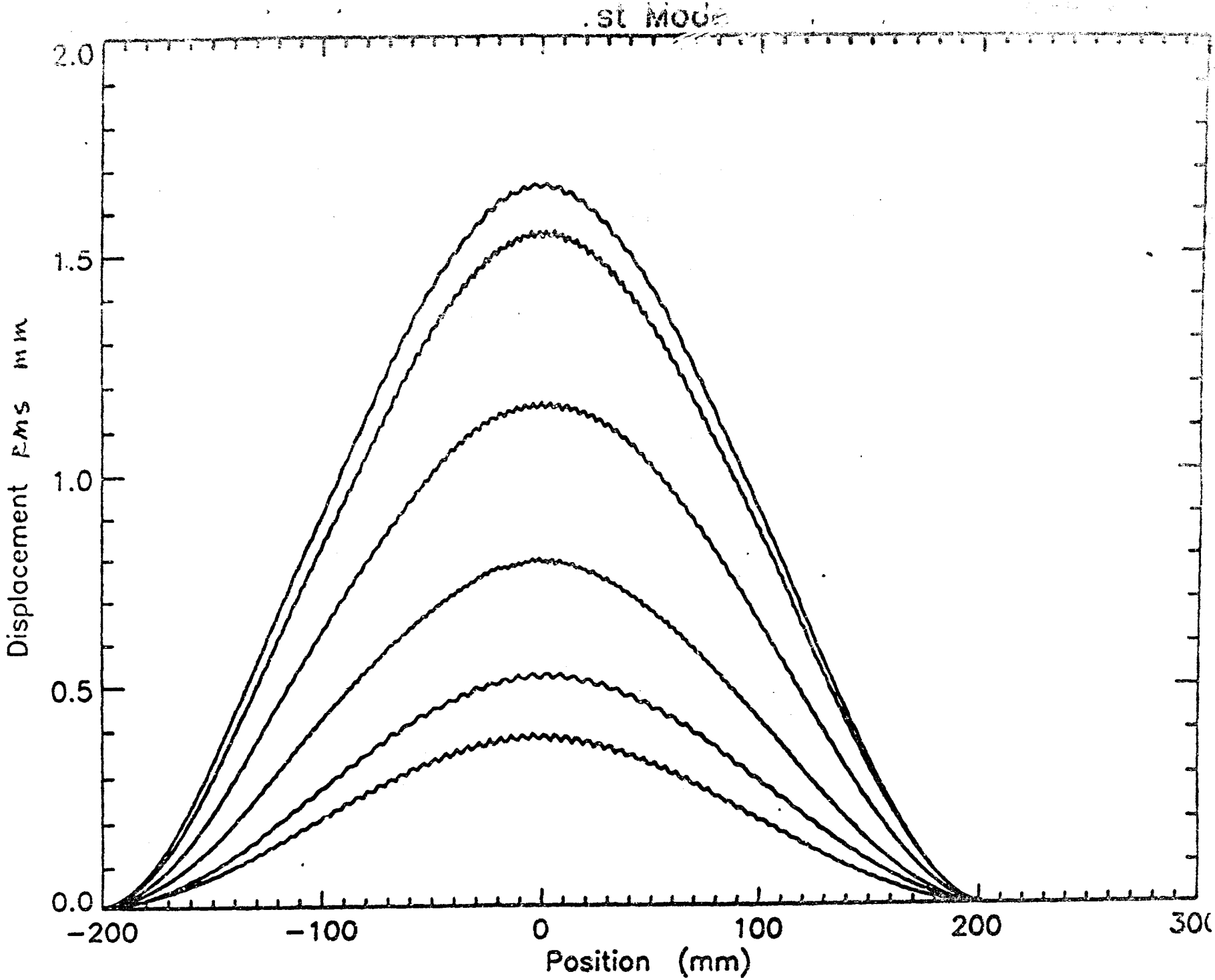

FIGURE 43 NONLINEAR DISPLACEMENT SHAPES, FIRST MODE, RAW DATA, C-C ALUMINUM

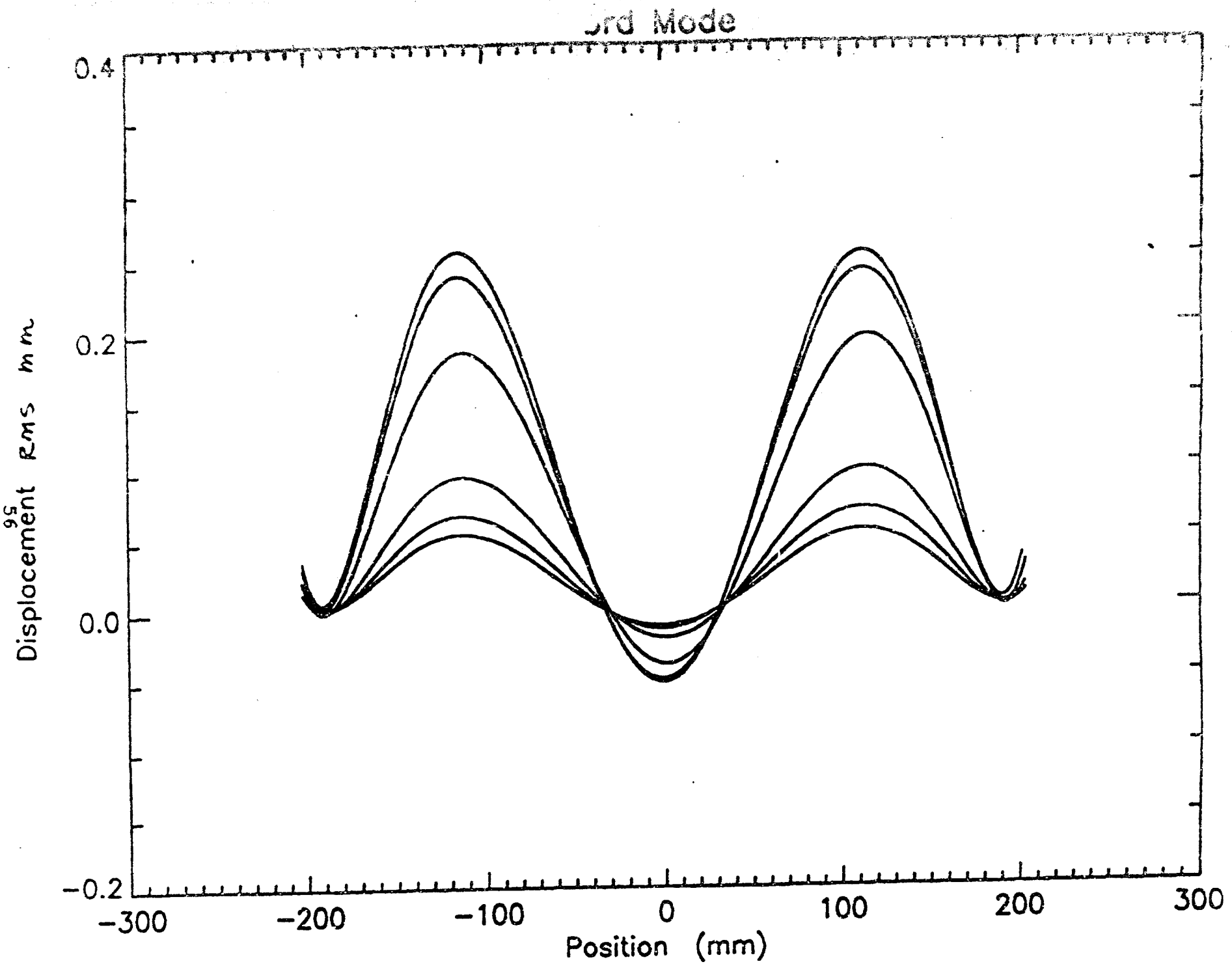

FIGURE 44 NONLINEAR DISPLACEMENT SHAPES, THIRD MODE, SEVENTH ORDER POLYNOMIAL FIT, C-C ALUMINUM BEAM

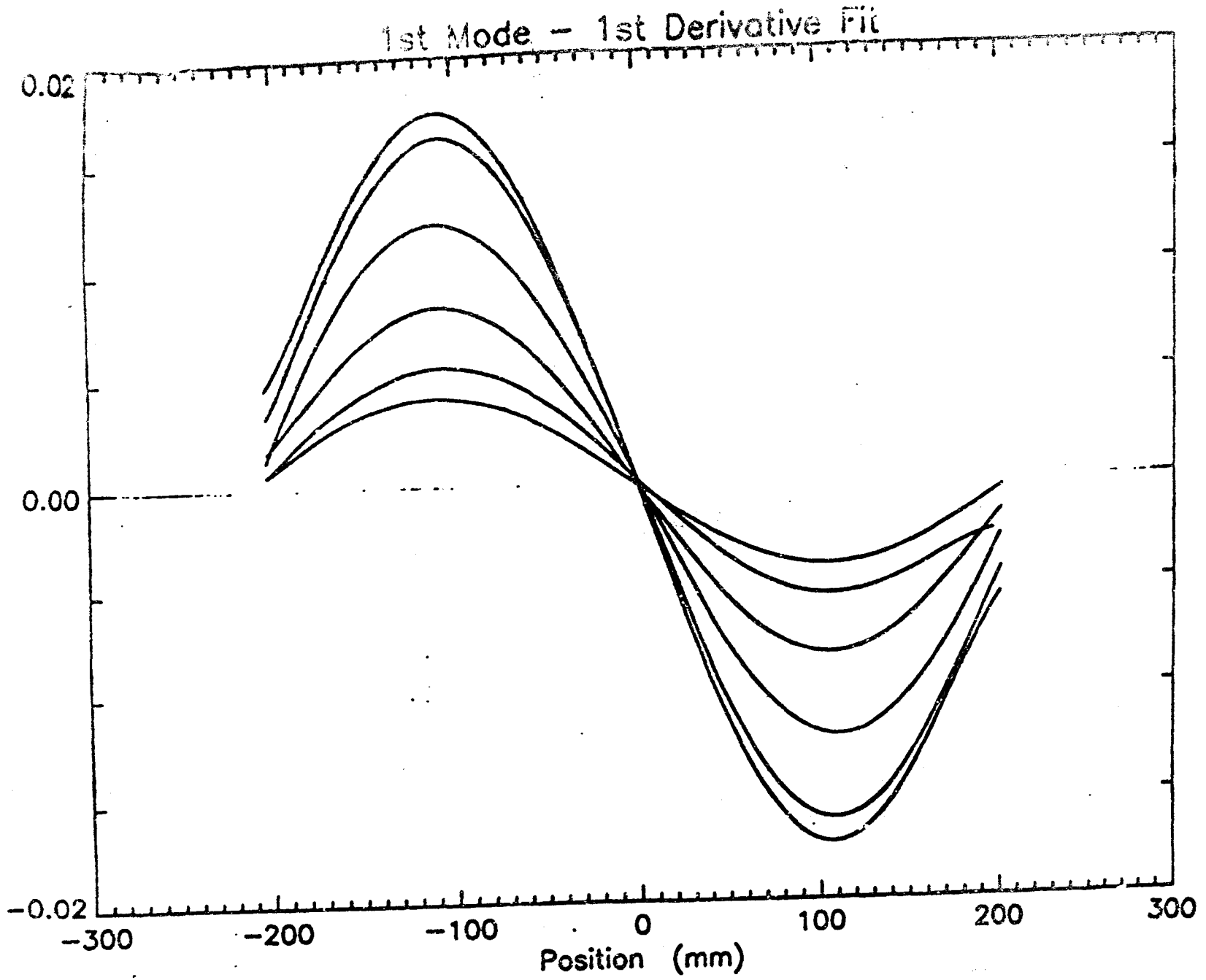

FIGURE 45 FIRST MODE, SEVENTH ORDER POLYNOMIAL CURVE FIT, FIRST DERIVATIVE, [illegible] ALUMINUM BEAM

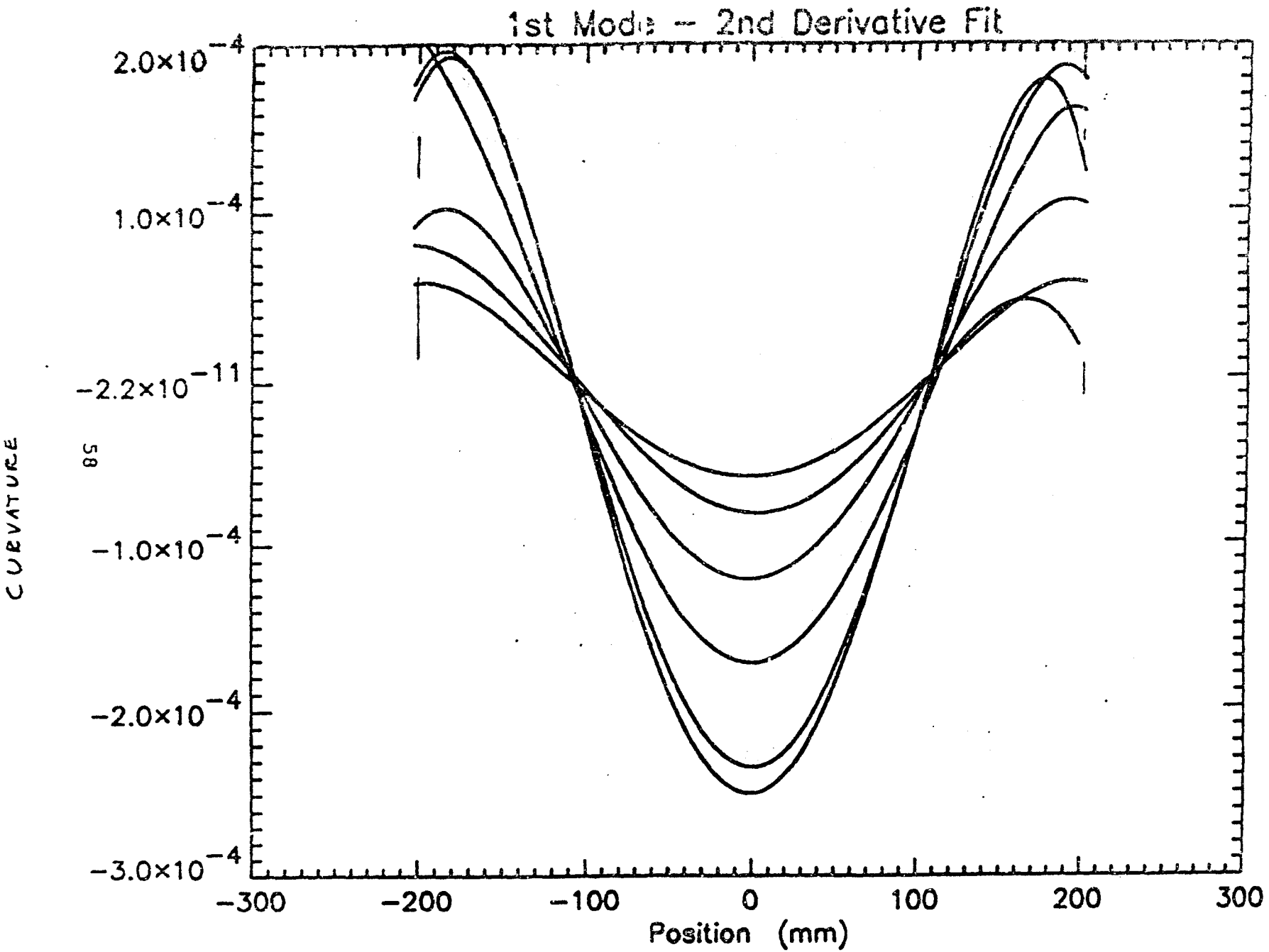

FIGURE 46 FIRST MODE, SEVENTH ORDER POLYNOMIAL CURVE FIT, SECOND DERIVATIVE,

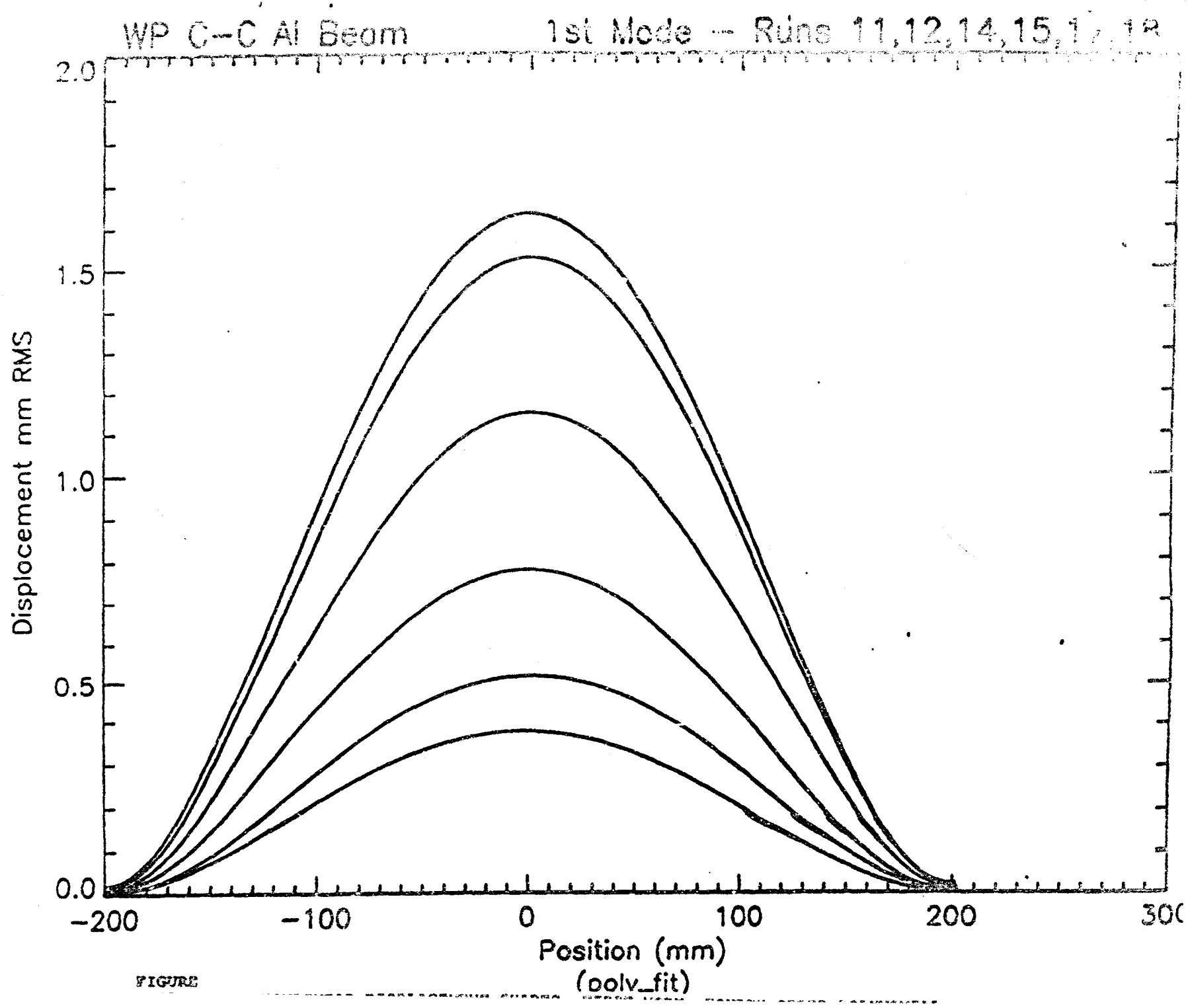
WP C-C Al Beam
1st Mode -- Runs 11,12,14,15,1
Displacement mm RMS
2.0
1.5
1.0
0.5
0.0
-200
-100
0
100
200
Position (mm)
(polv_fit)

FIGURE

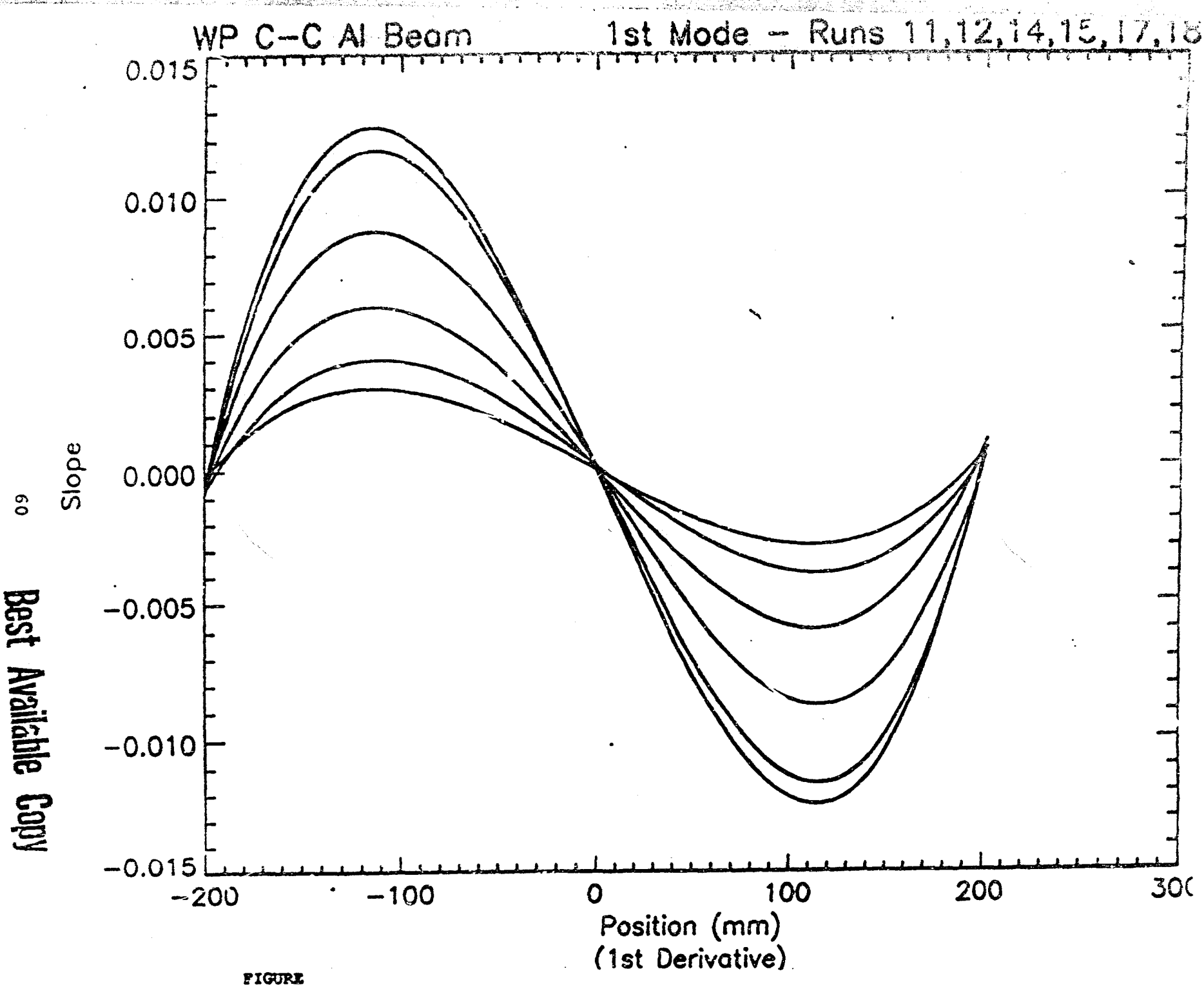

FIGURE 49 FIRST MODE. FOURTH ORDER POLYNOMIAL FIT. FIRST DERIVATIVE, C-C

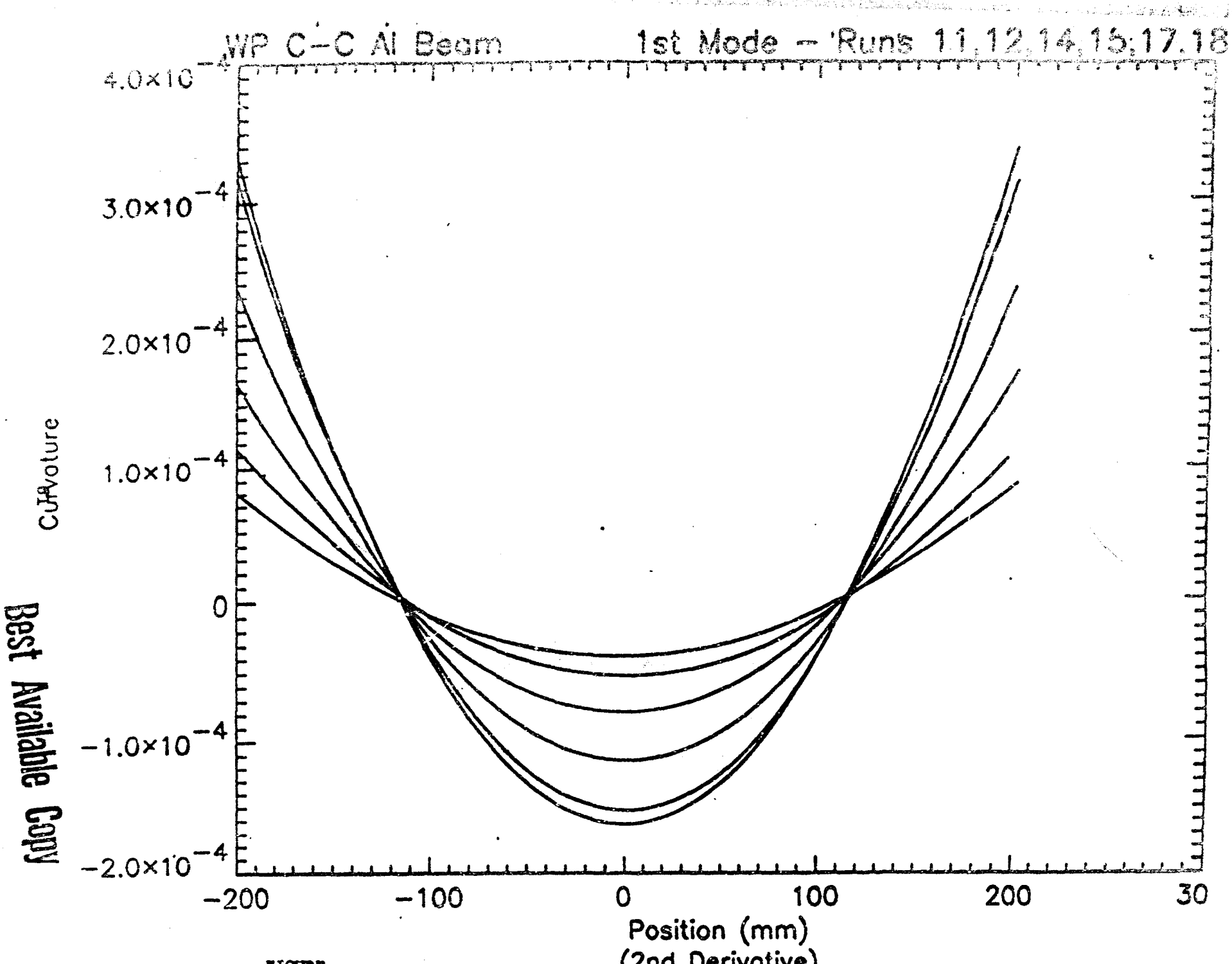

FIGURE 49

FIRST MODE, FOURTH ORDER POLYNOMIAL FIT, SECOND DERIVATIVE, C-C

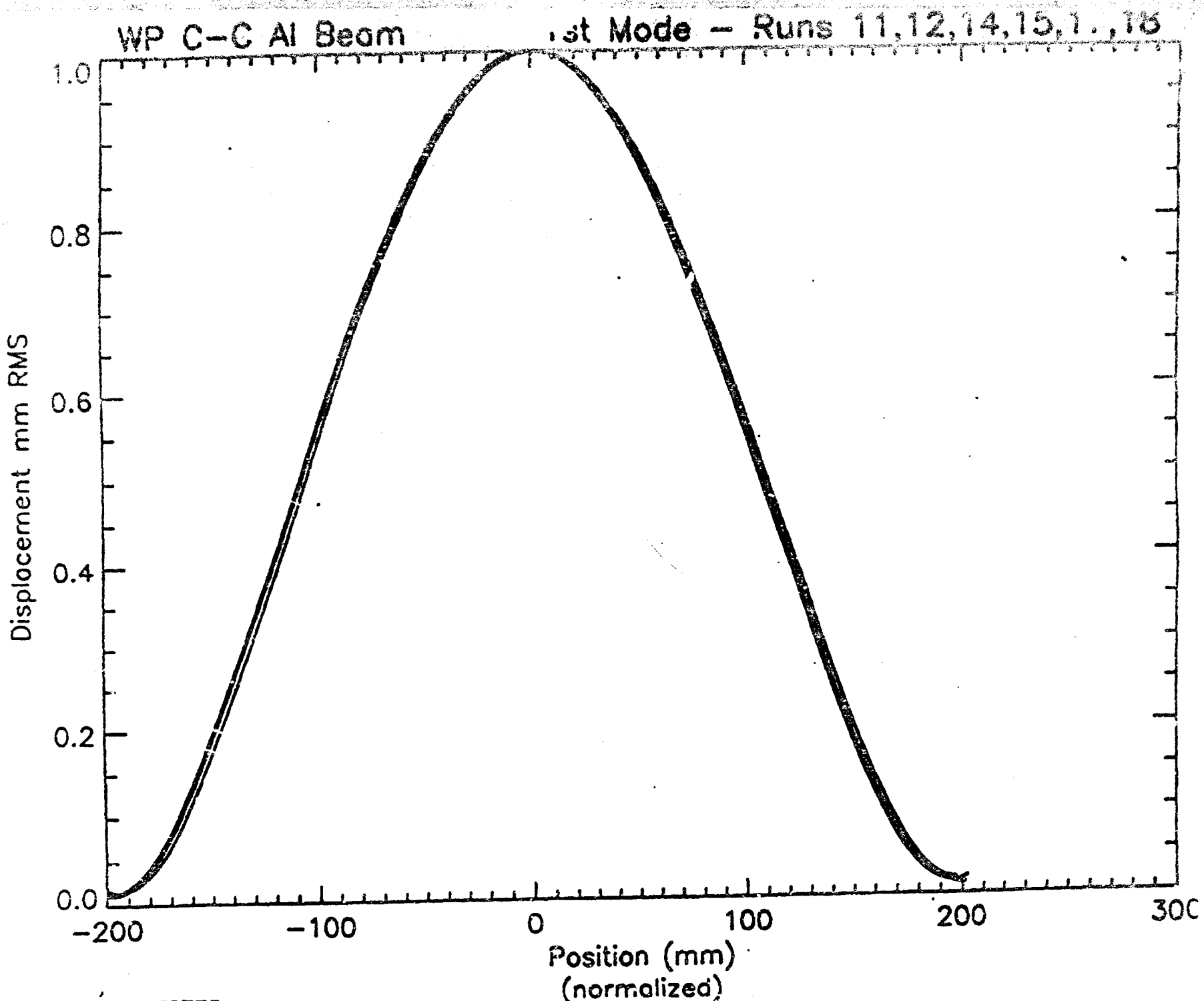

62

FIGURE 50 NORMALIZED NONLINEAR DISPLACEMENT SHAPES, FIRST MODE, C–C ALUMINUM

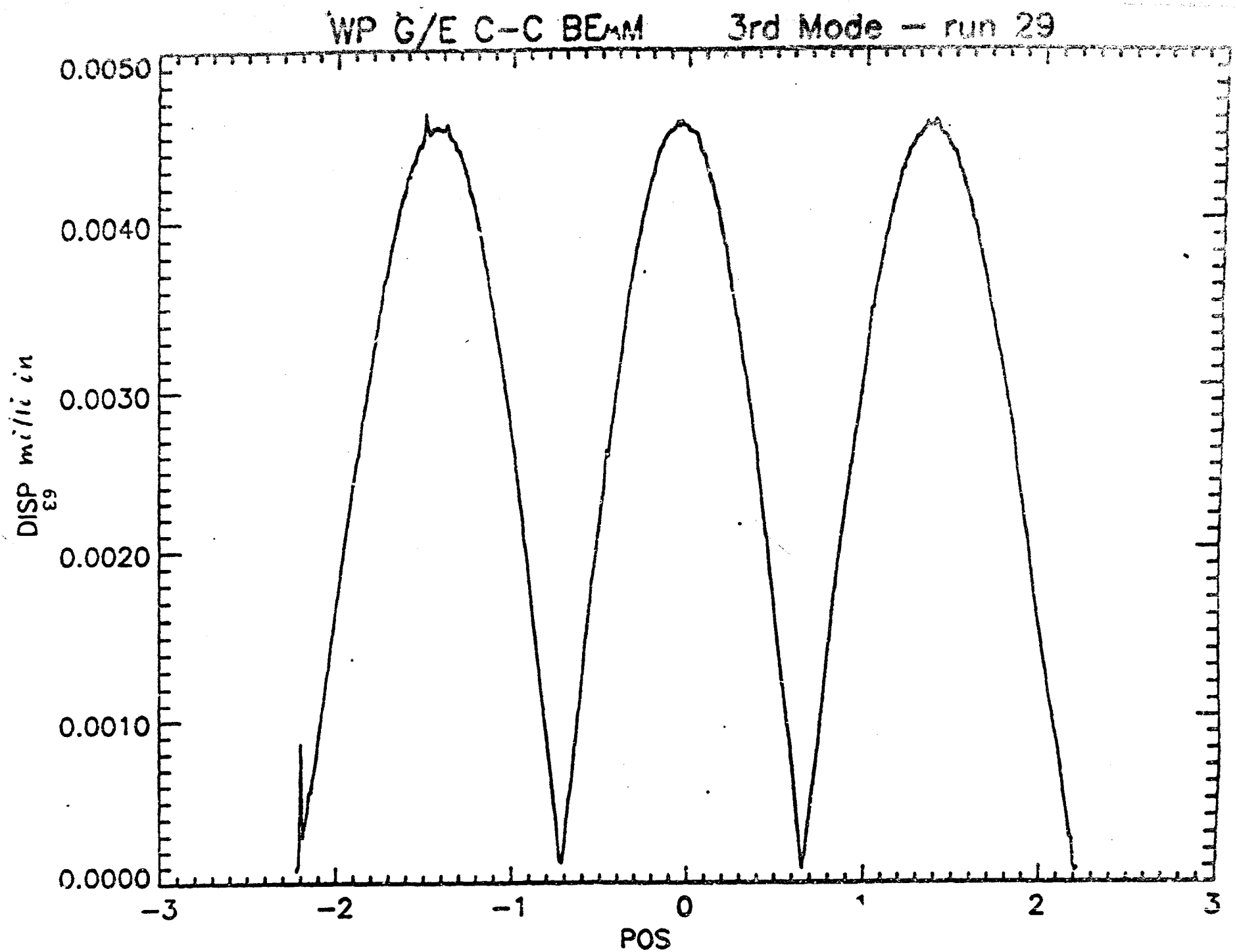

FIGURE

MODE SHAPE, THIRD MODE, ACOUSTIC EXCITATION, C-C CFRP BEAM

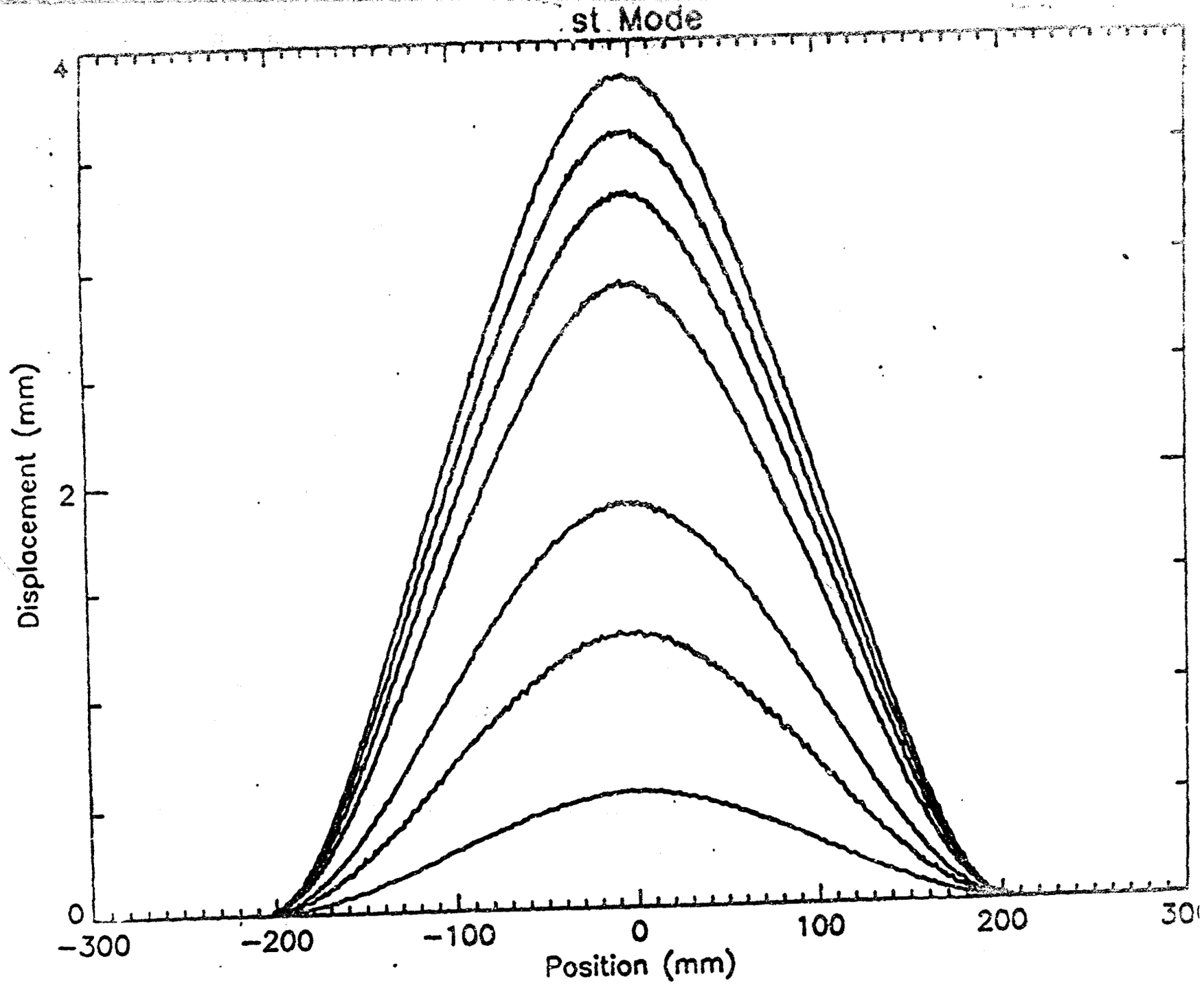

FIGURE 52 NONLINEAR DISPLACEMENT SHAPES, FIRST MODE, RAW DATA, C-C CFRP BEAM

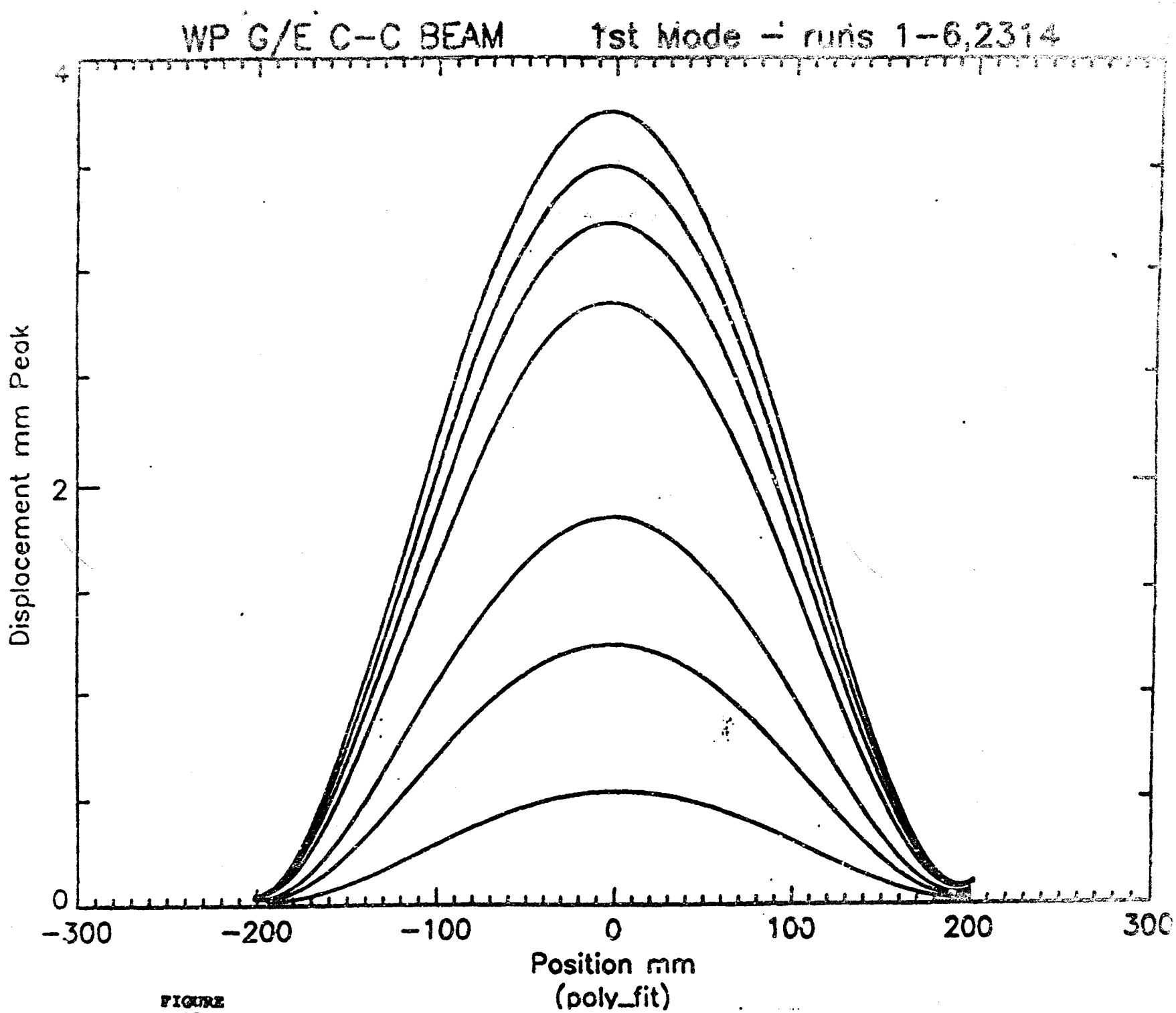

FIGURE 53 NONLINEAR DISPLACEMENT SHAPES, FIRST MODE, FOURTH ORDER POLYNOMIAL.

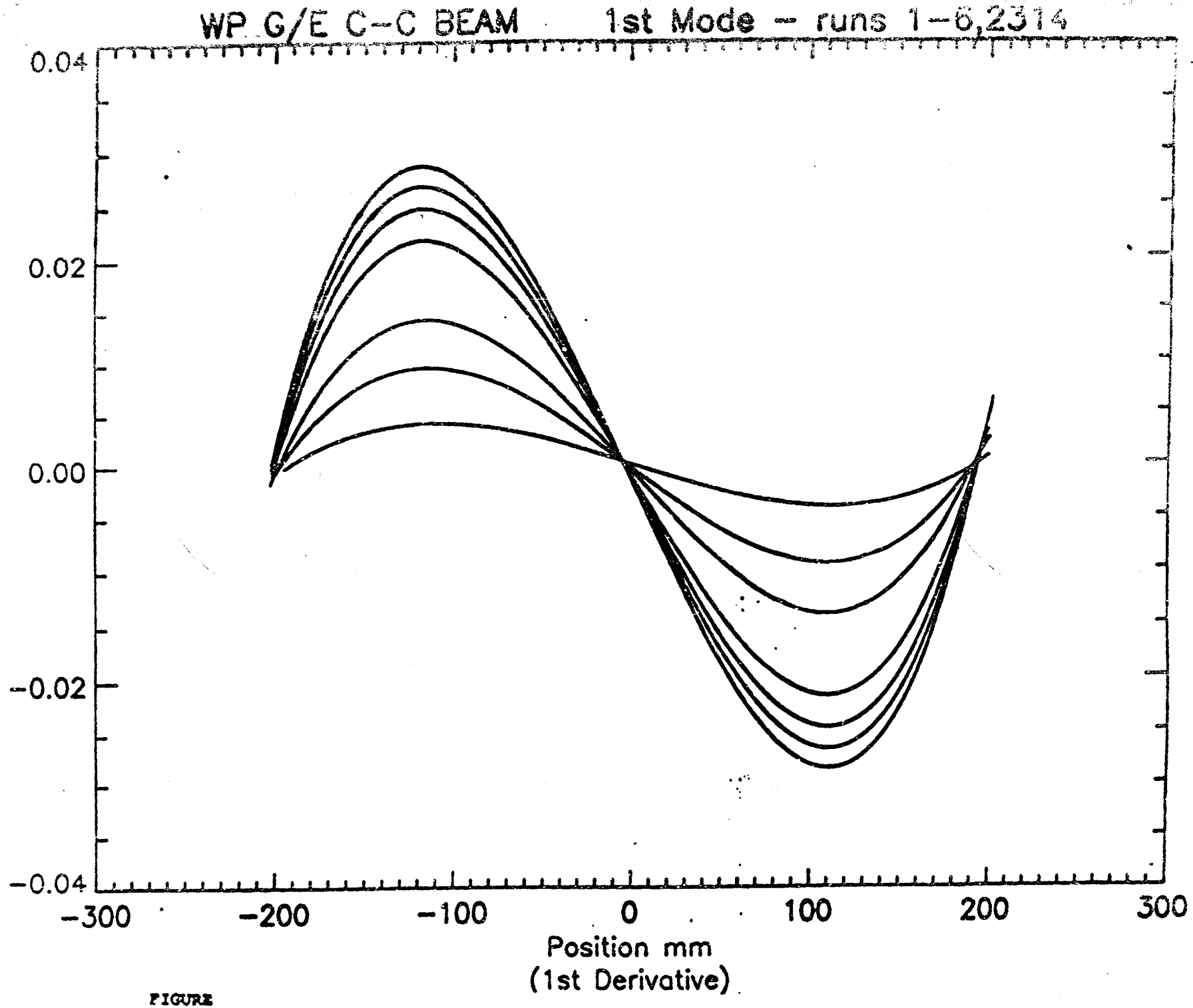

FIGURE 54 FIRST MODE, FOURTH ORDER POLYNOMIAL FIT, FIRST DERIVATE, C-C

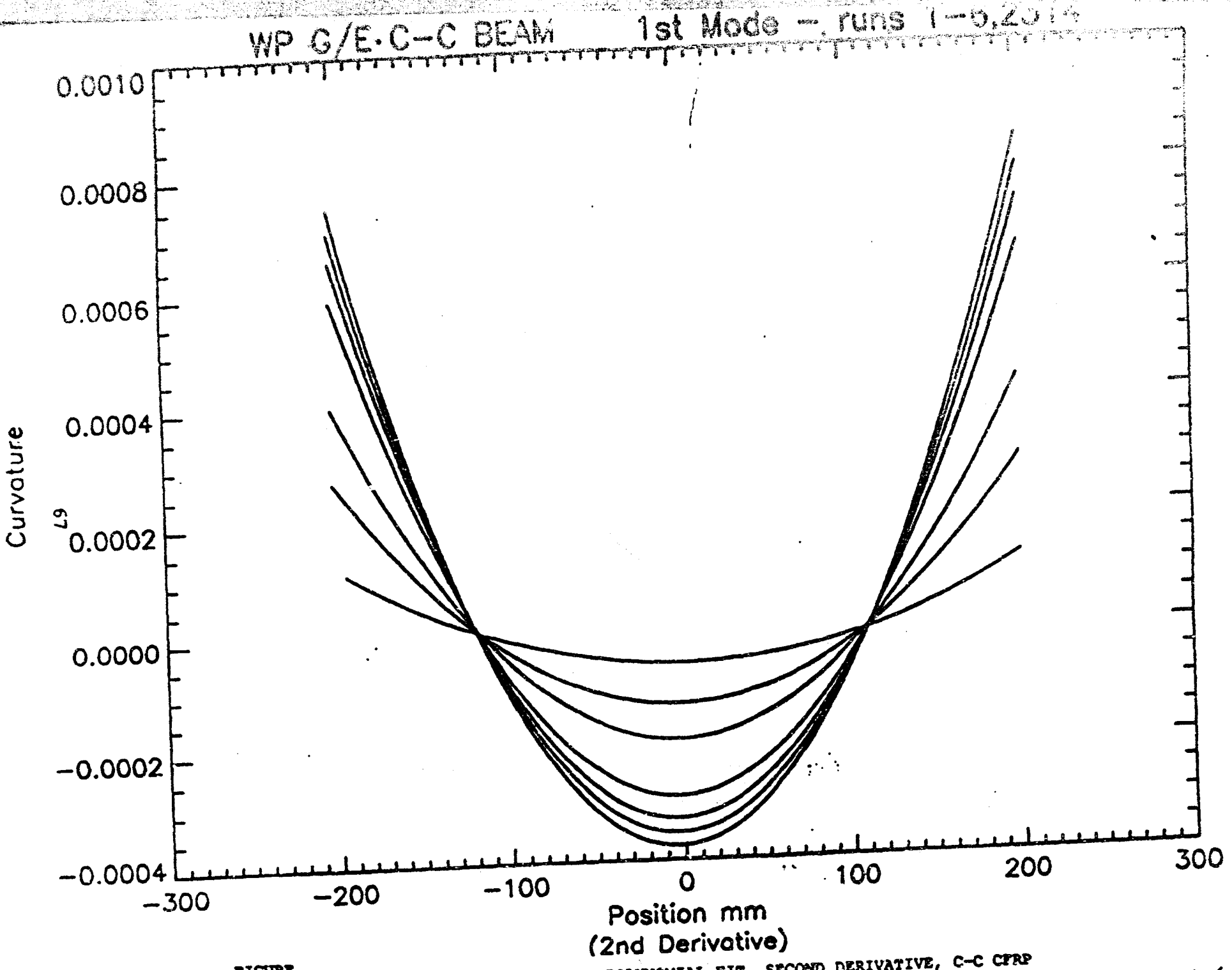

FIGURE 55 FIRST MODE, FOURTH ORDER POLYNOMIAL FIT, SECOND DERIVATIVE, C-C CFRP

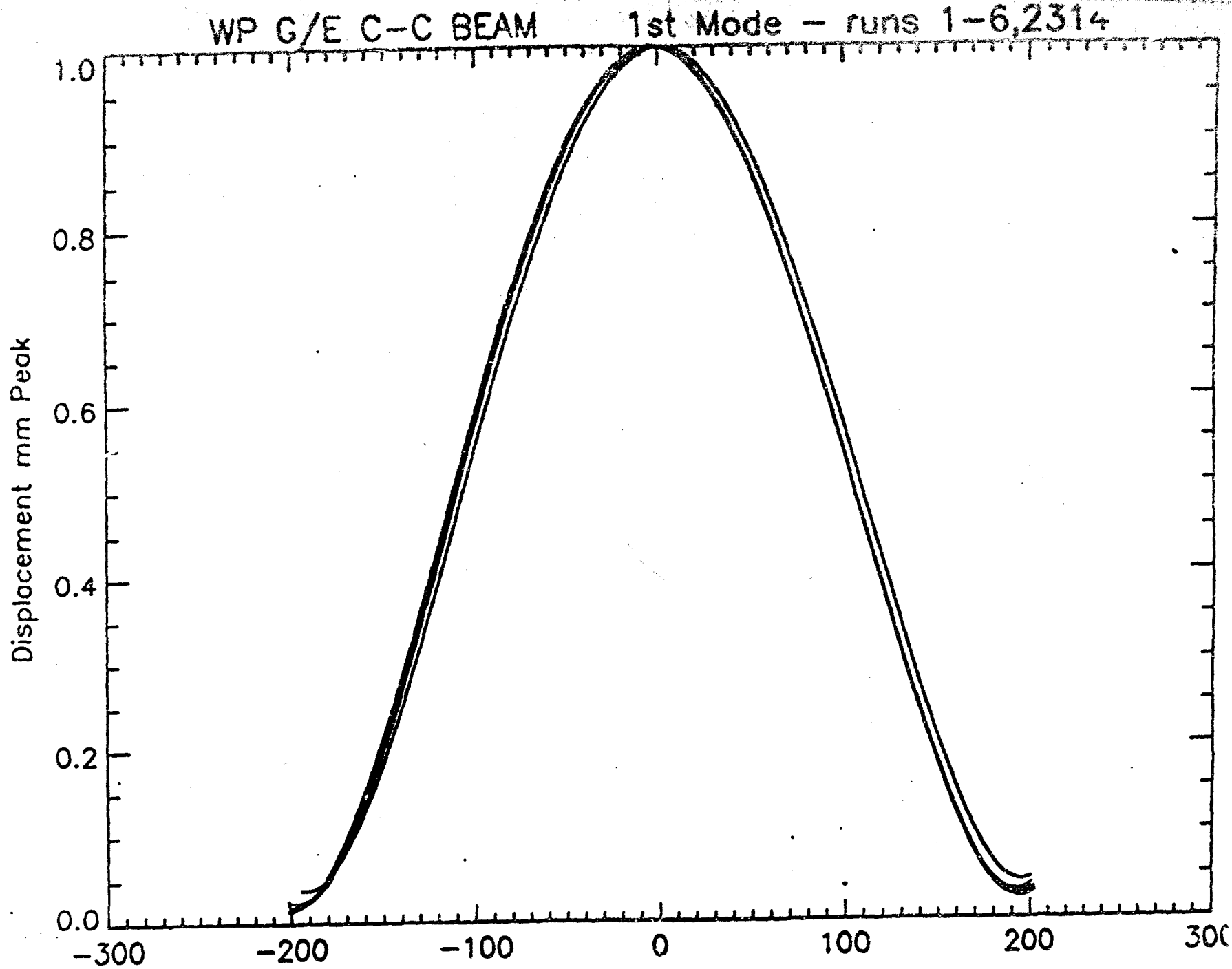
WP G/E C-C BEAM 1st Mode – runs 1-6,2314
Displacement mm Peak
1.0
0.8
0.6
0.4
0.2
0.0
-300
-200
-100
0
100
200
300
Position mm
(normalized)

89

FIGURE

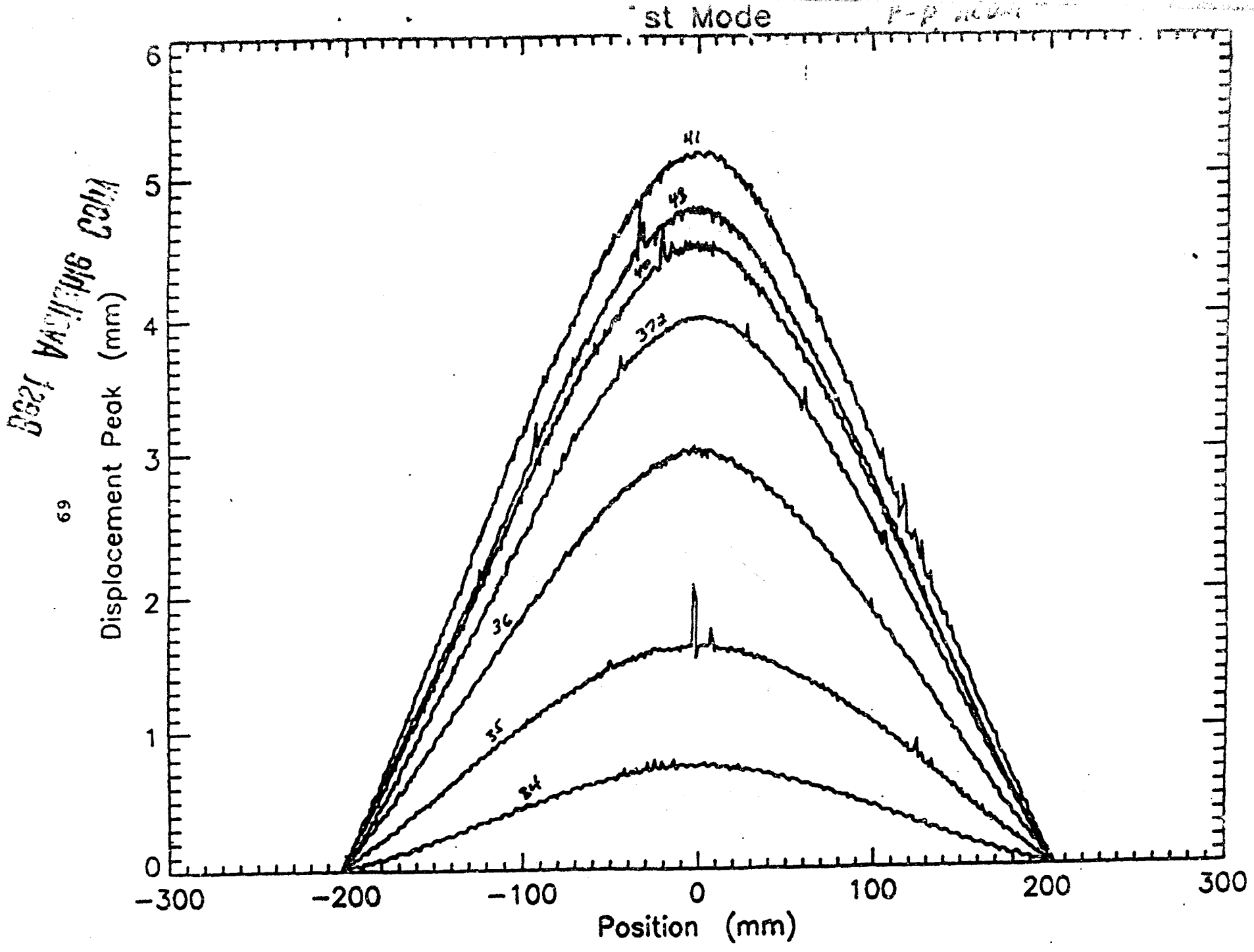

FIGURE 57 NONLINEAR DISPLACEMENT SHAPES, FIRST MODE, RAW DATA, P-P, ALUMINUM BEAM

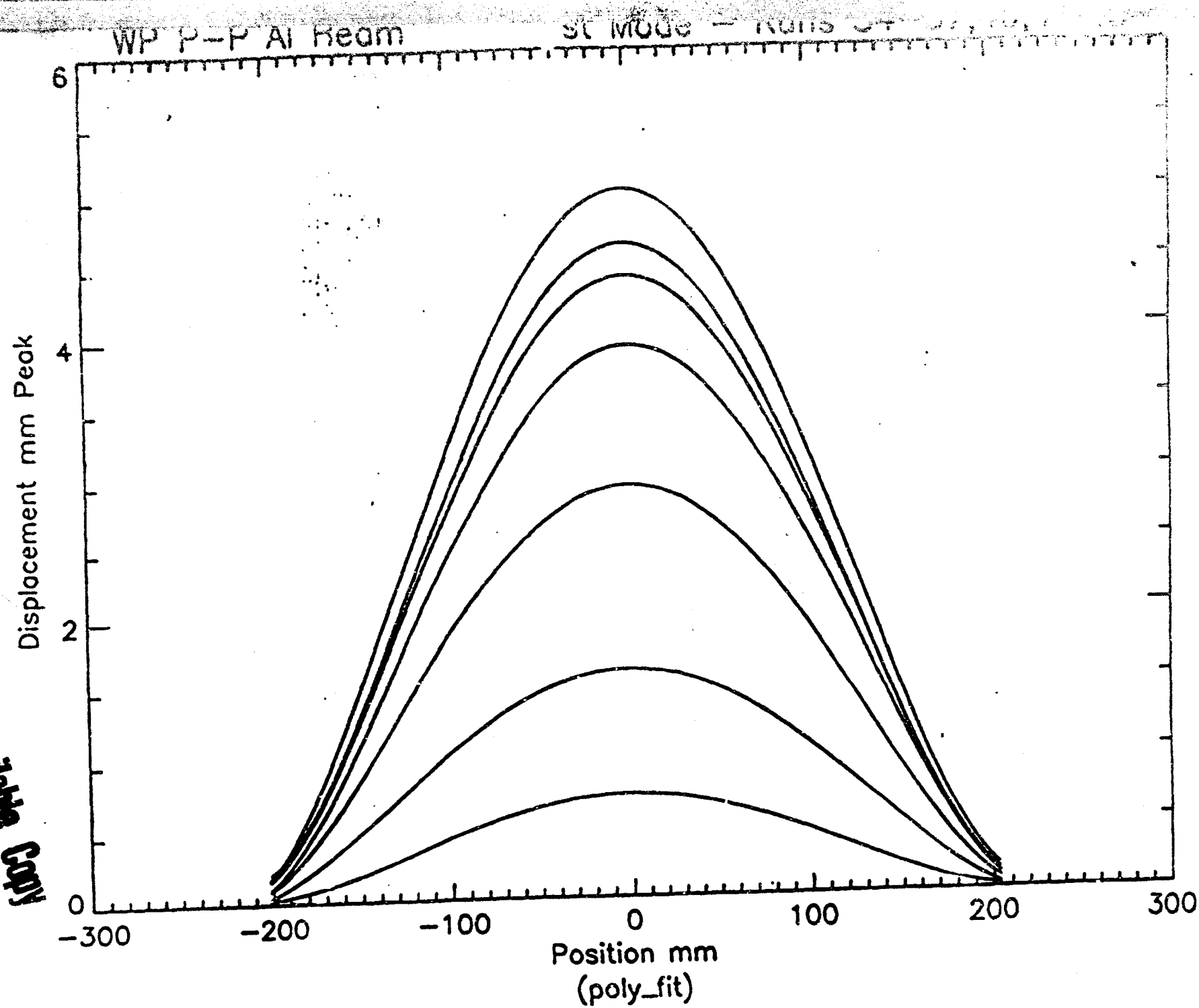

FIGURE 58 NONLINEAR DISPLACEMENT SHAPES, FIRST MODE, FOURTH ORDER POLYNOMIAL FIT, P-P ALUMINUM BEAM

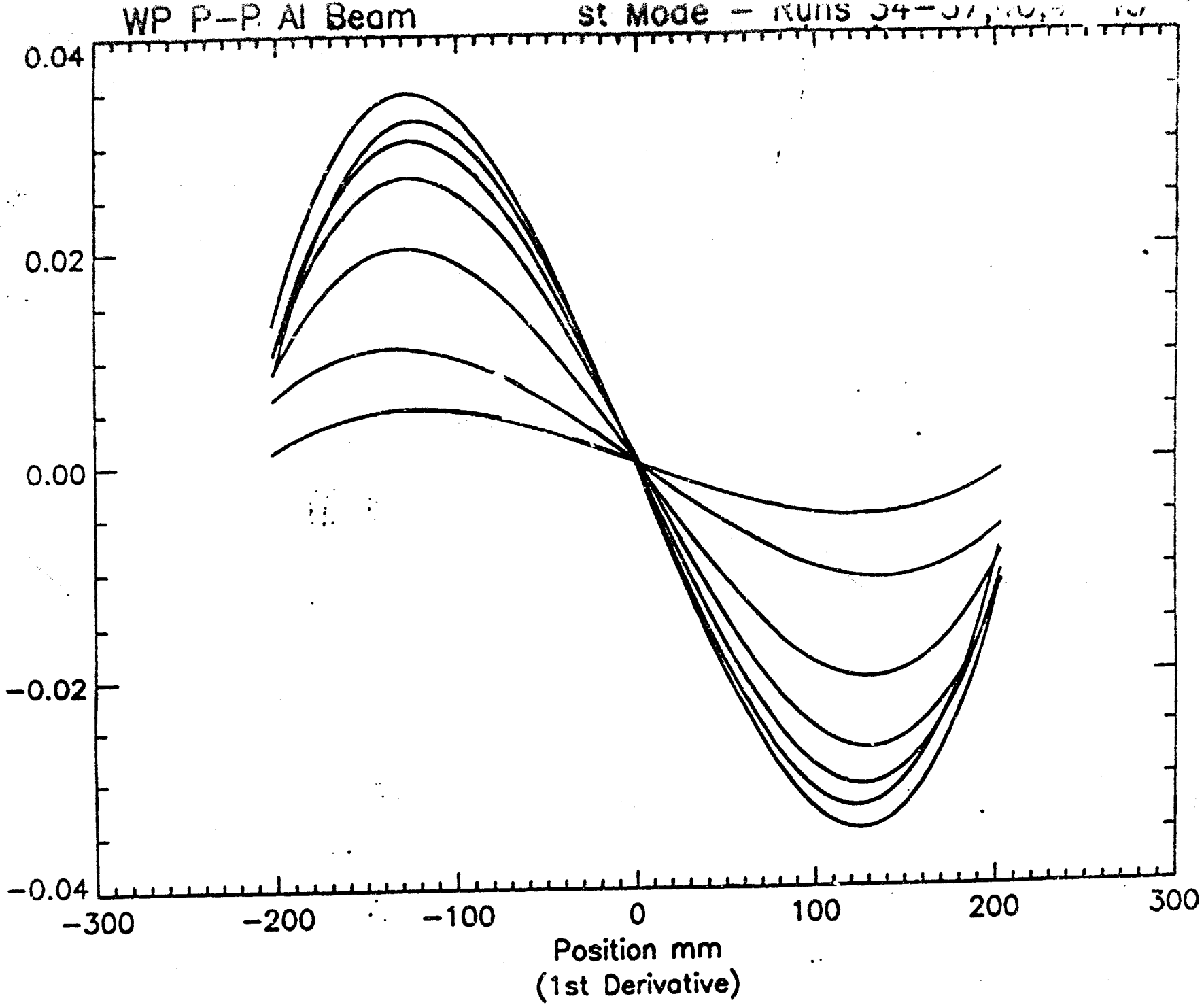

FIGURE 59 FIRST MODE, FOURTH ORDER POLYNOMIAL FIT, FIRST DERIVATIVE, P-P

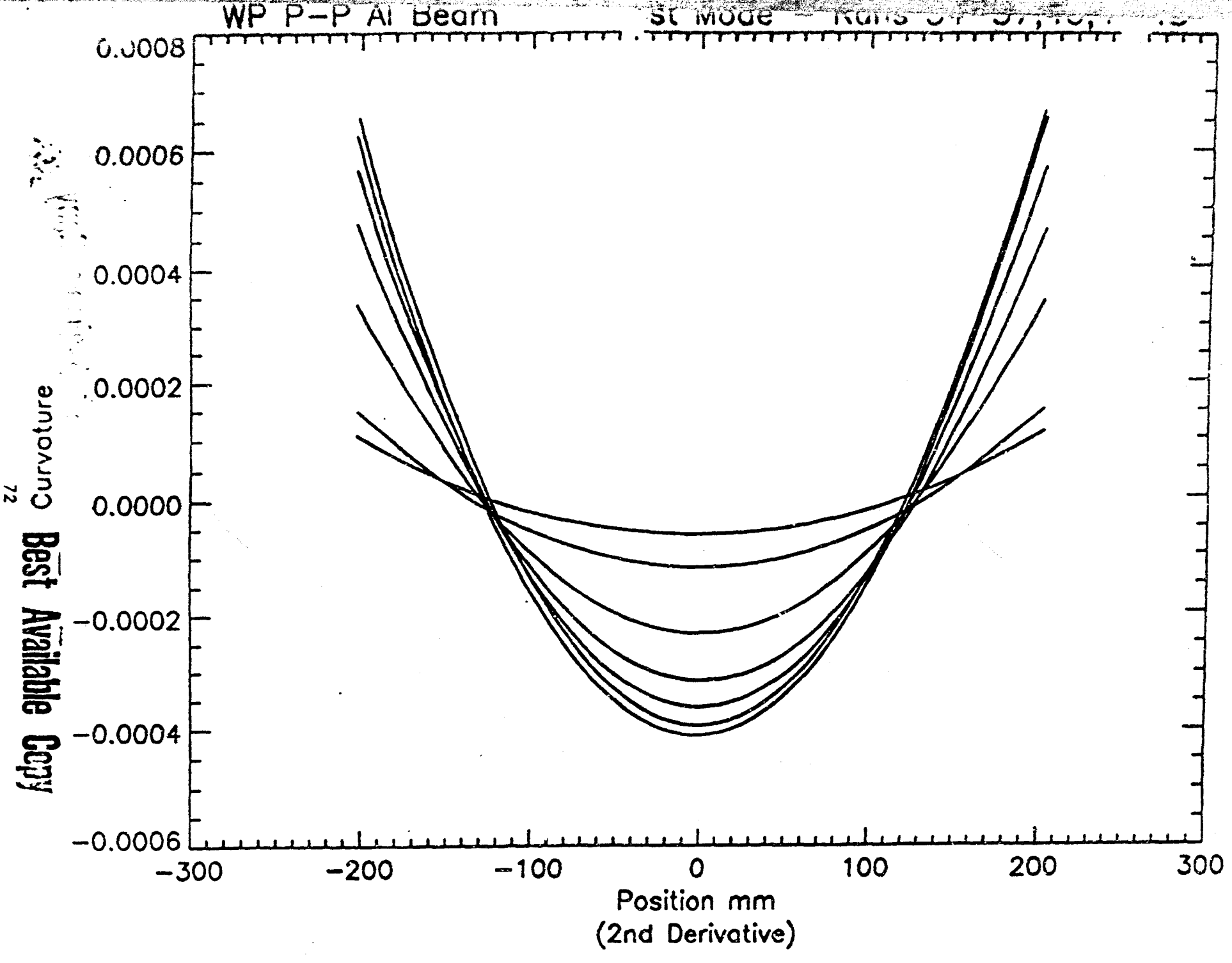
WP P-P Al Beam
0.0008
0.0006
0.0004
0.0002
0.0000
-0.0002
-0.0004
-0.0006
-300
-200
-100
0
100
200
300
Position mm
(2nd Derivative)
Curvature
Best Available Copy

FIGURE

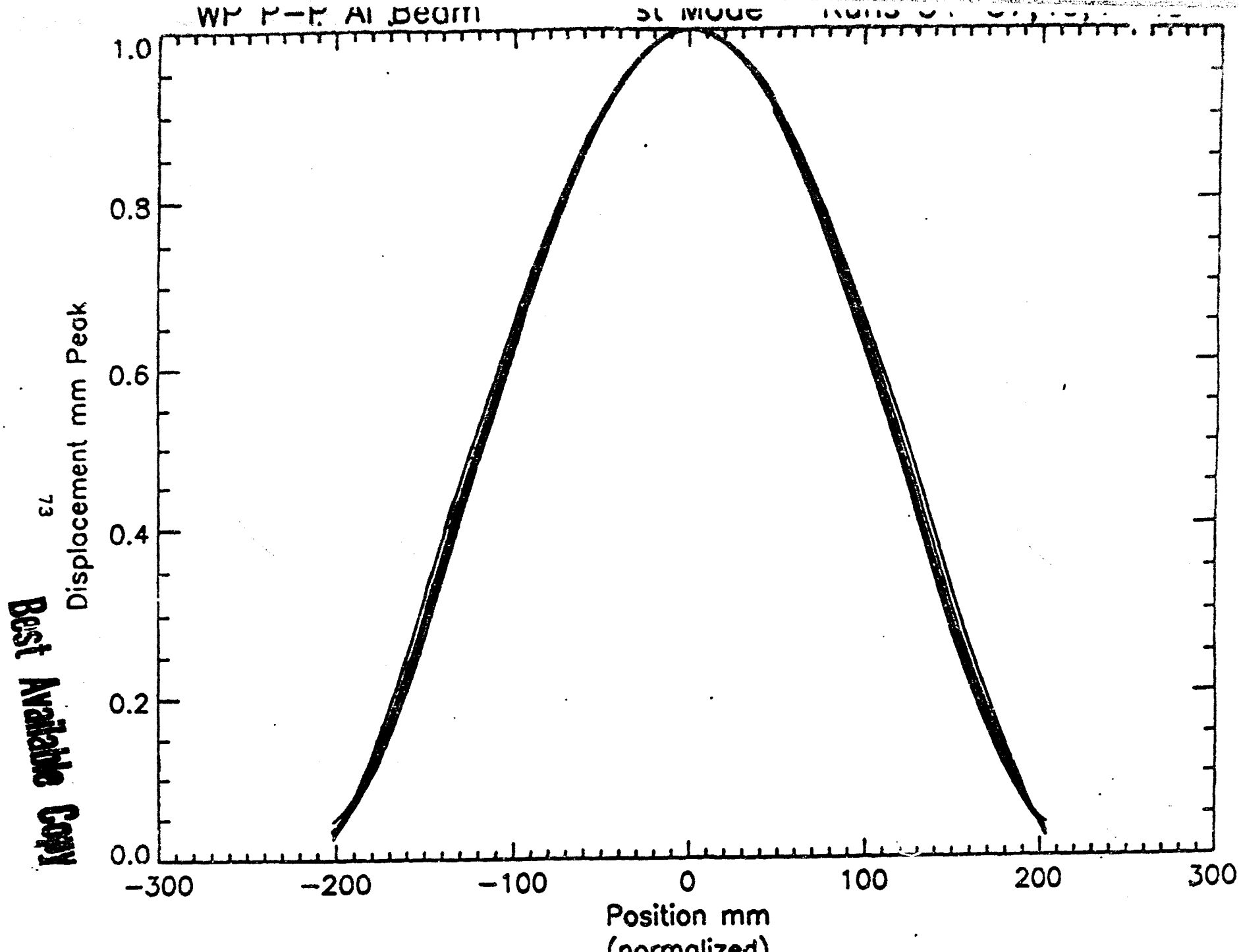

FIGURE [illegible] DISPLACEMENT SHAPES, FIRST MODE, P-P ALUMINUM

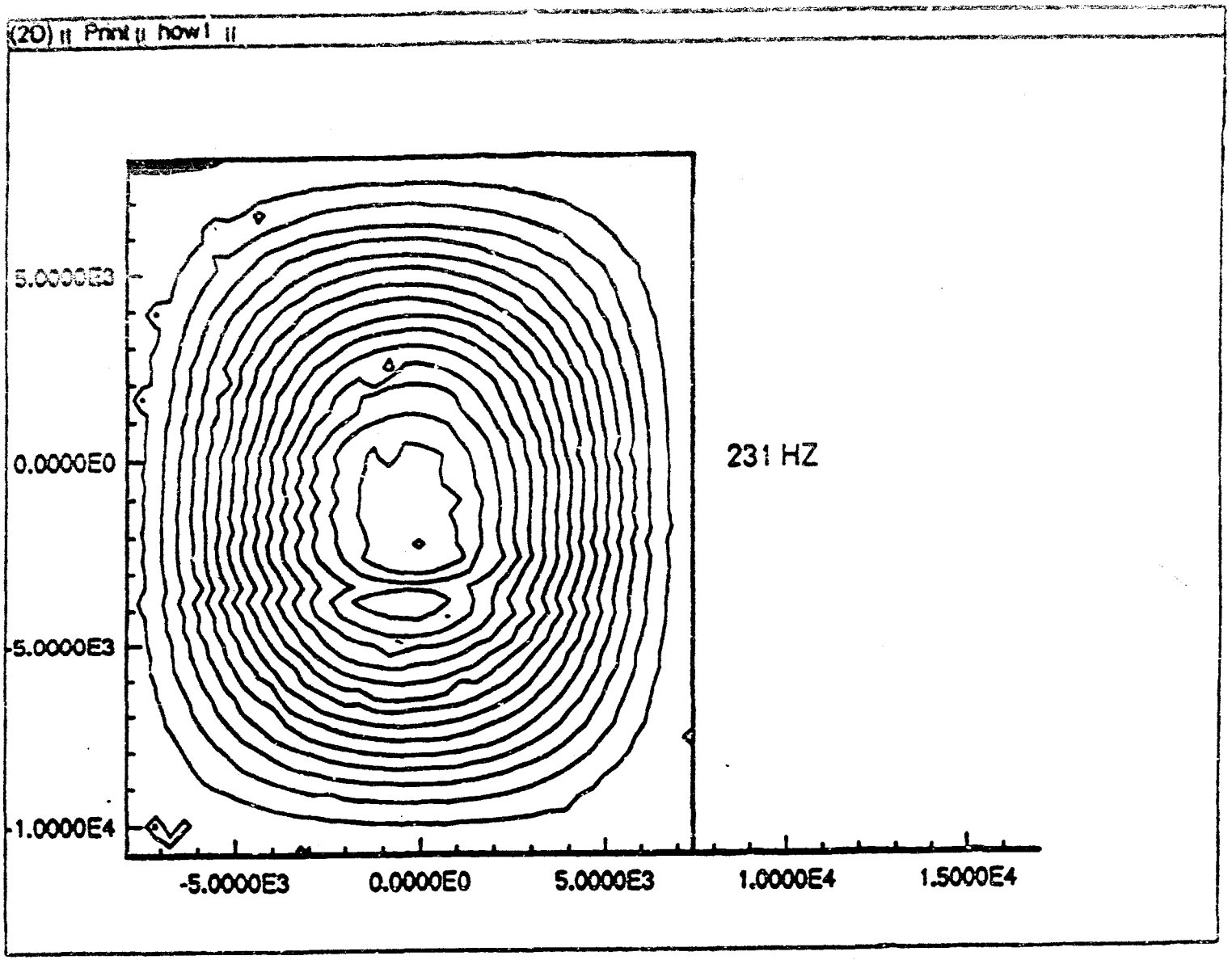

FIGURE 62 MODE SHAPE, 1:1, C-C ALUMINUM PLATE

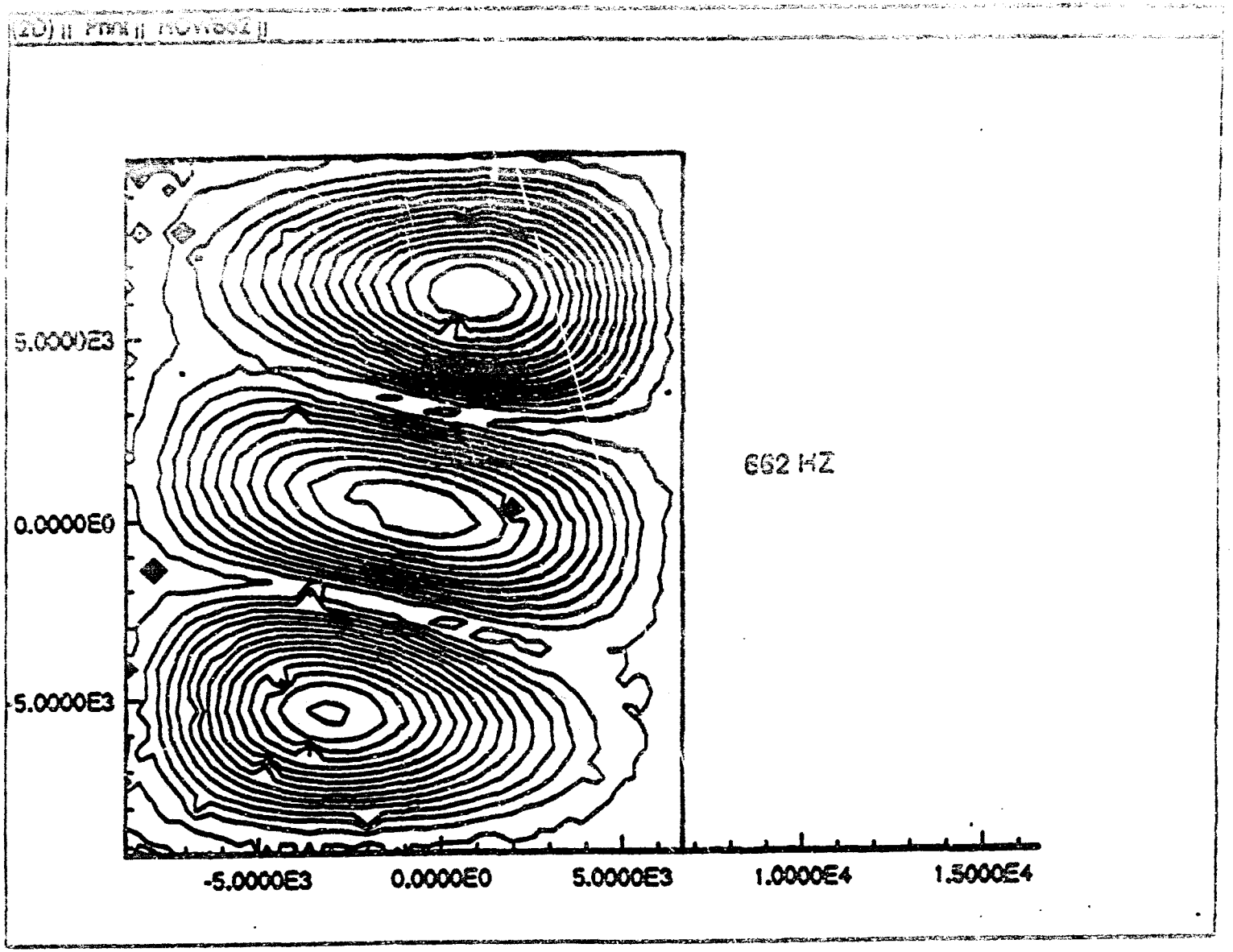

FIGURE 63 SKEWED MODE SHAPE, 3:1, C-C ALUMINUM PLATE

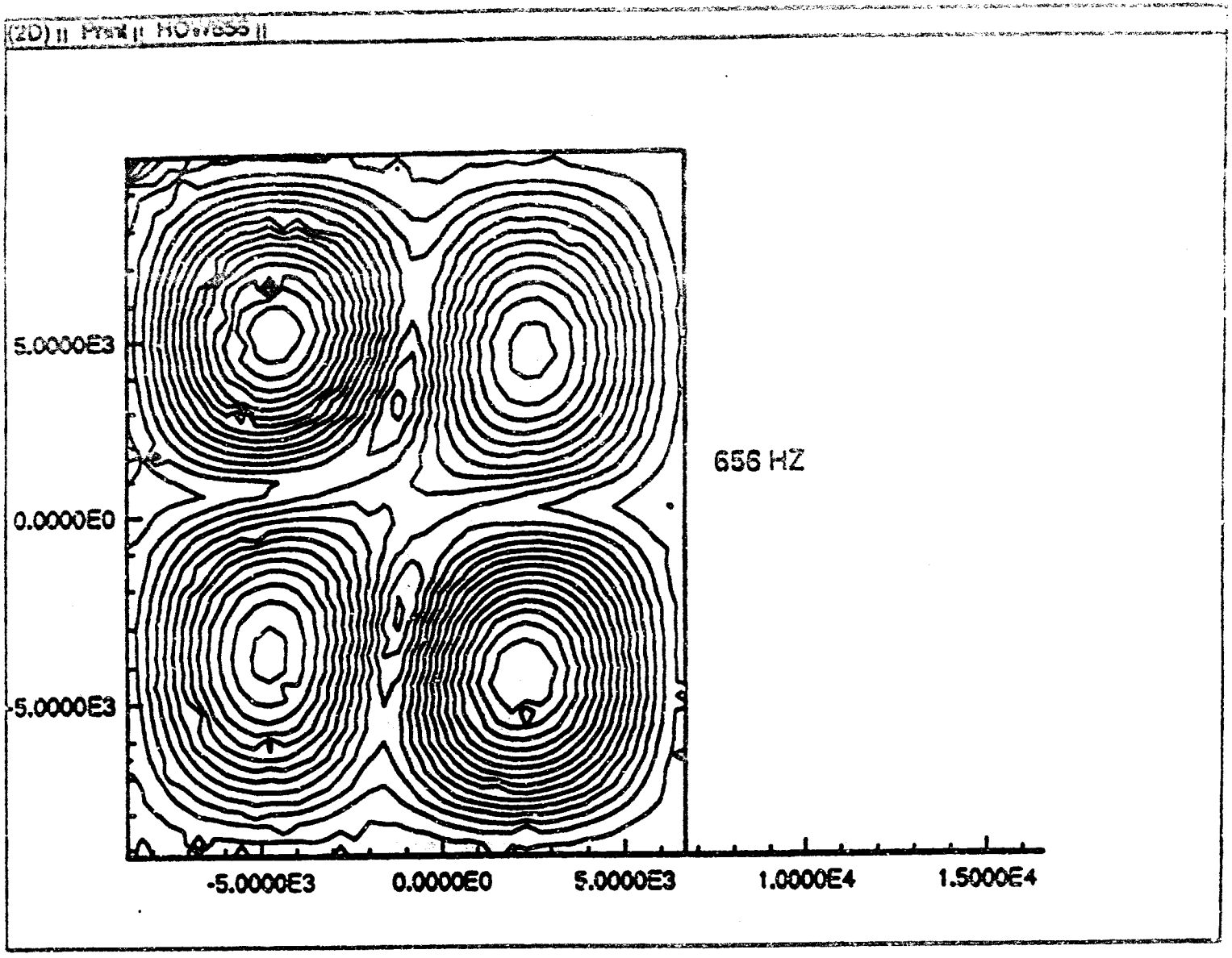

FIGURE 64 MODE SHAPE, 2:2, C-C ALUMINUM PLATE

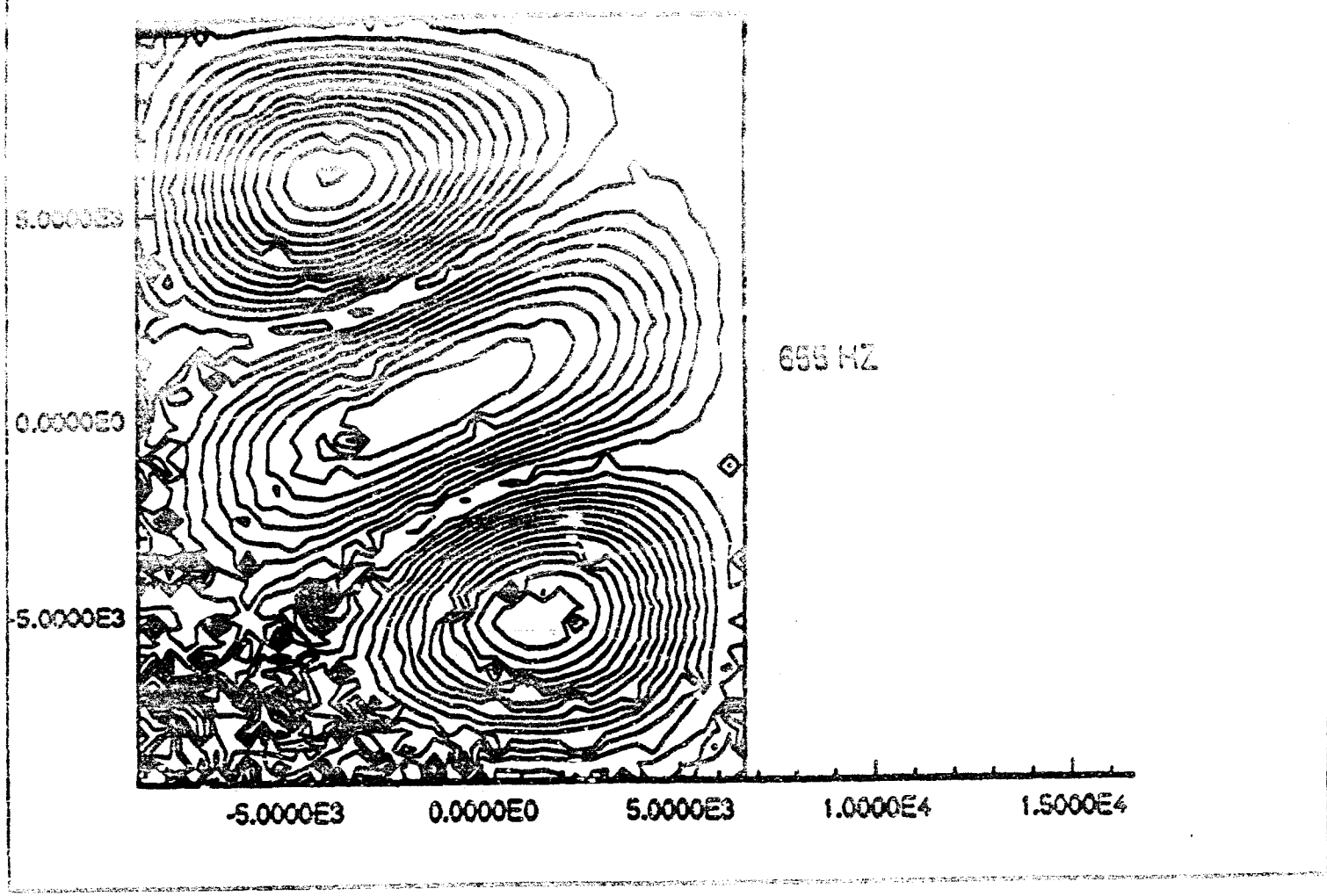

FIGURE 65 STEERED MODE IMAGE, 3:1, C-C ASPECT RATIO

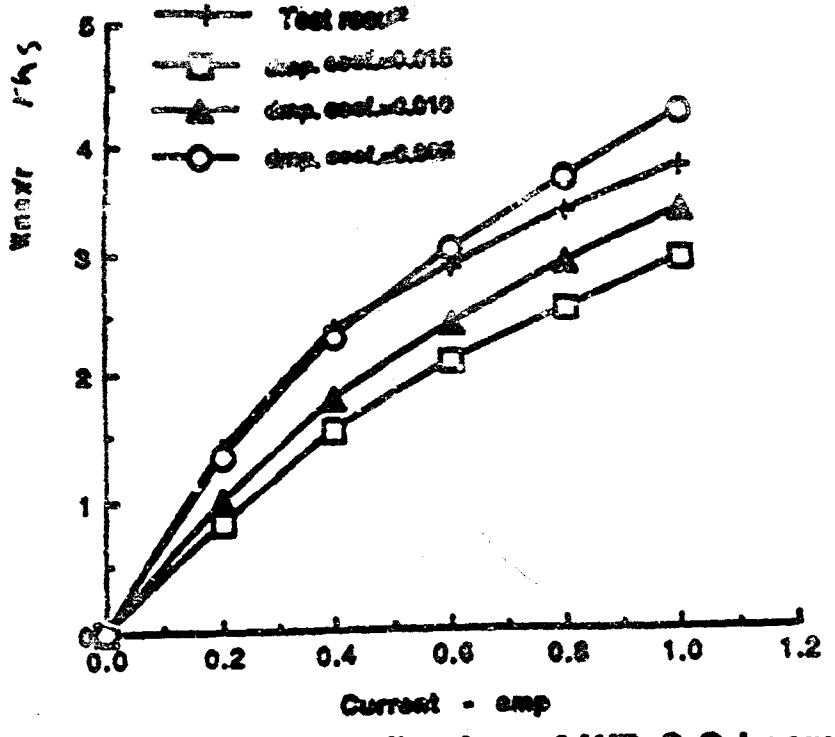

Fig. 1 Maximum deflection of WP C-C beam

66

FIGURE 66 COMPARISON OF C-C ALUMINUM BEAM DEFLECTION TEST RESULTS WITH FEM RESULTS

NO PRELOAD

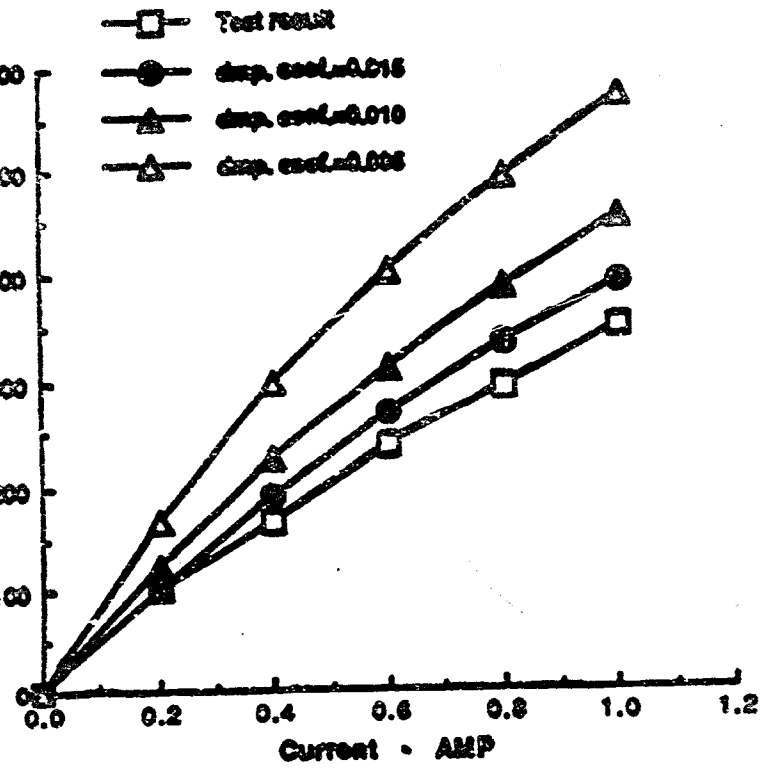

Fig. 67 RMS strain for WP C-C beam at center

67

FIGURE 67 COMPARISON OF C-C ALUMINUM BEAM STRAIN TEST RESULTS WITH FEM RESULTS, NO PRELOAD

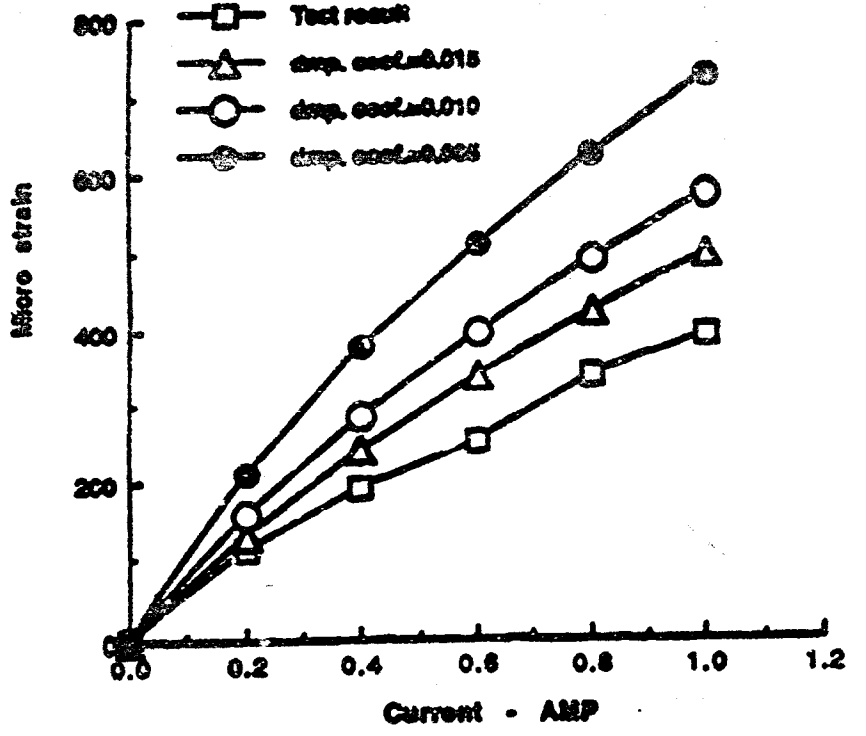

Fig. 6 RMS strain for WP C-C beam at clamped edge

68

FIGURE 68 COMPARISON OF C-C ALUMINUM BEAM STRAIN TEST RESULTS WITH FEM RESULTS,

STATIC DEFLECTION VS STRESS
CHIEN-YEH LARGE DEFLECTIONS-PLATE

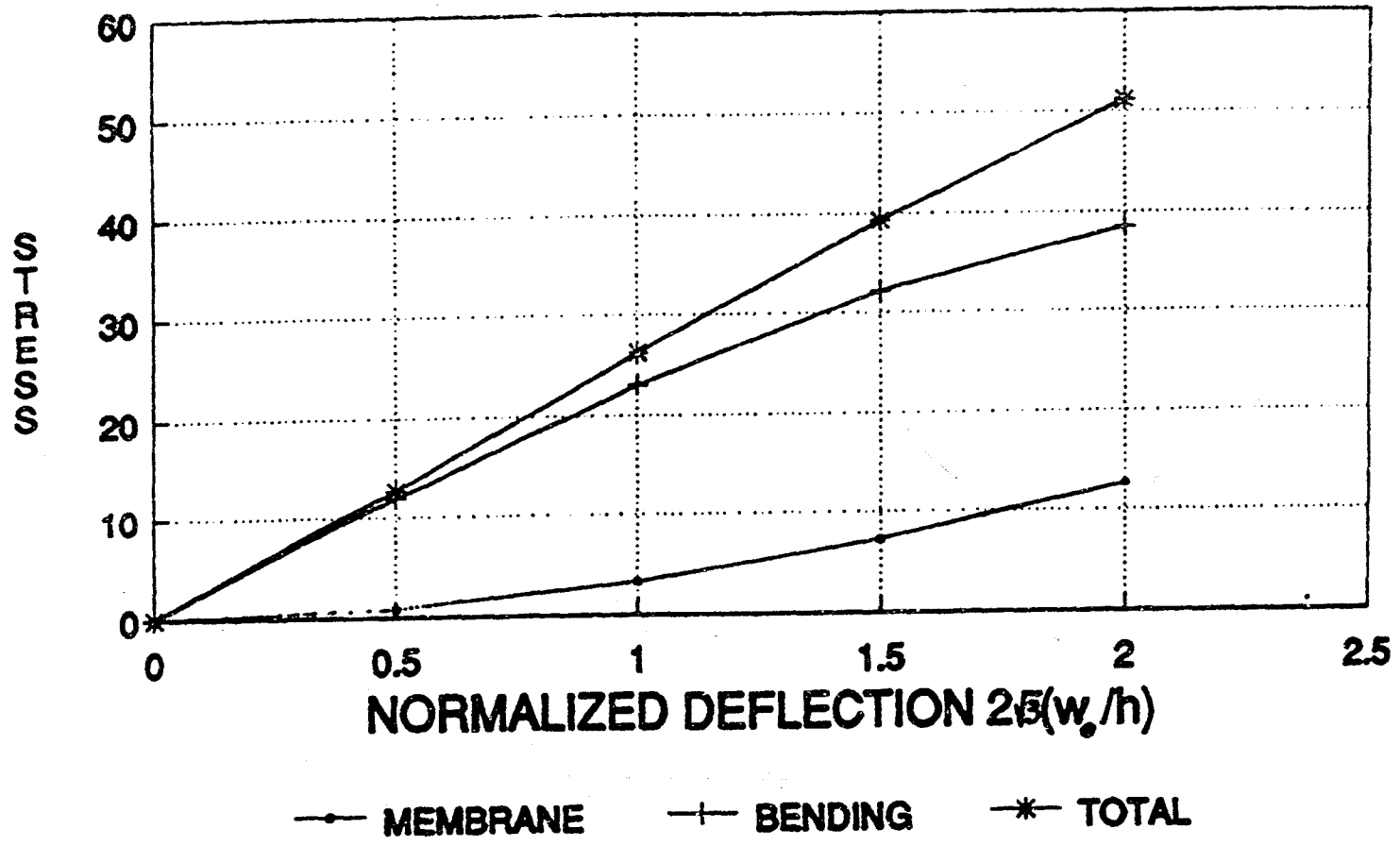

HW95 3NOV92

FIGURE 69 STATIC DEFLECTION VS STRESS, C-C PLATE, REF 3 RESULTS

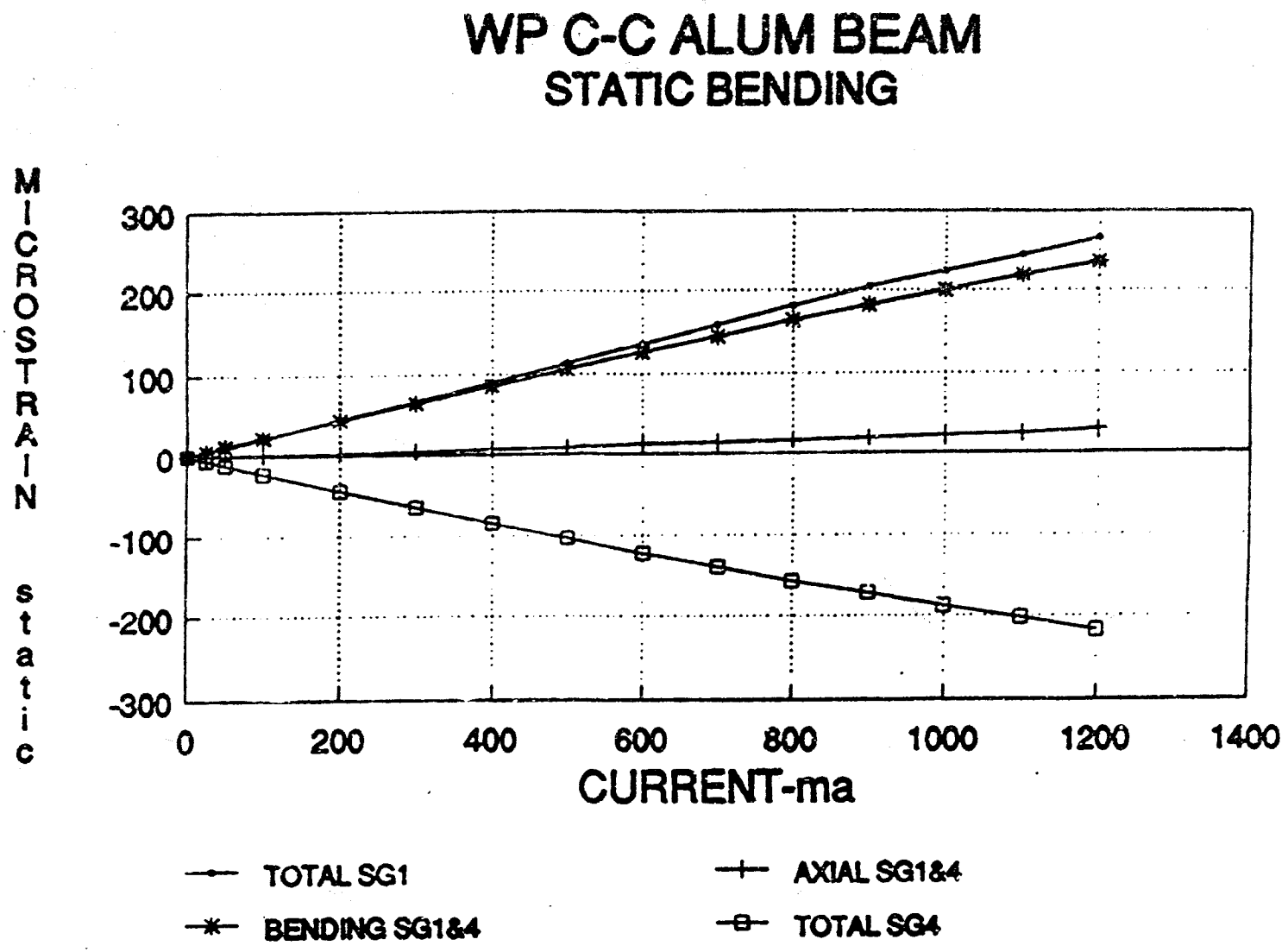

HW96 3NOV92

FIGURE 70 STATIC CURRENT VS STRAIN, C-C ALUMINUM BEAM TEST RESULTS